ISSN 0038-531X

Russian Original Vol. 48, No. 6, June, 1980

December, 1980

SATEAZ 48(6) 353-422 (1980)

SOVIET ATOMIC ENERGY

АТОМНАЯ ЭНЕРГИЯ
(ATOMNAYA ÉNERGIYA)

TRANSLATED FROM RUSSIAN

CONSULTANTS BUREAU, NEW YORK

SOVIET ATOMIC ENERGY

Soviet Atomic Energy is a translation of *Atomnaya Énergiya*, a publication of the Academy of Sciences of the USSR.

An agreement with the Copyright Agency of the USSR (VAAP) makes available both advance copies of the Russian journal and original glossy photographs and artwork. This serves to decrease the necessary time lag between publication of the original and publication of the translation and helps to improve the quality of the latter. The translation began with the first issue of the Russian journal.

Consultants Bureau journals appear about six months after the publication of the original Russian issue. For bibliographic accuracy, the English issue published by Consultants Bureau carries the same number and date as the original Russian from which it was translated. For example, a Russian issue published in December will appear in a Consultants Bureau English translation about the following June, but the translation issue will carry the December date. When ordering any volume or particular issue of a Consultants Bureau journal, please specify the date and, where applicable, the volume and issue numbers of the original Russian. The material you will receive will be a translation of that Russian volume or issue.

Subscription (2 volumes per year)

Vols. 46 & 47: $147.50 per volume (6 Issues)
Vols. 48 & 49: $167.50 per volume (6 Issues)

Single Issue: $50
Single Article: $7.50

Prices somewhat higher outside the United States.

CONSULTANTS BUREAU, NEW YORK AND LONDON

227 West 17th Street
New York, New York 10011

Published monthly. Second-class postage paid at Jamaica, New York 11431.

Soviet Atomic Energy is abstracted or indexed in *Chemical Abstracts, Chemical Titles, Pollution Abstracts, Science Research Abstracts, Parts A and B, Safety Science Abstracts Journal, Current Contents, Energy Research Abstracts,* and *Engineering Index.*

SOVIET ATOMIC ENERGY

A translation of *Atomnaya Énergiya*

December, 1980

Volume 48, Number 6 June, 1980

CONTENTS

CONTENTS

(continued)

The Russian press date (podpisano k pechati) of this issue was 5/22/1980. Publication therefore did not occur prior to this date, but must be assumed to have taken place reasonably soon thereafter.

ARTICLES

COMPARISON OF CALCULATIONS OF A TWO-DIMENSIONAL MODEL OF A FAST REACTOR

A. I. Voropaev, O. P. Chukhlova,
A. A. Van'kov, L. N. Kudryashov,
and R. V. Nikol'skii

UDC 621.039.51

The specification of a two-dimensional (R−Z) test model of a fast reactor with a power of 1200 MW (el.) was developed in 1976 by the European−American Committee of Reactor Physics (NEACRP) for comparison of the basic physical characteristics obtained in the different countries which determine the economics and safety of planned commercial fast reactors with sodium coolant [1].

The active zone with 10-m^3 volume contains two equally large subzones of different enrichment. The height of the active zone is 102 cm. The volume fractions of fuel, sodium, and steel are 41, 38, and 21%. The fuel is a homogeneous UO_2-PuO_2 mixture. The isotopic composition of the plutonium is as follows: 67.8% ^{239}Pu, 19.4% ^{240}Pu, 10.3% ^{241}Pu, and 2.5% ^{242}Pu. The thickness of the end shield is 33 cm and of the lateral shield − 47 cm. The moist material is the oxide of dumped uranium. The computational model corresponds to the start of reactor operation at power, i.e., no fission products and plutonium in the shields.

A systematic discussion of the calculations which have come in from the different countries has been carried out at the English National Laboratory [2]. The results presented by the USSR of calculations of this test model using the BNAB-70 system of constants are reviewed in [3]. A more detailed description of the model and computational details is also given there.

At the present time the new BNAB-78 system of constants [4], which is based on recent estimates of microscopic nuclear data and which are in agreement with the results of fundamental experiments on neutron balance in uranium and plutonium critical assemblies, is starting to be widely used in the computational practice of fast reactors in the USSR. Therefore, test calculations using this system of constants and a comparison of them with analogous calculations using other systems are of interest. Such a comparison was made [5, 6] for a spherical test model of a reactor. Results are presented below for a two-dimensional test model of a large breeder reactor (the NEACRP model).

The results given of calculations using BNAB-70 and BNAB-78 are obtained with the help of an NF-6 computer system [7] in which are implemented specific algorithms for preparation of the group macroscopic constants. Taking the effect of resonant self-screening into account and the calculation of the moderation cross section are done in specified approximations. The error due to these approximations is estimated (e.g., see [8]) to have these values: ±0.5% for k_{eff}, ±0.03% for the physical breeding ratio of the reactor (BR) and the breeding ratio of the active zone (BRA), and ±10% for the reactivity coefficients.

The results of the calculations of the test model carried out in the USSR using the BNAB-70 and BNAB-78 systems of constants are compared with the calculations of other countries in Table 1 and Fig. 1. The parameters BR and BRA are found from the neutron balance corresponding to a conditionally critical calculation, since the composition and dimensions of the reactor are fixed by the conditions of the specification. The following definitions are adopted:

$$\mathrm{BR} = \frac{C_r^8 + C_r^{40}}{(C+F)_r^9 + (C+F)_r^{41} + (C+F)_r^5}; \quad (1)$$

$$\mathrm{BRA} = \frac{C_{AZ}^8 + C_{AZ}^{40}}{(C+F)_r^9 + (C+F)_r^{41} + (C+P)_r^5}, \quad (2)$$

where C and F are integrals over the volume of the capture and fission rates in the active zone (AZ) or in the entire reactor (r). The superscripts "5", "8", "9", "40", and "41" refer to the isotopes ^{235}U, ^{238}U, ^{239}Pu, ^{240}Pu, and ^{241}Pu. The numbers in parentheses indicated in Table 1 are the results of recalculations of BR and BRA

Translated from Atomnaya Énergiya, Vol. 48, No. 6, pp. 355-357, June, 1980. Original article submitted October 15, 1979.

0038-531X/80/4806-0353 $07.50

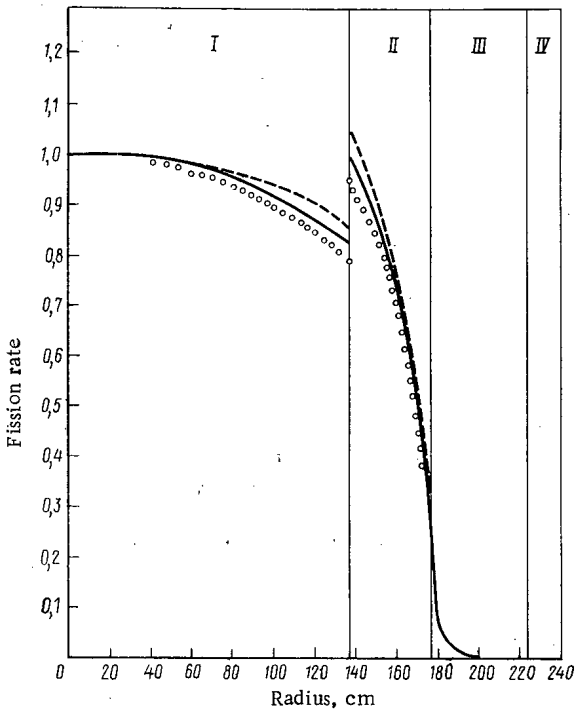

Fig. 1. Distribution of the heat-generation density in the central plane of the reactor: I) zone of small enrichment; II) zone of large enrichment; III) lateral shield; and IV) reflector made out of steel and sodium; —) USSR (BNAB-78), ---) USA, and ○) France.

TABLE 1. Comparison of Calculations of the Basic Physical Characteristics of the Test Model of a Fast Reactor

Country	Criticality and breeding parameters			Eff. of central boron rod, % k_{eff}		Effect of sodium removal, % k_{eff}			Variation of k_{eff} upon heating of the fuel from 1100°K to 2200°K, %	
	k_{eff}	BR	BRA	with respect to fuel	with respect to sodium	from zone of small enrichment	from entire active zone and end shield	from entire active zone and end shield of a "hot" reactor	orig. composition	upon removal of sodium from active zone and end shield
USSR:										
BNAB-70	1,009	1,48 (1,50)	1,06 (1,07)	—0,47	—0,39	1,9	1,7	2,0	—0,65	—0,34
BNAB-78	1,012	1,39 (1,42)	0,98 (0,99)	—0,37	—0,31	2,1	2,0	2,2	—0,58	—0,36
England	1,022	1,36 (1,42)	0,95 (0,97)	—0,40	—0,33	2,1	2,1	2,4	—0,74	—0,45
U.S.A.	0,993	1,39 (1,37)	0,99 (0,98)	—0,33	—0,28	2,4	2,4	2,7	—0,71	—0,46
France	1,013	1,39 (1,42)	0,98 (0,99)	—0,38	—0,36	2,2	2,2	2,5	—0,71	—0,48
West Germany	1,024	1,36 (1,42)	0,96 (0,98)	—0,40	—0,34	2,0	1,9	2,1	—0,65	—0,42
Japan	1,014	1,36 (1,39)	0,96 (0,97)	—0,32	—0,26	2,4	2,5	2,7	—0,78	—0,53
Av. value for foreign labs.	1,013	1,37 (1,40)	0,97 (0,98)	—0,37	—0,31	2,3	2,2	2,5	—0,72	—0,47

Remark: The numbers in parentheses give the result for the conditions of a critical reactor (see text).

for the conditions of a critical reactor with a change in the enrichment. Sensitivity coefficients calculated from generalized perturbation theory were used for the recalculation. The sensitivity coefficients are obtained under the condition of preserving the isotopic composition of the plutonium and the enrichment ratios in both subzones of the active zone [9].

In connection with the comparison of the efficiency of the central boron rod a variation of k_{eff} is indicated for the two cases in which the fuel in the central region of the reactor (R = 7.2 cm, H = HAZ) is replaced by a

TABLE 2. Comparison of Estimates of the Error in Calculating the Physical Parameters of a Large Fast Reactor

Parameter	Based on errors in nuclear data	Max. scatter of test calc. results
k_{eff}	±2 %	2,7 %
BR	±0,06	0,05
Eff. of boron rod	±10 %	20 %
Removal of sodium	±30 %	30 %
Heating of fuel	±30 %	30 %
Heat generation per unit volume of active zone	±5 %	10 %

boron rod and in which the boron rod is placed in the central region filled with sodium. The computational results of the variation of k_{eff} upon removal of sodium from different parts of the reactor are also given here. The cross sections of uranium and plutonium isotopes at 2200°K (T = 1100°K for all the preceding alternatives) correspond to a "hot" reactor.

Furthermore, the calculations of the variation of k_{eff} upon heating of the active zone from 1100 to 2200°K are compared in Table 1. The numbers in the next-to-last column correspond to the original composition, and those in the last column correspond to a reactor from whose active zone and end shield the sodium has been removed.

The distribution of the heat-generation density (without γ radiation taken into account) in the central plane of the reactor is shown in Fig. 1. The calculation using BNAB-70 practically coincides with that using BNAB-78 (maximum difference does not exceed 3%). The results of the American and French calculations are the bounding ones between which the results of the other countries are located.

On the basis of the above one can draw the following conclusions:

1. The transition from the BNAB-70 to the BNAB-78 system of constants has resulted in a decrease of BR by 0.08, which is produced entirely by a decrease in breeding in the active zone. The effective multiplication factor underwent an insignificant change (+0.3% k_{eff}). The efficiency of the central boron rod decreased by ≈25%. The sodium void effect became more positive. The changes in BR, BRA, and k_{eff} are in good agreement with the conclusions which follow from an analysis of experiments on large plutonium assemblies [10, 11] and with the results of international test calculations of a one-dimensional model of a fast reactor with an active-zone volume of 2.5 m^3 [5, 6]. We note that the good agreement of the criticality of the two-dimensional model in the calculations based on the BNAB-70 and BNAB-78 systems is a consequence of compensation of an overestimated contribution of ^{241}Pu (~1.5% k_{eff}) and an underestimated contribution of ^{238}U and ^{239}Pu to the reactivity in the BNAB-70 system of constants.

2. Calculations of the values of k_{eff}, BR, BRA, the efficiency of the boron rod, and the sodium void effect using the BNAB-78 system agree better with the results of foreign laboratories than the calcuations using the BNAB-70 system. However, the change in the reactivity upon heating of the fuel is less by 25% than all the foreign data in the calculations using the BNAB-78 system.

3. The estimates of the error in calculating the basic physical parameters of a large fast reactor obtained on the basis of an analysis of the errors existing today in the microscopic and integrated nuclear data [8] are compared in Table 2 with the scatter of the computational results in the test model under discussion. The closeness of these and the other results indicates that the error estimates of basic reactor parameters given in [8] are realistic. One can use them in design calculations of industrial fast reactors with oxide fuel and sodium coolant. However, one should anticipate increases by a factor of two to three in the computational errors of these parameters for reactors with a different coolant, a different kind of fuel, or with a design of the placement scheme of the breeding zones which is different from the traditional one [9]. The cause for this lies in the fact that the systems of constants used in design reactor calculations are matched for the best description of experiments on critical assemblies and operating breeder reactors with the traditional composition.

The authors are grateful to M. F. Troyanov for his support and discussion of the research at every stage.

LITERATURE CITED

1. C. Till, L. LeSage, and D. Wade, "Specifications for an international comparison calculation of a large sodium-cooled fast breeder reactor," Tech. Note, ANL (Aug., 1976).
2. L. LeSage et al., in: Proc. of ANS Topical Conf. on Advances in Reactor Physics, Gatlinburg, 10-12 Apr. 1978.
3. O. P. Chukhlova et al., Preprint FÉI-802, Obninsk (1977).
4. L. P. Abagyan et al., At. Energ., 48, No. 2, 117 (1980).
5. A. I. Voropaev, A. A. Van'kov, and A. M. Tsibulya, op. cit., 45, No. 6, 119 (1978).
6. A. I. Voropaev, A. A. Van'kov, and A. M. Tsibulya, op. cit., 47, No. 4, 274 (1979).
7. M. N. Zizin, O. A. Savochkina, and O. P. Chukhlova, Preprint P-40 (334), NIIAR, Dmitrovgrad (1977).
8. A. A. Van'kov, A. I. Voropaev, and L. N. Yurova, Analysis of a Reactor Physics Experiment [in Russian], Atomizdat, Moscow (1977).
9. R. V. Nikol'skii et al., "Prediction of the physical characteristics of prospective active zones of fast reactors on the basis of an analysis of critical assemblies and standard computational models," Lecture at the International Symposium of MAGATE on the Physics of Fast Reactors, Ekstan-Provence, 24-28 September 1979.
10. A. I. Voropaev et al., in: Problems of Nuclear Science and Technology [in Russian], Physical Constants Series, No. 20, Ch. 2, Atomizdat, Moscow (1975), p. 112.
11. A. I. Voropaev et al., op. cit., No. 25, 69 (1977).

PROCEDURE FOR CALCULATION OF FUEL DEPLETION TO DETERMINE THE PHYSICAL CHARACTERISTICS OF A FAST POWER REACTOR IN THE STEADY-STATE MODE

G. B. Usynin and V. A. Chirkov

UDC 662.039.526

The breeder properties of a fast reactor determine its physical characteristics: the breeding ratio BR, the doubling time T_2, the growth rate ω, the specific load of plutonium into the fuel cycle G, and the specific amount of excess plutonium r [1]. Since these characteristics depend on the instantaneous composition of the fuel, a unified approach to its computation is advisable. One can determine the listed characteristics for a reactor in a constant state (continuous overload conditions; the operational reserve of reactivity is equal to zero). We select for the calculation two different fuel conditions of the operation of a fast reactor: the steady-state fuel mode, in which the composition of the loaded and discharged fuel is constant, and the natural fuel mode, which is a particular case of the steady-state mode in which the composition of the loaded and discharged fuel is identical.

Natural Mode. Let us assume that the reactor is divided into J zones. We write the equations of material balance between the loaded and discharged fuel for the four plutonium isotopes ($^{239-242}$Pu):

$$\sum_{j=1}^{J} \frac{\mu_j}{T_j} \rho'_{i,j}(T_j)(1-\varepsilon_j) = B_i \sum_{j=1}^{J} \frac{\mu_j}{T_j} \rho^0_{i,j}. \quad (1)$$

Here μ_j and T_j are the mass of heavy atoms and the fuel delay time (operating period) in the j-th zone, $\rho^0_{i,j}$ and $\rho_{i,j}$ are the relative concentrations of the i-th isotope in the loaded and discharged fuel, and B_i is a coefficient which is equal to the ratio of the discharge rate of the i-th isotope to its loading rate. In the natural mode B_i for all four isotopes are equal to one another ($B = B_i$); ε_j are the fuel losses from the j-th zone in chemical reprocessing.

We obtain from the solution of the depletion equations [2]

$$\rho_{i,j}(t) = \sum_{k=238}^{242} f_{ik,j}(t)\, \rho^0_{k,j}, \quad (2)$$

Translated from Atomnaya Énergiya, Vol. 48, No. 6, pp. 357-360, June, 1980. Original article submitted August 20, 1979.

0038-531X/80/4806-0356$07.50

TABLE 1. Relative Concentration of Isotopes of the Reference Reactor *

Isotope i	Active zone					Shield		
	ρ_i^0	$\bar{\rho}_i$	ρ_i'	γ_i	$k_i = \frac{\rho_i^0}{\rho_{239}^0}$	ρ_i^0	$\bar{\rho}_i$	ρ_i'
^{238}U	0,8236	0,7768	0,7317	0	—	1	0,9885	0,9772
^{239}Pu	0,1394	0,1297	0,1207	1	1	0	0,0103	0,02
^{240}Pu	0,0305	0,0353	0,0391	0,1014	0,2186	0	$0,0^3147$	0,0004
^{241}Pu	0,0050	0,0058	0,0067	1,7784	0,03612	0	$0,0^53$	$0,0^411$
^{242}Pu	0,0014	0,0016	0,0019	0,1024	0,0100	0	0	0
Fission products	0	0,0509	0,10000	−0,0513	—	0	$0,0^2101$	$0,0^2238$

*A spherical reactor with a uniform reactive zone surround by a reflector. The radius of the active zone $R_{a.z.}$ = 84.196 cm; the thickness of the shield ΔR_S = 45.72 cm; the mass of heavy atoms in the active zone $\mu_{a.z.}$ = 7113 kg and in the shield μ_S = 32015 kg; the operating period of the active zone (at an average specific power of 400 kW/liter) is $T_{a.z.}$ = 727.6 days and of the shield $T_S = 1.38\,T_{a.z.}$ days.

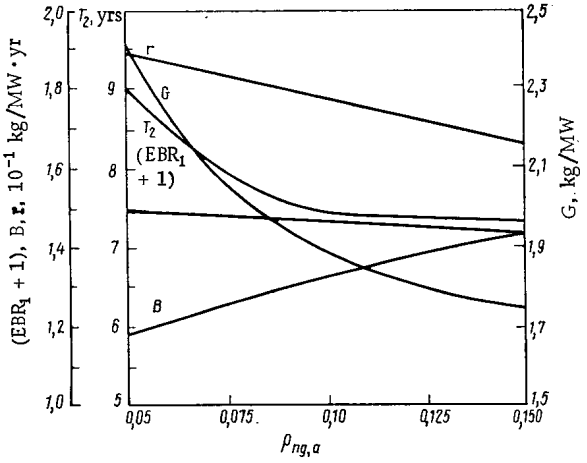

Fig. 1

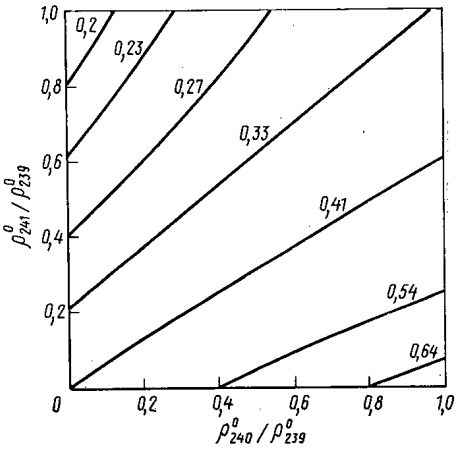

Fig. 2

Fig. 1. Dependence of $(EBR_1 + 1)$, B, r, G, T_2 on the depth of fuel depletion in the active zone of a reactor in the natural mode ($\varepsilon_j = 0$, $\rho'_{239,S} = 0.02$).

Fig. 2. Dependence of the excess breeding ratio EBR_1 on the composition of the plutonium consumed ($\varepsilon_j = 0$, $\rho'_{239,S} = 0.02$, and EBR_1 = const).

where $f_{ik,j}(t)$ are known functions of the cross sections and the time. The time $t = T_j$ for $\rho'_{i,j}(T_j)$ and $\bar{\rho}_{i,j}(T_j) = (1/T_j)\int_0^T \rho_{i,j}(t)\,dt$ is selected on the basis of the established fuel depletion (active zone) or plutonium accumulation (shield).

The criticality equation for the reactor and the conditions of constancy of the mass of heavy atoms in each zone are written in the form

$$\sum_j^J \left[\sum_{i=238}^{242} \mu_j \bar{\rho}_{i,j}\left(\frac{\delta k}{k}\right)_{i,j} + \mu_j \bar{\rho}_{ng,j}\left(\frac{\delta k}{k}\right)_{ng,j}\right] = S_{cr}; \tag{3}$$

$$\sum_{i=238}^{242} \rho^0_{i,j} = 1; \tag{4}$$

$$\sum_{i=238}^{242} \rho'_{i,j} + \rho'_{ng,j} = 1; \quad \sum_{i=238}^{242} \bar{\rho}_{i,j} + \bar{\rho}_{ng,j} = 1, \tag{5}$$

where $(\delta k/k)_{i,j}$ is the reactivity introduced by the i-th isotope into the j-th zone and $\rho'_{ng,j}$ and $\overline{\rho}_{ng,j}$ are the relative concentrations of fission products in the fuel. Since the isotopic composition of the plutonium loaded into the active zones of the reactor is identical, we obtain the following coupling equation:

$$\rho^0_{i,j} = A_j \rho^0_{i,j*}, \tag{6}$$

in which j* is the number of the active zone with respect to which the concentration in any i-th zone of the reactor is determined ($A_{j*} = 1$; $A_j = 0$ in the shields; $A_j \neq 0$ in all subzones of the active zone).

By substituting Eqs. (2) and (6) into (1), (3), and (5), we obtain a nonlinear algebraic system of six equations with six unknowns which is solved as follows. First one does a neutron physics calculation of the base version of the reactor in order to determine the cross sections, $(\delta k/k)$, etc. Then one arbitrarily specifies the values T_j in each zone and solves the system of equations (1), (3), and (5) in the six unknowns B and $\rho^0_{i,j*}$. This system has siz solutions. However, only one of them satisfies the physical sense of the problem. Next one determines $\rho^0_{i,j}$ and $\rho'_{i,j}$, and also the concentration of fission products and plutonium accumulation, compares them with the specified values, corrects the values T_j, and repeats the procedure. When necessary, one calculates a new the neutron physics of the base version.

Calculations have been performed according to the proposed procedure of the physical characteristics of a reference reactor [3]. A multigroup neutron physics calculation has been done according to a one-dimensional program [4] using the BNAB-70 system of constants. The method for calculating $(\delta k/k)_{i,j}$ is taken from [5]. The main expenditures of machine time in calculating the different versions are necessary for the neutron physics calculation of the reactor.

The initial data necessary to determine the physical characteristics of the reactor, which were determined from the following formulas:

$$\mathrm{EBR}_1 = \frac{\sum_{j=1}^{J} \frac{\mu_j}{T_j} \sum_{i=239}^{242} \gamma_i [(1-\varepsilon_j)\rho'_{i,j} - \rho^0_{i,j})]}{\sum_{j=1}^{J} \frac{\mu_j}{T_j} \rho'_{ng,j}}; \tag{7}$$

$$\mathrm{EBR}_2 = \frac{\sum_{j=1}^{J} \sum_{i=239}^{242} \gamma_i [N_c^{i-1} - N^i_{c,f}]_j}{\sum_{j=1}^{J} \sum_{i=238}^{242} (N^i_f)_j}, \tag{8}$$

where $\gamma_i = \sum_{j=1}^{J} \gamma_{i,j}\rho_{i,j}\mu_j / \sum_{j=1}^{J} \rho^0_{i,j}\mu_j$ is the relative cost of the i-th plutonium isotope $\left[\gamma_{i,j} = \left(\frac{\delta k}{k}\right)_{i,j} - \left(\frac{\delta k}{k}\right)_{238,j} / \left(\frac{\delta k}{k}\right)_{239,j} - \left(\frac{\delta k}{k}\right)_{238,j}\right]$; $N^i_{c,j}$ and $N^i_{f,j}$ are the number of captures and fission of the i-th isotope in the j-th zone; and EBR is the excess breeding ratio are given in Table 1.

The reactivity loss upon production of a unit of energy is

$$\frac{1}{k}\frac{dk}{dE} = \sum_{j=1}^{J} \frac{\mu_j}{T_j} \left[\sum_{i=238}^{242} \left(\frac{\delta k}{k}\right)_{i,j} (\rho'_{i,j} - \rho^0_{i,j}) + \left(\frac{\delta k}{k}\right)_{ng,j} \rho'_{ng,j} \right] \Big/ a \sum_{j=1}^{J} \frac{\mu_j}{T_j} \rho'_{ng,j}, \tag{9}$$

where a is the heating power of the fuel.

The doubling time $T_2 = \ln 2/\omega$ was determined from the equation [1]

$$\sum_{j=1}^{J} \frac{\mu_j \rho^0_j}{1-\exp(-\omega T_j/\varphi)} = \sum_{j=1}^{J} \frac{(1-\varepsilon_j)\mu_j \rho'_j}{1-\exp(-\omega T_j/\varphi)} \exp\left[-\omega\left(\frac{T_j}{\varphi} + T_{nj}\right)\right], \tag{10}$$

where T_{nj} is the average processing time of fuel from the j-th zone.

The annual excess amount of plutonium was calculated from the formula

$$r = \frac{1}{W} \sum_{j=1}^{T} \frac{\mu_j}{T_j} \sum_{j=239}^{242} \gamma_i [(1-\varepsilon_j)\rho'_{i,j} - \rho^0_{i,j}] = \frac{\mathrm{EBR}_1}{W} \sum_{j=1}^{J} \frac{\mu_j}{T_j} \rho'_{ng,j} = \frac{(B-1)}{W} \sum_{j=1}^{J} \frac{\mu_j}{T_j} \sum_{i=239}^{242} \gamma_i \rho^0_{i,j}, \tag{11}$$

where W is the reactor power. The specific load into the fuel cycle was found from the equation

$$G=\frac{1}{W}\sum_{j=1}^{J}\left(\mu_j\sum_{i=239}^{242}\gamma_i\bar{\rho}_i+\varphi\frac{\mu_j T_{nj}}{T_j}\sum_{i=239}^{242}\gamma_i\rho_i^0\right). \quad (12)$$

Below are given calculations of the physical characteristics of the reference reactor in the natural mode with $\varphi = 1$, $\varepsilon_j = 0$, and $T_{nj} = 1$ year:

EBR_1	0.463
EBR_2	0.460
$(1/k)(dk/dE)$, $(MW\cdot day)^{-1}$	$\sim(-0.0002')$
T_2, years	7.7
r, kg/(yr·MW)	0.178
G, kg/MW	1.893
B	1.329

The dependence of r, $(EBR_1 + 1)$, B, G, and T_2 on the depth of fuel depletion in the active zone is shown in Fig. 1. These characteristics depend also to a significant extent on the rate of plutonium accumulation in the shield and the losses upon chemical reprocessing, especially in the case of low depletion.

Steady-State Mode. In this case one writes the right-hand side of Eqs. (11) in the form $B_i k_i \sum_j (\mu_j/T_j)\rho^0_{239,j}$, where the coefficients $k_i=\rho_i^0/\rho_{239}^0$ characterize the composition of the loaded plutonium. For the steady-state mode one solves Eqs. (3) and (4) independently of Eqs. (1) with respect to only the two unknowns $\rho^0_{238,1}$ and $\rho^0_{239,j*}$, determines all the remaining concentrations, and corrects the fuel delay times in the zones, after which the operation is repeated. The dependence of EBR_1 on the composition of the plutonium consumed is shown in Fig. 2. As is evident from Fig. 2, an increase in k_{240} and a decrease in k_{241} result in an appreciable increase in the integrated breeding ratio.

We note in conclusion that one can take approximate account of compensating elements within the framework of the proposed method if one takes as the base version of the reactor one having an operational reserve of reactivity $\sim\left(\frac{1}{k}\frac{d\bar{k}}{dE}\right)\frac{E_p}{2}$, where E_p is the specified energy production between regular rechargings.

Conclusions. An effective procedure is proposed for calculation of the loading and discharge rates of fuel as well as its isotopic composition (in the continuous recharging mode), which is necessary for calculation of the physical characteristics of a reactor in the steady-state and natural fuel modes.

The procedure discussed permits determining the physical characteristics of the reactor in the natural mode as well as investigating their dependence on the composition of the fuel consumed.

The proposed algorithm makes possible the calculation of the physical characteristics with an arbitrary dependence of the microcross sections, fluxes, enrichment function, and other parameters over reactor volume and the optimization of reactors with a different heterogeneous structure.

The effectiveness of the procedure is achieved owing to the possibility of reducing a distributed problem (with an arbitrary number of partition zones) to a point one (with one zone).

LITERATURE CITED

1. V. S. Kagramanyan et al., At. Energ., 46, No. 4, 236 (1979).
2. G. B. Usynin, At. Energ., 25, No. 6, 466 (1968).
3. A. Baker et al., in: Proc. Symp. on Calculation for a Large Fast Reactor, TRG Rep. 2133 (R), Risley (1971).
4. A. I. Novozhilov et al., Kernenergie, 11, 329 (1975).
5. V. V. Orlov et al., ibid., 5, 112 (1969).

POWER DISTRIBUTION MONITORING AND CONTROL FOR A RBMK REACTOR

I. Ya. Emel'yanov, V. V. Postnikov, and Yu. I. Volod'ko

UDC 621.039.562

The RBMK reactors have involved various difficult problems in control of core processes, particularly in the monitoring and control of the power distribution. Reliable power-distribution control for reactors of this type is complicated by various factors: the high unit power and large size of the reactor, the xenon instability occurring in such reactors, the large number of monitoring points and control devices, which constitute a considerable load of the operator, the complicated microstructure of the power distribution, which is due to the large number of additional absorbers in the initial working period, and to the large numbers of adjacent fresh and partly worn out fuel-pin assemblies in the steady-state, in addition to the spatial instability due to the void, temperature, and other reactivity coefficients [1], and the complexity in monitoring the power distribution by heat-engineering methods in channels with a boiling coolant.

Some of these factors become more important to the structure of the control system for a reactor of any type as the size and unit power increase or as the specifications for automatic control are tightened.

The monitoring and control system for the RBMK-1000 includes three basic systems each having highly independent operation: the control and protection system CPS, the system for physical monitoring of the power distribution CPMPD and the Skala centralized monitoring system CMS. We consider the main functions and features of each system, with particular attention to the noval features of the structure and novel features of the structure and novel items of equipment.

The CPS [2] operates from lateral ionization chambers LIC. In the upgraded form, the CPS is supplemented with local automatic control LAC subsystems and local emergency protection LEP systems, in which triaxial fission chambers are used as the detectors [3].

The CPS is based to a certain extent on designs traditional for large uranium–graphite reactors and provides for monitoring of the power and reactor period together with automatic maintenance of the reactor power in the range 0.1-100%, as well as automatic emergency protection if the power level or rate of power increase exceed set limits, automatic emergency reactor protection from deviations in the power distribution at the periphery of the core corresponding to the first radial-azimuthal harmonics, monitoring of the relative power distribution at the periphery of the reactor, and manual control of the positions of the absorbing rods.

The lateral ionization chambers are placed in the reflector (four chambers) and behind the reflector (24 chambers), while there are 42 chambers within the reactor, whose positions are shown in the figure. The effectors in the control and protection system are absorbing rods of three types, which are placed in 179 special zirconium channels and are cooled by water, including the manual control rods MC, which number 146, the automatic control rods AC for the average reactor power, which number 12, and the short absorbing rods SAR, which number 21. Fifty-seven rods in the manual control system are used as emergency-protection rods and are withdrawn from the core during operation. The height distribution of the power is controlled by withdrawing the MC and AC rods upwards, while the SAR rods, which have absorbing parts of half the length, are withdrawn downwards.

The LAC system is designed for automatic control of reactor power and to stabilize the power distribution [4]. When the reactor works with LAC, one of the AC must be in the hot backup state. Switching from LAC to AC or vice versa is performed manually, or automatically, by means of the sevel effector organs for the LAC, which are analogous to the MC effectors, and the 42 LAC and LEP chambers are uniformly distributed over the core (Fig. 1). Each LAC rod is surrounded by two LEP chambers and four LAC chambers. The averaged corrected signal from the four LAC chambers is used to control the rod.

The SPMPD consists of two independent subsystems for monitoring the power distribution over the radius (SPMPDR) and the height (SPMPDH). Both systems work from the internal detectors ID that monitor

Translated from Atomnaya Énergiya, Vol. 48, No. 6, pp. 360-365, June, 1980. Original article submitted May 14, 1979.

0038-531X/80/4806-0360$07.50

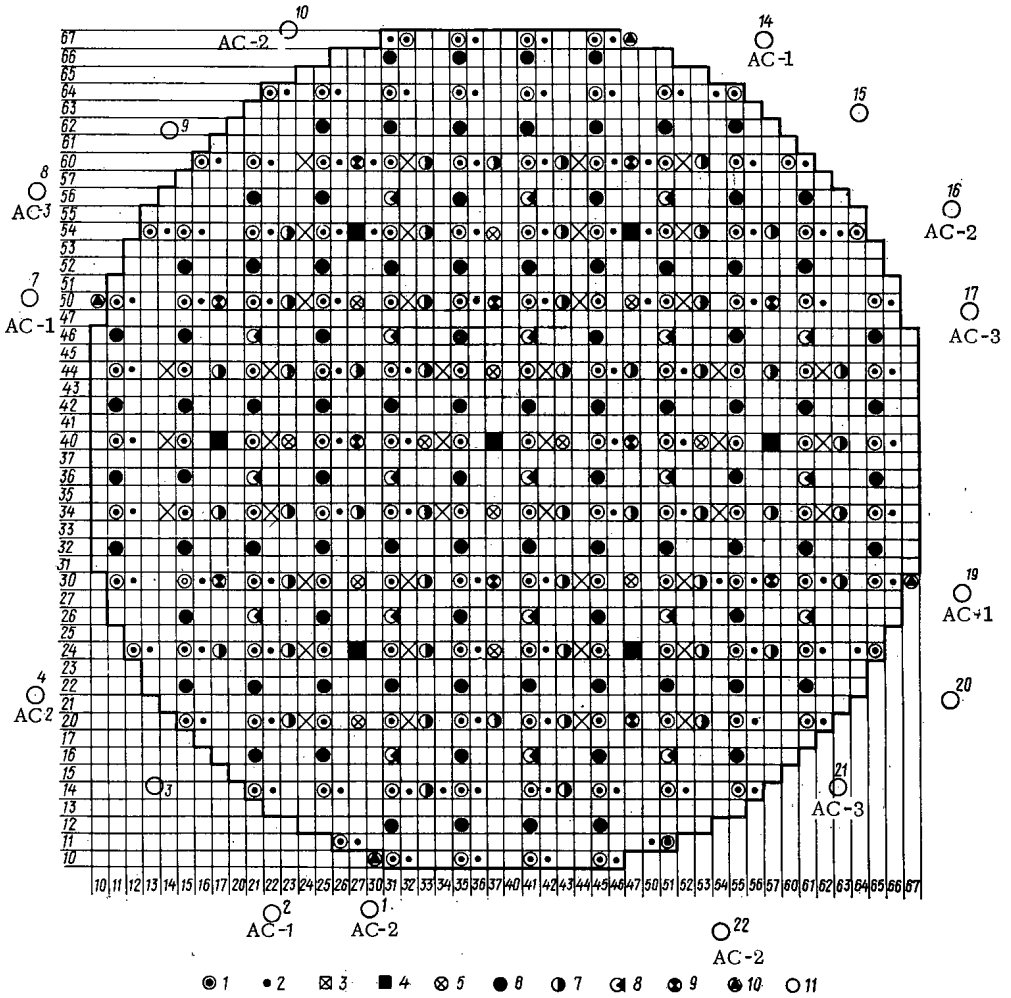

Fig. 1. Location of the control rods and ionization chambers of the CPS and of the SPMPD detectors in the RBMK-1000: 1) DMER; 2) channel for calibration γ chamber; 3) detector for the LAC and LEP systems; 4) LAC and LEP rods; 5) AC rod; 6) MC rod; 7) emergency-protection rod; 8) short absorbing rod; 9) DMEH; 10) fission chamber; 11) lateral ionization chamber (outside a reflector).

the radial power distribution DMER and the height distribution DMEH, which provide preprocessing of the signals, transmission to the computer, comparison of the signals with given levels, and generation of auidable and visible signals if the detector signals go outside set limits. The SPMPDR receives the signals from 130 DMER chambers placed in the fuel-pin assemblies, while the SPMPDH receives signals from 84 DMEH chambers placed at sevel points along the height in 12 of the DMEH channels.

The number and location of the ID were chosen on the basis that the permissible power in a fuel-pin assembly should only be slightly dependent on the power distribution over the height of a channel (up to axial nonuniformity coefficients of 1.7-2.0) and is determined in the main by the flow rate, pressure, and temperature of the water at the inlet to the pin assembly. Therefore, the SPMPDR provides the basic internal monitoring in the RBMK-1000; the DMEH chambers are intended in the main for monitoring the stability of the height distribution and to prevent excessive linear load on the fuel-pin assemblies in anomalous situations. The number and disposition of the DMER chambers are determined by the required monitoring and control accuracy. The mean-square error in discrete monitoring of fuel-pin power at the maximum distance from the DMER chambers is about 2% for the pitch chosen for the DMER lattice, which is much less than the errors required to produce an appreciable deterioration in the determination of the margin from the critical power in the fuel-rod assembly. Therefore, the DMER lattice has some redundancy as regards the necessary monitoring accuracy. The design is also intended to protect the fuel-pin assemblies from erroneous extraction of any individual automatic-control rod, where each control rod should be operated with at least one internal detector. There are seven DMEH chambers uniformly distributed over the height because of the specification for monitoring the first four axial harmonics even when two detectors in one channel fail.

The DMER detectors resemble the LAC and LEP detectors in lying in the central dry sleeves of the fuel-pin assembly, each of which is of the same design; a DMER chamber consists of a sensitive element filled with argon in a sealed body of corrosion-resistant steel together with a sealed high-temperature socket and a coupling line. The maximum working temperature of the sensing element in the DMER system is 350°C; an emission detector with a silver emitter is used. This detector is a radiation-resistant and heat-resistant coaxial cable made by a normal manufacturing technique used for high-temperature cables with mineral insulation.

During the design of the SPMPD for the RBMK-1000, the choice of sensing element for the power-distribution monitors was essentially restricted to emission detectors with emitters composed of rhodium and silver. Such detectors with silver emitters are rather faster in response [5], which is due to the shorter half-life of the silver radioisotopes, as well as to more favorable β-particle energy, which means that there is only a 13% contribution or less to the detector current from the component with half-life of 2.4 min, while there is practically no contribution from the component with half-life 259 days. Also, a silver emitter has a lower rate of burn-up (19% per year as against 34% per year for rhodium for a neutron flux density of 10^{14} neutrons/cm^2 · sec), together with a much lower dependence of the sensitivity on the neutron gas temperature. Further, a cable with a silver core is easier to manufacture and more reliable, which is extremely important for routine production and operation.

The working life of the DMER is not less than the working life of a fuel-pin assembly (3-4 years). Operating results led to some minor changes in the detector, which amounts mainly to simplification and replacement of some of the soldered joints by welded ones. It was found that the period of a fault-free operation for such a detector working with air in the central tube of the fuel-pin assembly at about 300°C (with the body removed) was much less than that in argon, which is the filling used for the standard DMER, since the working life was then only one year.

The seven DMEH are located in a dry sealed sleeve filled with a mixture of argon and helium. The sleeve is set up in a channel analogous to the CPS channels and is cooled with water having an outlet temperature of up to 75°C. The sensitive element in a DMEH is the same as in the DMER and is a cylindrical spiral of length 2.6 m. Periodic checks are provided by a tube having an internal cavity isolated from the volume of the sleeve placed along the axis. The DMER and DMEH can be replaced, along with the LAC and LEP chambers, with the reactor working. The maximum currents in the DMER and DMEH at the normal reactor power are about 15 μA.

It is necessary to maintain a reasonably high insulation resistance R_{in} in the detectors, since R_{in} has a direct effect on the current formation in the detector and thus on the accuracy [6]. The insulation resistance varies only slightly during the working life and constitutes 10^8-10^{10} Ω with the reactor shut down for 90-95% of the detectors or 10^7-10^8 Ω with a reactor power of 25-100% of nominal. If R_{in} falls below $5 \cdot 10^5$ Ω, there is a spontaneous change in the sensitivity of more than 10% that is unrelated to the input impedance of the secondary apparatus, which is less than 100 Ω. The DMER and DMEH are checked mainly by scanning the fuel-pin assemblies adjacent to the DMER as well as the central sleeves of the DMEH with the reactor working by means of small triaxial fission chambers.

The secondary electronic equipment in the SPMPDR differs from the apparatus in other such systems mainly in that it combines the functions of monitoring the power distribution and producing signals when permitted levels are exceeded with the function of monitoring the relative power distribution, which includes outputting information on deviations from the specified distribution. The relative power distribution is monitored by comparing the reference levels and corresponding signals for each of the DMER as normalized to the total signal from the DMER. A display in front of the operator presents signals when the reference levels are exceeded by more than 5 and 10% and when the levels fall by more than 10%. The normalization reduces the error of the system arising from the lag in the DMER during fast changes in reactor power, while the information displayed to the operator on the form of the power distribution is unaltered as the power changes. The operator can estimate the deviations from the specified relative power distribution by altering the reference levels in the relative monitoring channel over the range ± 15%. The total-current recorder for the DMER is the main instrument for monitoring the reactor power.

The secondary electronic equipment in the SPMPDH also combines the functions of absolute and relative monitoring of the power distribution. The structure of this system differs from that of the previous one only in that the signal from each DMEH is normalized to the total current of the seven DMEH in one channel, not to the total current of all detectors.

The SPMPD provides monitoring of the power distribution in the range from 10 to 100% of the nominal power as well as monitoring of the thermal power of the reactor in the range from 5 to 100%.

The Skala central monitoring system [7] is based on a V-3M computer and provides monitoring, processing, display, and recording of most of the engineering parameters of the reactor and of the power station as a whole. The signals from the central system are processed by the PRIZMA program, which calculates the power for all the fuel-pin assemblies, the limiting permissible power for each fuel-pin assembly corresponding to a given probability of crisis-free operation in the assembly, the reserve-power coefficient K_r relative to the limiting acceptable power for each fuel-pin assembly and the same for the reactor as a whole, calculation of the steam content in each fuel-pin assembly, the power production by each assembly and by the reactor as a whole, the reactivity margins, the burn-up in the DMER and DMEH, the recommended water flow rates through the fuel-pin assemblies, the reference and maximal signal levels for the DMER and DMEH, the amplitudes of the axial harmonics representing height deviations in the energy distribution at the points bearing the DMEH assemblies, overall reactor parameters (reactor power indicated by the SPMPD and the heat-engineering instruments, nonuniformity coefficients for the power distribution, total power and flow rate in individual parts of the reactor), the recommended displacements for the control and protection system rods, etc. PRIZMA also performs the diagnostic processing for certain forms of reactor equipment and also accumulates data on the peripherals for subsequent statistical analysis, while providing cyclic recording of data for analysis of emergency situations. Any cell in which the calculated or measured parameter (K_r, fuel-pin assembly power, water flow rate, etc.) differs from the specified one is displayed to the operator. The results are printed out as patterns with indication of the type of each channel (fuel-pin assembly, MC, SAR, AC, DMER, etc.) together with the parameters channel by channel: water flow rate, steam content, position of CPS rod. The pattern is accompanied by a brief summary of the general reactor parameters and a list of the 6-10 most highly stressed fuel-pin assemblies with the maximum power and minimum K_r. The calculations are performed in 5-8 min.

The software for the operation of the RBMK is designed to overcome the complexity or impossibility of direct monitoring of many parameters, including ones related to safe operation of the core. These parameters are monitored indirectly by calculations in the Skala system on the basis of results from more complex calculations performed by an external BÉSM-6 computer. The data exchange between the BÉSM-6 and the central monitoring system for the RBMK-1000 at Kursk and Chernobyl nuclear power stations is performed automatically by means of Akkord 1200M interfaces. The software for operating the RBMK-1000 includes the following: PRIZMA for the in-station computer, BOKRUS for periodic physical calculations on the BÉSM-6 giving the opimum power distribution and the positions of the control rods, BOKR, LEN, and KVARTs for BÉSM-6 processing of the measurements involved in checking the DMER, and ANALOG for periodic checking of the PRIZMA with the BÉSM-6.

The profiles for the distributions of parameters such as the fuel-pin power, the channel water flow rates, and the reference levels in the SPMPD substantially influence the safety and economy of the RBMK. A parameter that is to be used in optimizing any of the parameters of the reactor in design and operation is obviously the referred cost η per kWh subject to the various constraints imposed primarily by the requirements of power station safety. In individual instances where most of the parameters have been specified, it is permissible to optimize a single parameter that influences η. For example, in defining the mutual distributions of the power distribution and flow rates, one uses the maximum probability of crisis-free operation in the core for the RBMK-1000. The basic input data are here the specified macroscopic distribution for the power production over the radius, which influences the limiting permissible reactor power, and the specific power production in the fuel, together with the dynamic stability in the power distribution and the reactivity balance. The specified macroscopic power distribution is determined from optimization calculations on the external computer for each enlarged state of operation.

The sequence for controlling the power distribution in the RBMK-1000 includes observation on the power distribution from the SPMPD signals, the display, and the printout patterns from the special monitor, together with the parameters related to the power distribution (distribution of K_r, distribution of the water flow rates, and general loop engineering parameters), which may involve outputting recommendations on changing the water flow rates, the reference levels in the SPMPD, the positions of the correctors for the CPS chambers, all of which employ recommendations from the central monitoring system. Further, there may be actions involving direct control of the power distribution by displacement of the control rods and by altering the levels of the AC or LAC transducers, together with changes in the modes of operation of the monitoring and control systems (switching of the AC and LAC, calls for recording SPMPD signals, the calling of central monitor system data, etc.). The number of manual operations involving the CPS rod is reduced in stationary state by factors of

2-5 by transforming from automatic control to local automatic control. If power overload occurs in a fuel-pin assembly, the power distribution can be regulated with or without the LAC, and the work of the operator is simplified in the first case. Each reloading operation for a fuel-pin assembly is preceded by adjustment of the flow rate in the reloading region. Manual control of the power distribution is provided by alternate operation of the manual controls and the SAR, which eliminates general reactor or local deviations in radius and height.

The monitoring and control systems thus constitute a hierarchic structure with virtually independent base subsystems, which are combined as regards monitoring functions by means of the central monitoring system, which lies at the top. Such structures provide high reliability and viability in the entire system, but they impose a considerable load on the operator and other staff, who are involved in ensuring consistent operation of the individual low-level systems via manual control of the power distribution and so on.

It has become necessary to improve the control systems for the power distribution in the RBMK reactors, and the following factors are involved:

1) increasing the specific thermal loads on the fuel and other parts of the core, with substantial increase in the number of monitoring points and number of control units for the next generation of RBMK (RBMK-1500 and RBMKP-2400);

2) the ongoing tightening of specifications for reactor safety and reliability in nuclear power station equipment;

3) the need to reduce the load on the operator and to improve the economy of the power station; and

4) the need for the power station to operate in load-tracking modes.

Experience with the RBMK-1000 has given rise to practical proposals for improving these reactors; in order to improve the power-distribution control systems, it will be necessary to make further use of computers in the light of the above factors. Extension of the sphere of the computers in control involves new problems, particularly safety aspects. It is necessary to define the correct combination of analog independent systems with systems based on standard computers. One possible approach is a combined monitoring and control system that includes the CPS traditional for the RBMK-1000 that works with the lateral ionization chambers, together with a system for monitoring and controlling the power distribution (SMPD) employing analog instruments working with the 252 radial and 80 height internal detectors and providing local protection against major deviations from the specified margins for avoiding crisis and linear heat loading in the fuel-pin assemblies, together with transmission of the normalized signals from the internal detectors to the analog local automatic controls and computer, and finally a control computing system consisting of several subsystems each with its own computer and a higher-level computer, or else one in which each subsystem employs several computers.

Such a system will have a hierarchic structure, and the first level contains analog systems (CPS and SMPD), which normalize and transmit detector signals to the second-level systems, which employ computers and which process the data to present information to the operator while providing automatic management of the energy distribution (via the CPS), as well as diagnosis of equipment states and local emergency protection on the basis of current crisis margins and heat loads on the fuel-pin assemblies. At the third level there is a high-power computer that performs complicated physical and optimization calculations and which provides coupling to the external computer in the power system.

The independent digital protection subsystem in the second level calculates the maximum permissible signals from the internal detectors and compares these with the current signals, which provides a digital protection function, while the CPS and SMPD provide analog protection. The control functions of the CPS and SMPD back up the analog functions executed by the control computing system. The DMER are provided by fast emission detectors of cable type, in which the emitter contains hafnium, while the DMEH are assemblies of two triaxial gamma chambers. Each of the 20 channels used in height monitoring employs dry sleeves cooled by water in the CPS loop, and four such assemblies are set up in each channel. A characteristic feature of the system is that it provides local automatic emergency protection of the reactor from erroneous removal of any control rod. The system is designed for completely automatic control of the power distribution under stationary and transient conditions.

Future improvement of the automatic facilities and computer backup for power stations with RBMK should not be accompanied by an increase in the amount of information output to the operator, but instead should involve automating control and output of information to the operator only of essential data indicating

anomalous situations not envisaged in the monitoring and control algorithms. The operator should be protected from redundant routine information in order to be able to concentrate attention on the basic factors that determine the safety and efficiency of the reactor.

LITERATURE CITED

1. A. P. Aleksandrov and N. A. Dollezhal', At. Energ., 43, No. 5, 337 (1977).
2. I. Ya. Emel'yanov, in: Nuclear Science and Engineering: Reactor Physics and Engineering Series, Issue 1(21) [in Russian], TsNIIatominform, Moscow (1978), p. 36.
3. I. Ya. Emel'yanov et al., At. Energ., 43, No. 1, 44 (1977).
4. I. Ya. Emel'yanov et al., in: Nuclear Science and Engineering: Reactor Physics and Engineering Series, Issue 1(5) [in Russian], TsNIIatominform, Moscow (1979), p. 3.
5. I. Ya. Emel'yanov et al., At. Energ., 34, No. 3, 203 (1973).
6. I. Ya. Emel'yanov et al., ibid., 37, No. 1, 72 (1974).
7. V. I. Adas'ko et al., "Systems for monitoring and controlling engineering processes in nuclear power stations by means of control computers," International Electrotechnical Congress, Moscow, June 1977, Section 7 [in Russian].

ANALYSIS OF THERMOHYDRAULIC STABILITY IN CHANNELS OF A BOILING REACTOR

V. N. Smolin, S. V. Shpanskii,
V. I. Esikov, T. K. Sedova,
and V. P. Shishov

UDC 532.5.529

Thermohydraulic stability of the operating conditions in parallel steam-generating channels is one of the factors which ensures the reliability of cooling of the fuel elements of nuclear reactors. The problem of determining the limit of thermohydraulic stability was first formulated and solved at the contemporary level in the research of Morozov [1]. The stability of a one-dimensional time-dependent model of flow in a channel incorporating the linearized equations of thermohydraulics with empirical relations closing them was investigated in his research. Some theoretical questions associated with the application of such an approach to complex systems have been discussed by Molochnikov [2].

A program for calculating the limit of thermohydraulic stability by the D-partition method was proposed in [3] which is based on the algorithm of [1]. However, the program of [3] permits calculating only a vertical channel of constant cross section without local drag in intermediate cross sections. The evaporative channels of boiling reactors constitute a complex system of sections of various transfer cross sections. They can include sections with various slopes and have local drag along the channel length. Therefore, the problem of practical implementation of the method of calculating stability in flexible and efficiently running computer programs has still not been definitely solved.

We will discuss the system of equations of the thermohydraulics of a one-dimensional fluid flow which includes the continuity, momentum, and energy equations, which have the following form for a channel of constant cross section without local drag (without the kinetic energy and pressure energy taken into account):

$$\left.\begin{aligned} &f\frac{\partial\rho}{\partial\tau}+\frac{\partial G}{\partial z}=0;\\ &\frac{\partial G}{\partial\tau}+\frac{1}{f}\frac{\partial}{\partial z}(G^2v)+f\frac{\partial p}{\partial z}=-g\rho f\sin\theta-\\ &\qquad -\Pi^{\circ}T^{\circ}-\Pi^{i}T^{i};\\ &f\frac{\partial I}{\partial\tau}+\frac{\partial}{\partial z}(Gi)=\Pi^{\circ}q^{\circ}+\Pi^{i}q^{i}. \end{aligned}\right\} \tag{1}$$

It is taken into consideration here that the wetted perimeter of the channel may consist in the general case of two surfaces – an "outer" one (the surface of the channel lining) and an "inner" one (the surface of the rods).

For a steady flow, system (1) takes the form:

$$\left.\begin{aligned} &G(z)=G(0);\\ &i(z)=i(0)+\frac{1}{G_0}\int_0^z(\Pi^{\circ}q^{\circ}+\Pi^{i}q^{i})\,dz;\\ &p(z)=p(0)+\frac{G^2}{f^2}[v(z)-v(0)]+g\sin\theta\int_0^z\rho\,dz+\\ &\qquad +\frac{1}{f_0}\int_0^z(\Pi^{\circ}T^{\circ}+\Pi^{i}T^{i})\,dz. \end{aligned}\right\} \tag{2}$$

After linearization, a Laplace transformation, and reduction to canonical form, system (1) for small deviations (variations) of the operating parameters is converted into a system of ordinary differential equations whose vector form is

Translated from Atomnaya Énergiya, Vol. 48, No. 6, pp. 366-369, June, 1980. Original article submitted July 23, 1979.

0038-531X/80/4806-0366$07.50

$$dX/dz = AX, \tag{3}$$

where X is a vector whose components are the Laplace-transformed variations of the flow rate, pressure, and enthalpy:

$$X(s, z) = \begin{pmatrix} \widetilde{G}(s, z) \\ \widetilde{p}(s, z) \\ \widetilde{i}(s, z) \end{pmatrix}. \tag{4}$$

The boundary-value problem in which the vector of the boundary conditions is

$$\Gamma = \begin{pmatrix} \widetilde{i}(s, 0) \\ \widetilde{p}(s, 0) \\ \widetilde{p}(s, H) \end{pmatrix}$$

is discussed for system (3).

Any solution of system (3) has the form

$$X(s, z) = \Phi(s, z) X(s, 0), \tag{5}$$

where $\Phi(s, z)$ is the fundamental matrix of system (3) normalized at z = 0, whose columns are linearly independent solutions of the system (3):

$$\Phi(s, z) = \begin{pmatrix} \widetilde{G}_1(s, z) & \widetilde{G}_2(s, z) & \widetilde{G}_3(s, z) \\ \widetilde{p}_1(s, z) & \widetilde{p}_2(s, z) & \widetilde{p}_3(s, z) \\ \widetilde{i}_1(s, z) & \widetilde{i}_2(s, z) & \widetilde{i}_3(s, z) \end{pmatrix}.$$

The vector of the boundary conditions is associated with the conditions at the entrance by the relationship

$$\Gamma = F(s) X(s, 0), \tag{6}$$

where the matrix F(s) has the form

$$F(s) = \begin{pmatrix} 0 & 1 & 0 \\ \widetilde{p}_1(s, H) & \widetilde{p}_2(s, H) & \widetilde{p}_3(s, H) \\ & 0 & 1 \end{pmatrix}. \tag{7}$$

Using Eqs. (5) and (6), we obtain an equation which relates the solution of system (3) to the vector of the boundary conditions, viz.,

$$F(s) \Phi^{-1}(s, z) X(s, z) = \Gamma.$$

One can write the characteristic equation whose roots determine the behavior of solution (4) in the form

$$\det F(s) = 0 \tag{8}$$

with the properties of the fundamental matrix taken into account.

By substituting Eq. (7) into Eq. (8) and expanding the determinant, we obtain the characteristic equation

$$p_1(s, H) = 0. \tag{9}$$

Thus, there is no need to find the fundamental matrix in order to analyze the stability of system (3), but it is sufficient to find a solution with the initial conditions: $\widetilde{G}(s, 0) = 1$, $\widetilde{p}(s, 0) = 0$, and $\widetilde{i}(s, 0) = 0$.

This conclusion is valid for a channel with local drag along its length or with variation in its cross section. In this case the characteristic equation is of form (9). The channel is treated as a series of smooth sections with constant cross section whose boundaries are cross sections with local drag or variation or cross section. The splicing of the solutions at the boundary of sections is accomplished on the basis of a well-known relation for the pressure losses by local drag, which is considered as quasisteady, with the introduction of a term which takes account of the pressure difference due to variation of cross section:

$$\Delta p(z_d) = \left(\xi_d + \frac{f^2(z_d - 0)}{f^2(z_d + 0)} - 1\right) \frac{G^2 v}{2 f^2(z_d - 0)}.$$

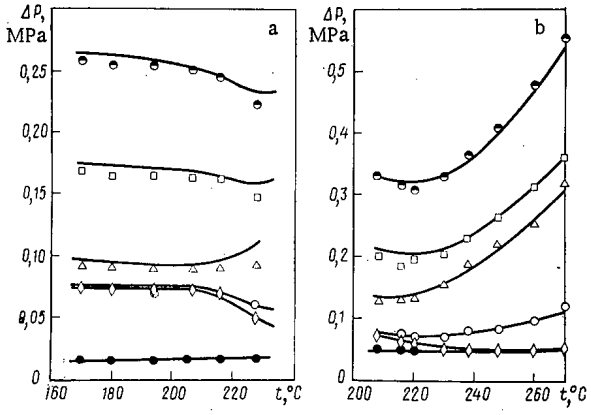

Fig. 1

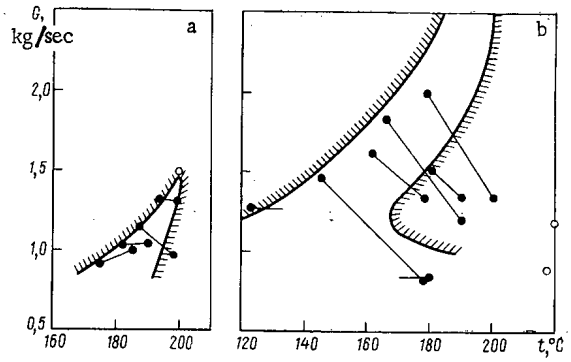

Fig. 2

Fig. 1. Comparison of the experimental and calculated thermohydraulic characteristics of a model of the circuit of a channel of the RBMK-1500 reactor (a) at a pressure of 4.8 MPa and a power of 265 kW and (b) at a pressure of 6.87 MPa and a power of 614 kW: ◓) circuit, □) channel, △) zone of heat generation, ◇) exit section of the channel, ○) steam–water communication, and ●) water communication.

Fig. 2. Comparison of experimental data with the calculated stability limit at a pressure of 3.0 MPa and (a) a power of 260 kW and (b) 615 kW: ○) pulsation-free conditions, ●) region of pulsation conditions.

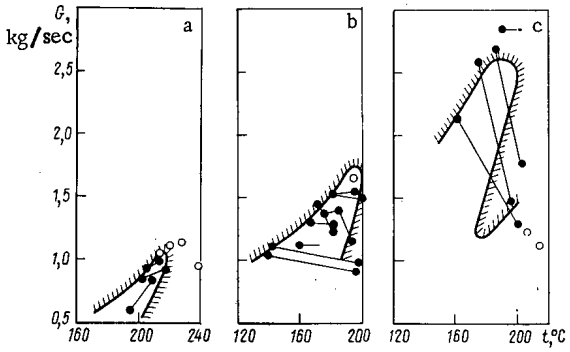

Fig. 3

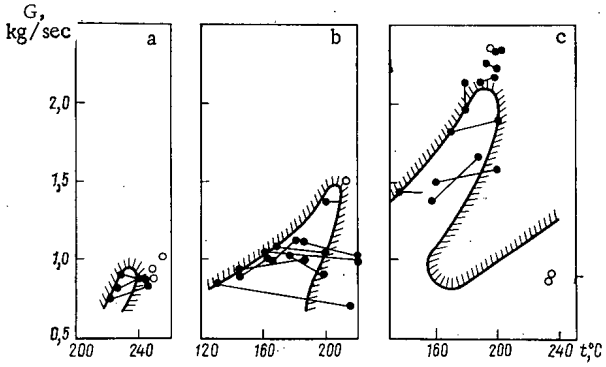

Fig. 4

Fig. 3. Comparison of the experimental data with the calculated stability limit at a pressure of 5.0 MPa and (a) a power of 265 kW, (b) 620 kW, and (c) 1000 kW. The symbols are the same as in Fig. 2.

Fig. 4. Comparison of experimental data with the calculated stability limit at a pressure of 7.0 MPa and (a) a power of 260 kW, (b) 625 kW, and (c) 1015 kW. The symbols are the same as in Fig. 2.

It is assumed that the flow rate and the enthalpy do not vary due to local drag. These conditions lead after linearization and Laplace transformation to the splicing equation in cross section z_d:

$$X(s,\ z_d+0) = F_d X(s,\ z_d-0),$$

where the matrix F_d has the form

$$F_d = \begin{pmatrix} 1 & 0 & 0 \\ K_G & 1 & K_i \\ 0 & 0 & 1 \end{pmatrix};$$

$$K_G = \frac{G}{2f^2(z_d - 0)}\left(\frac{f^2(z_d - 0)}{f^2(z_d + 0)} - 1 + \xi_d\right)\left(2v + G\frac{\partial v}{\partial G}\right);$$

$$K_i = \frac{G^2}{2f^2(z_d - 0)}\frac{\partial v}{\partial i}\left(\frac{f^2(z_d - 0)}{f^2(z_d + 0)} + \xi_d\right).$$

In order to close this system of thermohydraulic equations, a number of empirical relations are used which are considered as quasisteady. The hydraulic friction is taken into account on the basis of the formula

$$\Delta p_f = K_{\partial\Phi}\lambda\frac{\Delta z}{d_h}\frac{G^2 v}{2f^2},$$

from which we obtain

$$T^o\Pi^o + T^i\Pi^i = K_{\partial\Phi}\frac{G^2 v}{8f^2}(\lambda^o\Pi^o + \lambda^i\Pi^i).$$

The coefficient of hydraulic friction of a single-phase flow is determined from the formula [4]

$$\lambda = 0.1\left(1.46\Delta + \frac{100}{\mathrm{Re}}\right)^{0.25}.$$

The coefficient which takes account of the difference between the friction of a two-phase flow and that of a single-phase flow is found from the equation

$$K_{\partial\Phi} = 1 + 3\varphi(1 - \varphi^2)\left(\sqrt[4]{\frac{221.15}{p}} - 1\right).$$

The form of the relation is obtained by analysis of the data of [5], and the numerical coefficient "3" is selected according to the results of a determination of the hydraulic characteristics of a model of an RBMK-1500 channel [6].

We take heat exchange with the walls into account approximately by the formula

$$q = q_{hg} - b_w C_w \rho_w \frac{dt_w}{d\tau},$$

where q_{hg} is the thermal flux due to heat generation which is constant in time and b_w is the geometrical characteristic of the channel wall (the ratio of the area of the transverse cross section of the wall to the perimeter of the heat exchange). The wall temperature for a single-phase flow is calculated with the help of the formula

$$\mathrm{Nu} = 0.023\mathrm{Re}^{0.8}\mathrm{Pr}^{0.4}.$$

The procedure has been adopted for calculating the steam content of a two-phase flow which is proposed in [7] and modified in [8], which includes the equation given below for the start of boiling, shear, and enthalpy of the liquid phase. The enthalpy of the start of intense surface boiling has been adopted as the limit of a two-phase flow viz.,

$$i_{sb} = i' - 7.5\frac{qf}{G}\left(\frac{qd_h}{r\rho''\nu'}\right)^{0.08}\left(\frac{4G}{\Pi\mu'}\right)^{0.2}.$$

We determine shear of the phases from the formula

$$s = 1 + \frac{\left(1.062 + 2.654/\left(1 + \frac{1-x}{x}\frac{v_l}{v''}\right)^2\right)d_h^{0.25}}{\sqrt{G/fv_l}}\left(1 - \frac{p}{221.15}\right).$$

The enthalpy of the liquid phase is calculated from the equation

$$i_l = i' - (i + i' - 2i_{sb})\exp\left(-2\frac{i - i_{sb}}{i' - i_{sb}}\right).$$

We find the true mass and volume steam content from the formulas

$$x = \frac{i - i_l}{i'' - i_l},$$

$$\varphi = 1\Big/\left(1 + \frac{1-x}{x}s\frac{v_l}{v''}\right).$$

The roots of Eq. (9) are analyzed by the D-partition method; the boundary of the regions of existence of different numbers of roots with a positive real part is found by specifying the purely imaginary values of the

Laplace transformation parameter $s = j\omega$ and it is checked whether or not the operating point belongs to a region which does not contain a single root with a positive real part.

As has been shown in [1], it is possible in the majority of practical cases to neglect the effect of a pressure variation on the remaining parameters. Then the continuity and energy equations in the system (3) are independent of the momentum equation, and after transformation for purely imaginary values $s = j\omega$ they take the form:

$$\left.\begin{aligned}
\frac{dG_R}{dz} &= A_1 G_1 + A_2 i_I;\\
\frac{dG_I}{dz} &= A_1 G_R - A_2 i_R;\\
\frac{di_R}{dz} &= A_3 G_R + A_4 G_I + A_5 i_R + A_6 i_I;\\
\frac{di_I}{dz} &= -A_4 G_R + A_3 G_I - A_6 i_R + A_5 i_I.
\end{aligned}\right\} \tag{10}$$

The integrated momentum equation for a smooth section of the channel takes the form

$$\Delta p_R = -\frac{\omega}{f}\int_{z_{st}}^{z_{end}} G_I\,dz + \int_{z_{st}}^{z_{end}} (A_7 G_R + A_8 i_R)\,dz + \tag{11}$$

$$+ B_1(z_{end})\,G_R(z_{end}) - B_1(z_{st})\,G_R(z_{st}) + B_2(z_{end})\,i_R(z_{end}) - B_2(z_{st})\,i_R(z_{st});$$

$$\Delta p_I = \frac{\omega}{f}\int_{z_{st}}^{z_{end}} G_R\,dz + \int_{z_{st}}^{z_{end}} (A_7 G_I + A_8 i_I)\,dz + \tag{12}$$

$$+ B_1(z_{end})\,G_I(z_{end}) - B_1(z_{st})\,G_I(z_{st}) + B_2(z_{end})\,i_I(z_{end}) - B_2(z_{st})\,i_I(z_{st}).$$

System (10) is solved with the initial conditions

$$\left.\begin{aligned}
&G_R(0) = 1\\
&G_I(0) = i_R(0) = i_I(0) = 0
\end{aligned}\right\}. \tag{13}$$

The integrated momentum equation takes the simple form

$$\Delta p_R = \frac{\Delta z G \Pi}{8 f^3 \rho}\left(2\lambda + \mathrm{Re}\,\frac{\partial\lambda}{\partial\,\mathrm{Re}}\right) G_R(0);$$

$$\Delta p_I = \frac{\Delta z \omega}{f} G_R(0)$$

for an input heated smooth section.

The complex plane $\tilde{p}_1(s, H)$, on which the D-partition curve $\tilde{p}_1(j\omega, H) = p_R(\omega, H) + jp_I(\omega, H)$ is constructed, is selected as the D-partition plane. The values of $p_R(\omega, H)$ and $p_I(\omega, H)$ are determined from Eqs. (11) and (12), in which the solutions of the system (10) with the initial conditions (13) are used. The "operating point" on the D-partition plane is the origin of coordinates $p_R = 0$ and $p_I = 0$. Thus, the system is stable if the curve $\tilde{p}_1(j\omega, H)$ intersects the p_R axis in the positive region.

The outlined procedure for calculating stability has been implemented in the computer program CAHS (calculation of hydrodynamic stability). The program is written in ALGOL for a BÉSM-6 computer and permits calculating the limit of both aperiodic and oscillatory instability of a steam-generating channel consisting of sections of different geometry and having local drag in arbitrary cross sections. The program CAHS has been tested by comparing the computational results from the program with experimental data on stability limits in a model of the circuit of a channel of the RBMK-1500 reactor [6].

The model of the circuit consisted of water communication at the input into a channel of length 11.4 m, the heat-generation zone of the channel consisting of a bundle of seven rods with an outer diameter of 13.5 mm and a length of 7 m, the output part of the channel ~11 m in length, and steam–water communication at the channel exit ~29 m in length. The circuit was divided into 51 computational sections. All the spacer lattices were taken into account as local drag. The heat capacity of the walls of the heat-generating rods and thermal losses along the circuit were taken into account.

Comparison of the experimental hydraulic characteristics of the circuit and its sections with those calculated from Eq. (2) with the empirical dependences given above is presented in Fig. 1. Sufficiently satisfactory agreement of calculation with experiment is obtained, which indicates the validity of these dependences.

The stability limits are calculated for pressures of 1.0, 3.0, 5.0, and 7.0 MPa and powers in the channel of 90, 250, 600, and 1000 kW. Comparison of the results of the calculation with the experiments is given in Figs. 2-4. Good agreement for this kind of calculation is obtained with the experiments over the entire parameter range investigated.

LIST OF SYMBOLS

a – thermal conductivity, m^2/sec
C_p – specific heat, $J/kg \cdot deg$
d_h – hydraulic diameter, m
f – transfer cross section, m^2
g – gravitational acceleration, m/sec^2
G – coolant flow rate, kg/sec
H – total length of channel, m
i – enthalpy, J/kg
I – volume enthalpy, J/m^3
j – imaginary unit
p – pressure, Pa
П – perimeter, m
r – heat of vaporization, J/kg
q – thermal flux, W/m^2
s – Laplace transformation parameter
T – tangential stress, N/m^2
v – specific volume, m^3/kg
x – mass steam content
z – coordinate along the channel axis, m
α – heat-exchange coefficient, $W/m^2 \cdot deg$
Δ – absolute roughness, m
φ – true volume steam content
λ_t – thermal conductivity, $J/m \cdot deg$
μ – dynamic viscosity, Pa
ν – kinematic viscosity, m^2/sec
ρ – density, kg/m^3
θ – angle of inclination to horizontal
τ – time, sec
ω – frequency, Hz
t – temperature, °C

INDICES

st, end – start and end of the channel section under discussion; (′), (″) – water and steam on the saturation line; l – liquid phase; d – local drag; o, i "outer" and "inner" parts of the perimeter; R, I – real and imaginary parts of a complex quantity; and $\sim$ – a quantity which has been Laplace-transformed.

LITERATURE CITED

1. I. I. Morozov and V. A. Gerliga, The Stability of Boiling Equipment [in Russian], Atomizdat, Moscow (1969).
2. Yu. S. Molochnikov, in: Some Questions of the Reliability of Nuclear Reactors [in Russian], A. I. Klemin and M. M. Strigulin, Atomizdat, Moscow (1969), p. 289.
3. M. S. Lavrova et al., Preprint IAE-2238, Moscow (1972).
4. I. E. Idel'chik, Handbook on Hydraulic Drag [in Russian], Énergiya, Moscow (1975).
5. G. Wallace, One-Dimensional Two-Phase Flow [Russian translation], Mir, Moscow (1972).
6. V. N. Smolin et al., "Investigation of the thermohydraulic stability in a model of the circuit of a channel of the RBMK-1500 reactor," Lecture at the Sixth All-Union Conference on Heat Exchange and Hydraulic Drag in Units of Power Machines and Equipment, Leningrad (1979).
7. P. Kroeger and N. Zuber, Int. J. Heat Mass Transfer, 11, No. 2, 211 (1968).
8. V. S. Osmachkin and V. D. Borisov, Preprint IAE-1957, Moscow (1971).

APPROXIMATE METHODS OF CALCULATING NEUTRON DISTRIBUTIONS

S. S. Gorodkov

UDC 621.039.51.12:539.125.52

Neutron distributions in reactors are commonly calculated by the homogeneous-diffusion method in which all cells of the reactor are replaced by homogeneous cells, and neutron transport in them is described by the diffusion equation

$$D^i\Delta\Phi(\mathbf{r}) - \Sigma_a^i\Phi(\mathbf{r}) + S^i = 0. \quad (1)$$

The coefficients D^i, Σ_a^i (homogeneous constants) and S^i are constant within a single cell. The traditional method for obtaining Σ_a^i is to average the true absorption cross section over the neutron flux obtained from a kinetic calculation of an infinite uniform lattice consisting of cells of the i-th kind. A homogeneous-diffusion cell with Σ_a^i is equivalent to the initial cell with respect to the probability of neutron absorption in it. There is no direct relation between D^i and any characteristic of the initial cell. In this method of homogenization an approximate relation between D and Σ_{tr} is established by making the simplifying assumptions that either $l_a \ll l_s$, or that the neutron flux varies in an infinite uniform lattice. These assumptions are not valid for all real cases.

Another method of homogenization is based on Selengut's assumption [1] that from the outside an equivalent homogeneous cell should not be distinguishable from the initial cell. This approach was most completely developed by [2]. The cells must be equivalent with respect to the γ_0-symmetric and γ_1-antisymmetric components of the neutron current and flux at the surface of a cell. The values of γ_0 and γ_1 are calculated for a single cell surrounded by an infinite moderator in which the source is located at a large distance from the center. This leads to a symmetric or antisymmetric solution. The diffusion calculation of an infinite uniform lattice using D and Σ_a obtained from γ_0 and γ_1 does not lead to a result in agreement with the kinetic calculation, but by a simple renormalization of the flux and the neutron source in Eq. (1) proposed by Bonalumi, agreement is achieved in this case also. Thus, the evaluation of the homogeneous constants of a single cell requires three kinetic calculations.

In the heterogeneous-diffusion method developed by Galanin and Feinberg [3], all cells are filled with a moderator, and a fuel element or an absorbing rod is simulated by a line source or sink, so that neutrons are distributed according to the equation

$$D^0\Delta\Phi(\mathbf{r}) - \Sigma_a^0\Phi(\mathbf{r}) + \beta_0\Phi^{ext}\delta(\mathbf{r}) = 0, \quad (2)$$

where Φ^{ext} is the neutron flux at point $\mathbf{r} = 0$ produced by all sources outside the cell, and β_0 is a monopole heterogeneous constant characterizing the rod. A term of the dipole type

$$-2\beta_1\nabla\Phi^{ext}\nabla\delta(\mathbf{r}) \quad (3)$$

is sometimes introduced in Eq. (2) to take account of the difference between the transport characteristics of the rod and the moderator.

The heterogeneous method was developed under the assumption that the diffusion approximation is valid in the moderator, and therefore it is assumed is applicable, e.g., for calculating closely spaced uranium–water lattices which can be calculated by the homogeneous-diffusion program. If it is assumed that neutron transport in a model cell is described by Eqs. (2) and (3), parameters β_0 and β_1 can be chosen so that this cell will be equivalent to the initial cell in the same sense as a homogeneous cell. Therefore, along with the homogenization method the heterogenization method can be used, and apparently with equal success. If the constants of one type are known, it is not necessary to resort to kinetic calculations of individual cells in order to find the constants of the other. It is necessary to establish in what characteristics equivalence is required, to determine from the known homogeneous

Translated from Atomnaya Énergiya, Vol. 48, No. 6, pp. 370-373, June, 1980. Original article submitted April 23, 1979.

0038-531X/80/4806-0372$07.50

(heterogeneous) constants the specific values of these characteristics, and then to find the heterogeneous (homogeneous) constants giving the same values. Equivalent homogeneous and heterogeneous cells differ in the external properties of the second and higher azimuthal harmonics of the neutron flux. Therefore, the difference in the two calculations, not aggravated by other approximations, will indicate the error due to the difference in higher azimuthal characteristics of the initial and equivalent cells. And how do the negligible anisotropy of the neutron flux and other possible effects show up? What in general is the error of these approaches resulting from the fact that having assumed a certain form of equivalence it is possible at once to replace the kinetic calculation by a diffusion calculation?

It is impossible to give specific answers to these questions beforehand. A clear notion of the error of one method or another can only be obtained by a comparison with a series of precise calculations. With this in mind, we considered a one-velocity calculation of a hexagonal lattice by the Monte Carlo method [4]. An element of symmetry of the lattice is shown in Fig. 1. The reflection condition is shown outside its boundary on the right. The pitch of the lattice was 0.8 cm. The outside 66 cells are pure water ($\Sigma_a = 0.02$ cm^{-1}, $\Sigma_t = 2.02$ cm^{-1}), and the inner 61 cells contain 0.3 cm radius rods with $\Sigma_s = 0.3$ cm^{-1} surrounded by water. Absorbers with $\Sigma_a^{abs} \neq \Sigma_a^{fuel}$ (the absorption cross section of the other rods) can be placed in cell number 7. In the six variants Σ_a^{abs} and Σ_a^{fuel} were assigned the values shown in Table 1. It was assumed that neutron scattering is isotropic in the laboratory system, and that the neutron sources are steady in water and zero in the rods. The Monte Carlo method was used to calculate a cell with a source in water and reflection from the boundary, and a cell surrounded by water with a source at a considerable distance, ensuring a symmetric or antisymmetric distribution of the neutron flux in the cell.

The methods were first compared for a simpler example of a neutron distribution described by the diffusion equation in the infinite layered medium shown in Fig. 2. Water cells have the same properties as analogous cells of the kinetic test, and the fuel cells have the same characteristics as the homogenized fuel cells. The source strengths in the fuel and water cells have the same ratio as the volumes of moderator in analogous cells of the kinetic test, and the sum of the sources over cells 1-4 is equal to 1.

We note that the solution of the diffusion problem by any method being investigated is naturally not a universal test of it. Certain sources of error vanish, but the value of others stands out. In addition, it will be useful to note whether rules established in a simple case are retained when factors that were neglected are included, or whether these factors will act like noise, blurring a clear picture.

After the homogenization constants have been determined for the homogeneous equations, and the heterogeneous constants for the heterogeneous equations, there arises the question of how to solve these equations. In the homogeneous case the boundaries of a cell can be squared up along vertical lines (cf. Fig. 2). The two-region one-dimensional problem obtained is solved analytically, and the result is compared with the exact solution of the diffusion test. The diffusion equations with line sources in an infinite moderator also can be solved exactly by using a Green's function.

As a rule, a two-dimensional homogeneous-diffusion problem cannot be reduced to a one-dimensional problem, and its solution requires spanning the computational field with a certain net and replacing the differential operators by **finite-difference** operators over this net. A very coarse net with one node per cell is most frequently used. Since this approximation, called hereafter the homogeneous-net approximation, is difficult to test for hexagonal cells by a change of pitch, it is more interesting to compare it with the exact calculation.

The finite-difference approximation was developed by mathematicians under conditions such that the result approaches the exact solution as the pitch of the net approaches zero. Physicists would be interested in a scheme giving the smallest deviation for a given pitch, and without a significant complication of the form of the equations. One such scheme can be obtained by the Laletin–El'shin method [5] in which the transport equation is solved by synthesizing several sets of solutions in individual cells. The relations between the amplitudes of such solutions have the form of linear equations. If the input set is a Bonalumi complex of solutions, the linear equations have the same form as the homogeneous–net equations, differing from them in coefficients, the meaning of the variables, and the physical results. Another approach for increasing the accuracy of the **finite-difference** approximation was proposed by Marakazov [6].

The various methods employed in the diffusion test were compared through $A_{1,2} = \bar{\Phi}_{1,2}\Sigma_a V$ – the absorption in the first and second fuel cells, and $A = A_1 + A_2$, which for a given source normalization will be the thermal utilization. The input data and results of the comparison are given in Tables 2 and 3.

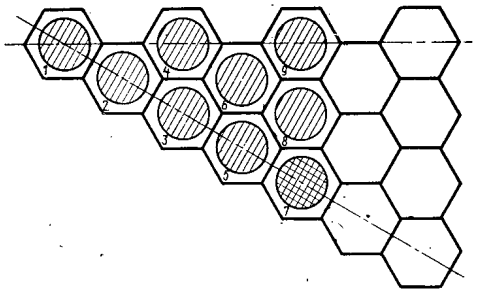

Fig. 1. Element of symmetry of lattice for two-dimensional kinetic test.

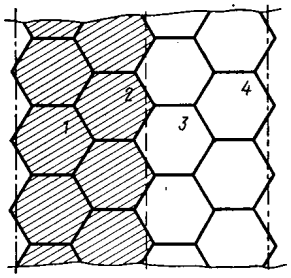

Fig. 2. Problem for diffusion test: $\Sigma_a^{3,4} = 0.02$; $D^{3,4} = 0.1652$

Variant	$\Sigma_a^{1,2}$	$D^{1,2}$
1	0.2502	0.238
2	0.4625	0.207
3	0.8004	0.167

TABLE 1. Input Data for Hexagonal Lattice

Characteristic	Variant					
	1	2	3	4	5	6
Σ^{fuel}, cm^{-1}	0,5	0,5	1,0	1,0	2,0	2,0
Σ_a^{abs}, cm^{-1}	0,5	2,0	1,0	2,0	2,0	4,0

TABLE 2. Input Data and Results of Exact Solution for the Diffusion Test

Characteristic	Variant		
	1	2	3
$\Sigma_a^{1,2}$, cm^{-1}	0,250	0,463	0,800
$D^{1,2}$, cm^{-1}	0,238	0,207	0,167
$\Sigma_a^{3,4}$, cm^{-1}	0,020	0,020	0,020
$D^{3,4}$, cm^{-1}	0,165	0,165	0,165
A_1	0,377	0,342	0,285
A_2	0,488	0,549	0,619

TABLE 3. Deviations of Approximate Solutions of Diffusion Problem from Exact Solution

Approximation	Variant	$(A - A_{exact}) \cdot 10^2$	$\delta A_1/A_1$, %	$\delta A_2/A_2$, %
Homogeneous-net	1	0,80	—0,40	—1,37
	2	1,00	0,65	—2,24
	3	1,36	3,45	—3,82
Laletin—El'shin	1	0,20	0,22	—0,45
	2	0,22	0,95	—1,04
	3	0,25	3,00	—1,72
Σ_a-Heterogeniza-tion	1	0,08	0,28	—0,26
	2	0,10	0,72	—0,70
	3	0,13	2,23	—1,31
γ-Heterogeniza-tion	1	0,10	0,10	0,11
	2	0,11	0,10	0,11
	3	0,11	0,10	0,11
Marakazov [6]	1	0,06	0,15	—0,06
	2	0,10	0,60	—0,25
	3	0,17	1,76	—0,59

TABLE 4. Deviation of Approximate Solutions of Kinetic Problem from the Solution by the Monte Carlo Method

Approximation	Variant	$\delta\theta \cdot 10^3$	$\sqrt{\overline{\delta\Phi_R^2}}/\Phi_R$, %	$\delta\Phi_7/\Phi_7$, %	Approximation	Variant	$\delta\theta \cdot 10^3$	$\sqrt{\overline{\delta\Phi_R^2}}/\Phi_R$, %	$\delta\Phi_7/\Phi_7$, %
Homogeneous-net	1	—1,3	0,7	—0,5		1	—1,6	1,5	0,5
	3	—2,0	1,3	—2,3		3	—1,8	1,1	0,0
	5	—2,8	3,9	—5,8		5	—1,1	2,0	—2,5
	2	—2,7	1,7	—6,3	Laletin—El'shin	2	—1,5	2,0	0,0
	4	—0,9	3,5	—8,8		4	—0,5	1,6	—3,1
	6	—3,5	4,0	—9,8		6	—1,5	1,6	—3,3
Σ_a-Hetero-genization	1	—0,8	2,6	3,8	Ditto with simplified cell calculations	1	0,4	0,9	0,3
	3	—0,7	3,0	3,8		3	0,7	0,8	—0,3
	5	—1,6	1,7	2,3		5	1,1	0,9	—1,2
	2	1,6	3,2	6,3		2	1,6	1,5	0,5
	4	2,5	1,0	2,2		4	1,8	1,9	—2,5
	6	1,6	2,1	3,5		6	0,7	0,8	—1,0
γ-Heterogeniza-tion	1	—0,1	1,8	2,2					
	3	0,0	2,2	2,3					
	5	0,9	0,8	1,0					
	2	0,4	2,8	5,1	Error of calculation by Monte Carlo method		0,6	0,5	1,0
	4	1,6	0,7	1,2					
	6	0,8	1,1	1,7					

Note: θ, thermal utilization; Φ_R, average neutron flux in rods; and Φ_7, average neutron flux in an absorbing rod.

The quality of γ-equivalent heterogenization should be noted. It indicates the clear advantage of Selengut equivalence over the traditional Σ_a-equivalence. The large error of the homogeneous-net method can be substantially decreased by using the Laletin—El'shin and Marakazov methods.

On the basis of the diffusion test, in which the errors are due only to the coarse net and higher harmonics, it is possible to estimate each method accurately, but in the kinetic test, the results of which are shown in Table 4, the situation turns out to be more complicated. No one of the methods investigated is quantitatively better than all the others. It is true that γ-heterogenization and the Laletin—El'shin methods using three cell calculations instead of two give somewhat better results. It should be noted, however, that in the problem under discussion, where most of the neutrons are created outside the fuel cells, the calculation of a uniform lattice to obtain Σ_a to use in the homogeneous-net and Σ_a-heterogeneous approximations is not sufficiently characteristic. The use of less adequate unit cell calculations does not necessarily worsen the results. For example,

in calculations by the Laletin–El'shin method the use of symmetric cell calculations in the G_3 approximation and antisymmetric calculations in the P_2 approximation, without taking account of absorption in water, improved the agreement with the exact solution at most points. This and the fact that the first variant shows that the homogeneous-net method is most the "best" indicate an increase in the statistical part of the error due to the various factors which were not taken into account. In this problem the number of such factors is small. In more realistic cases these factors include complex composition and geometry, resonances, energy spectra, heat and mass transfer, three dimensionality, etc. If no one of the methods demonstrates an overwhelming advantage over the others in a simple problem, one can hardly expect this in more complicated problems. Therefore, in calculating neutron distributions in large power reactors using characteristics of individual cells, one method is as good as another.

Thus, the choice of this or that method of calculating a specific assembly is made largely on technological grounds. In problems with hexagonal cells and substantially different diffusion coefficients (VVÉR), homogeneous program are preferable, while in problems with square cells containing relatively narrow channels (RBMK), a homogeneous five-point algorithm will be an appreciable error, and a heterogeneous algorithm, particularly in the monopole variant, becomes preferable.

The author thanks A. S. Il'yashenko and A. D. Frank-Kamenetskii for calculating the characteristics of individual cells by the Monte Carlo method, and L. V. Maiorov and Ya. V. Shevelev for a discussion of the results of the work.

LITERATURE CITED

1. D. Selengut, Trans. Am. Nucl. Soc., 3, 398 (1960).
2. R. Bonalumi, Energ. Nucl., 20, 39 (1973); 21, 231 (1974).
3. A. D. Galanin, Thermal Reactor Theory, Pergamon, New York (1960).
4. L. V. Maiorov, G. Ya. Trukhachev, and A. D. Frank-Kamenetskii, in: Methods of Calculating Thermal Neutron Distributions in Reactor Lattices [in Russian], Atomizdat, Moscow (1974), p. 216.
5. N. I. Laletin and A. V. El'shin, At. Energ., 43, No. 4, 247 (1977).
6. A. A. Marakazov, Preprint IAÉ-2781, Moscow (1977).

NUMERICAL STUDY OF THE DISTRIBUTION FROM A PULSED SOURCE OF 14-MeV NEUTRONS IN AN INFINITE TWO-LAYER CYLINDRICAL MEDIUM

A. A. Morozov, R. A. Rezvanov, and A. I. Khisamutdinov

UDC 539.125.52:518.61

Statement of the Problem. The present article extends the work of [1] to the study of the distribution from a pulsed isotropic point source of 14-MeV neutrons. Above the energy of 1.4 MeV considered in [1], various inelastic processes occur, and the use of a library of detailed "pointwise" nuclear data such as the ENDL library [2] becomes necessary and justified. At $E_0 = 1.4$ MeV the standard ABBN system of group constants [3] and ENDL give nearly the same results (cf. [1]). In the present work the neutron distribution is calculated numerically by the Monte Carlo method on the basis of the ENDL library. The method and program used are the same as in [1]. The choice of 14 MeV was dictated by the availability of generators producing neutrons of this energy.

Suppose an infinite homogeneous medium (stratum) is penetrated by an infinitely long cylindrical hole of radius R. The hole is filled with water (H_2O), and the stratum consists of $(1 - m)$ parts by volume of sandstone (SiO_2) of density 2.65 g/cm^3 and m parts of water (H_2O) ($0 \leq m \leq 1$). A point monoenergetic isotropic pulsed neutron source is located in the hole. To calculate the neutron distribution it is necessary to evaluate integrals over a spherical volume V of radius 2 cm inside the hole:

$$J = 1/V\Delta T \int\int\int_{(V)} d\mathbf{r} \int_{T}^{T+\Delta T} dt \int_{E}^{E+\Delta E} dE' \int \Phi(\mathbf{r}, E', \Omega, t)\, d\Omega. \quad (1)$$

Here r is the spatial coordinate; E', energy; Ω, direction vector; t, time; $\Phi(\mathbf{r}, E', \Omega, t)$, differential neutron flux; and T and $T + \Delta T$, E and $E + \Delta E$, boundaries of the time and energy intervals, respectively. The space–time and energy distributions of neutrons and the dependence of the energy distributions on m are determined by the functionals J.

Model of the Interaction of Neutrons with Matter. In the thermal region ($E < 0.215$ eV) a one-velocity model of the diffusion of 0.0252-eV neutrons was assumed with isotropic scattering in the laboratory system. The total macroscopic cross sections Σ and macroscopic scattering cross sections Σ_S, were chosen in accord with the known published values of the diffusion coefficients D and lifetime τ. For H_2O we took $\Sigma = 2.0952$ cm^{-1}, $\Sigma_S = 2.0725$ cm^{-1}, and for SiO_2 $\Sigma = 0.2486$ cm^{-1}, $\Sigma_S = 0.2444$ cm^{-1}. The model chosen for the interaction with matter of neutrons having energies $E > 0.215$ eV was based on the ENDL library.

Results of Calculations. To investigate the effect of the choice of neutron data on the neutron distribution, calculations were performed and the results compared with data from [2] (Tables 1 and 2). Table 1 compares the calculated time distribution of the thermal neutron ($E < 0.215$ eV) flux density at the probe (distance from source to center of sphere $z = 10$ cm on the axis of the hole for $m = 0.2$). The error of the results was not reported in [2].

The numbers in the first column of Table 1 are the values of the upper limit of the time interval $T + \Delta T$; the numbers in a row refer to the corresponding interval (T, $T + \Delta T$); the value of T is found in the preceding row of the first column; for the first time interval $T = 0$. Table 2 compares the calculated epithermal (0.215–100 eV) neutron flux density on the axis of the hole with data from [2] recalculated by using the Fermi spectrum in the 0.125–100 eV energy range for the steady-state case.

Tables 1 and 2 show qualitatively the same dependence but widely different absolute values. Figures 1–4 show the results calculated for five different energy ranges and two positions of the source–sphere center axis (V): centric (c) when this axis coincides with the axis of the hole and eccentric (e) when this axis is 7.85 cm from the axis of the hole. The calculations were performed for R = 9.85 cm; the limits of the time intervals were chosen so as to obtain a satisfactorily sharp representation of the time spectra. In particular, in Figs.

Translated from Atomnaya Énergiya, Vol. 48, No. 6, pp. 374–376, June, 1980. Original article submitted February 14, 1979.

0038-531X/80/4806-0377$07.50

TABLE 1. Comparison of Thermal Neutron Flux Calculated Using INNK-MK Program with Data from [2] $(cm^2 \cdot sec)^{-1}$

$T + \Delta T$	Results using INNK-MK	Data from [2]
100	$2{,}1 \cdot 10^{0}$ (13,1 %)	$6{,}4 \cdot 10^{0}$
200	$1{,}5 \cdot 10^{0}$ (13,9 %)	$3{,}6 \cdot 10^{0}$
300	$8{,}1 \cdot 10^{-1}$ (13,0 %)	$2{,}1 \cdot 10^{0}$
400	$4{,}8 \cdot 10^{-1}$ (13,8 %)	$1{,}2 \cdot 10^{0}$
500	$2{,}7 \cdot 10^{-1}$ (19,1 %)	$6{,}1 \cdot 10^{-1}$
600	$1{,}6 \cdot 10^{-1}$ (14,2 %)	$3{,}3 \cdot 10^{-1}$
700	$9{,}8 \cdot 10^{-2}$ (17,1 %)	$2{,}2 \cdot 10^{-1}$

Note: Error is indicated in parentheses.

TABLE 2. Comparison of Epithermal Neutron Flux Density with Data from [2] $(cm^2 \cdot sec)^{-1}$

z, cm	Present work	Data from [2]
0	$2{,}448 \cdot 10^{-4}$ (13,1 %)	$4{,}92 \cdot 10^{-4}$
10	$9{,}101 \cdot 10^{-5}$ (24,9 %)	$2{,}09 \cdot 10^{-4}$

Note: Error is indicated in parentheses.

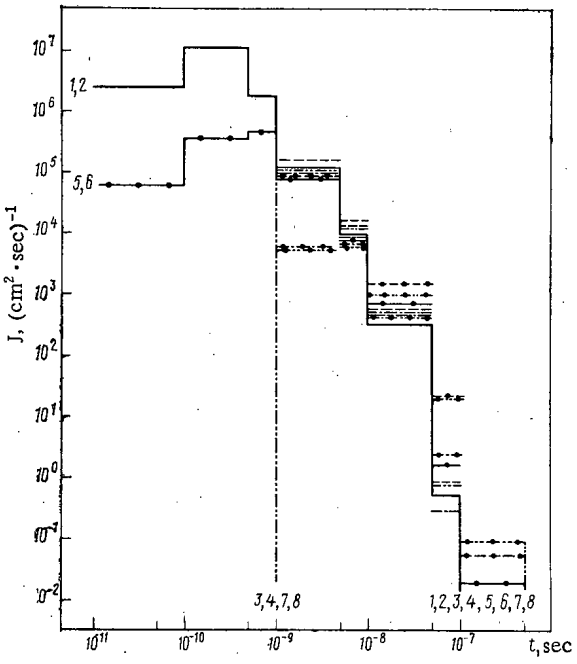

Fig. 1

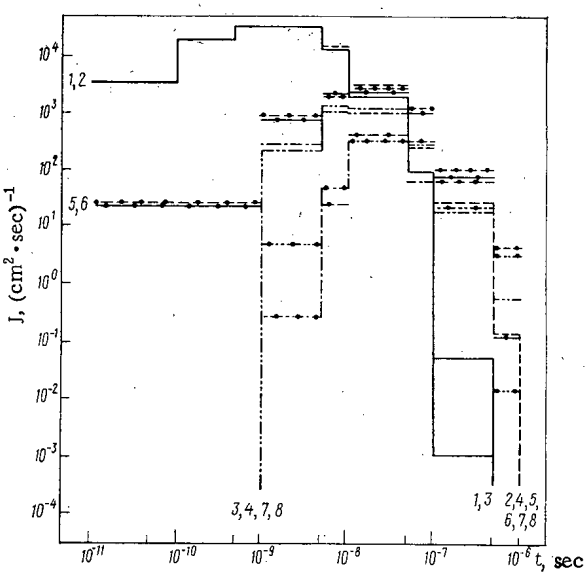

Fig. 2

Fig. 1. Time dependence of the neutron flux in the 1.4-14-MeV range (1-4) and the 0.2-1.4-MeV range (5-8): ——) curve 1, z = 0, c case; ---) curve 2, z = 0, e case; - · -) curve 3, z = 10 cm, c case: - · · -) curve 4, z = 10 cm, e case; •) corresponding curves 5-8.

Fig. 2. Time dependence of neutron flux in the 4.65-keV-0.2-MeV range (1-4) and the 100-eV-4.65-keV range (5-8). Notation same as in Fig. 1.

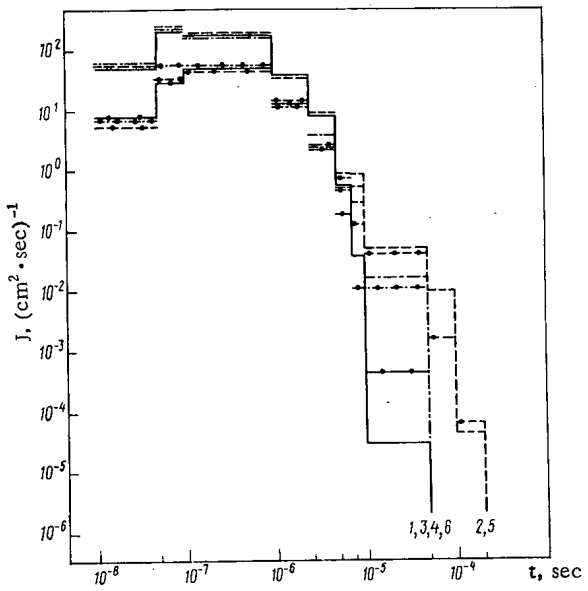

Fig. 3

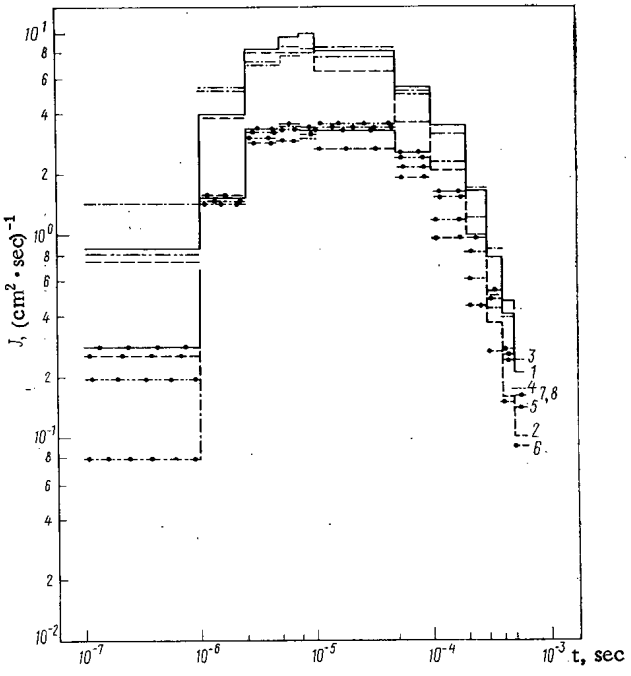

Fig. 4

Fig. 3. Time dependence of neutron flux in the 0.215-100-eV range: ——) curve 1, z = 0, m = 0, c case: ---) curve 2, z = 0, m = 0, e case; - · -) curve 3, z = 0, m = 0.2, e case; •) corresponding curves 4-6 for z = 10 cm.

Fig. 4. Time dependence of neutron flux in the 0-0.215-eV range. Notation for curves 1 and 2 same as in Fig. 3; - · -) curve 3, z = 0, m = 0.2, : case; - · · -) curve 4, z = 0, m = 0.2, e case; •) corresponding curves for z = 10 cm.

1-4 the positions of the maxima for these spectra can be distinguished.

A comparison of the values of J for thermal and epithermal neutrons for initial energies of 1.4 MeV [1] and 14 MeV shows that

$$J_{1.4\,\mathrm{MeV}}/J_{14\,\mathrm{MeV}} \approx (5 \div 10).$$

Let us compare the results for the centric and eccentric positions of the source–sphere center axis (V). For thermal neutrons the values of J are larger for the centric position than for the eccentric. For the other energy intervals the behavior is the following: at the maxima the values are nearly the same, but at later times the values for the eccentric position decrease smoothly.

Certain characteristic features of the dependence of J on m for epithermal neutrons can be understood from Fig. 3. At z = 0 the values of J for m = 0 and m = 0.2 begin to differ from $t \approx 10^{-5}$ sec, and at z = 10 cm from $t \approx 7.5 \cdot 10^{-6}$ sec. For m = 0 the spectrum extends to $2 \cdot 10^{-4}$ sec, but for m = 0.2, only to $5 \cdot 10^{-5}$ sec.

Thus, the $1 \cdot 10^{-5}$–$5 \cdot 10^{-5}$ sec interval can be used to determine the moisture content of the stratum for $m \geq 0.2$; for $m < 0.2$ it is necessary to use intervals with a larger value of the time. We note that these statements give concrete form to certain prognostic conclusions in [6] where the dependence of the slowing down density on m was analyzed for a source $E_0 = 2.45$ MeV. For the general character of the time, that for a stratum penetrated by a hole, the epithermal neutron flux is cut off sharply at a certain t; the cutoff time increases with decreasing m and with the displacement of the instrument from the axis of the hole.

Computation Time and Errors. The calculation of all the curves of Figs. 1-4 required 42 h of machine time on a BÉSM-6. The standard relative error of the results was ~10-15%.

With an increase in the probe distance z there is an increase in the volume of computational work (v.c.w.) necessary to achieve a given accuracy. Thus, in the eccentric position for epithermal neutrons in the time interval 10^{-7}–10^{-5} sec the values of the v.c.w. to obtain the same accuracy of the results at probe distances z = 0, 10, 20, 30 cm will be approximately in the ratio 1 : 2 : 7 : 9. For thermal neutrons the estimate of

the v.c.w. will evidently be the same. For fast neutrons the v.c.w. increases more rapidly with increasing z. For example, for $E_0 = 1.4$ MeV in the centric position in the energy range 100 eV–4.65 keV the values of the v.c.w. for the neutron density close to the time maximum for probe distances z = 0, 10, 20 cm are in the approximate ratio 1:16:400.

All the numerical values of the neutron fluxes and their statistical errors are given in a report of the Computation Center of the Siberian Branch of the Academy of Sciences of the USSR.

LITERATURE CITED

1. A. A. Morozov and A. I. Khisamutdinov, Preprint No. 78 VTs Sib. Otd Akad. Nauk SSSR, Novosibirsk (1977).
2. Evaluated Nuclear Data Library, Lawrence Livermore Laboratory (1975).
3. L. P. Abagyan et al., Group Constants for Calculating Nuclear Reactors [in Russian], Atomizdat, Moscow (1964).
4. R. A. Rezvanov, V. Ya. Gommershtadt, and V. E. Lebedev, in: Nuclear Geophysics, Proc. of VNII of Nuclear Geophysics and Geochemistry [in Russian], No. 7, Nedra, Moscow (1969), p. 75.
5. Yu. S. Shimelevich et al., Physical Principles of Pulsed Neutron Methods of Studying Boreholes [in Russian], Nedra, Moscow (1976).
6. R. A. Rezvanov, Fiz. Zemli, 3, 105 (1970).

DETERMINATION OF THE DETAILS OF THE RESONANCE STRUCTURE OF BOTH THE TOTAL CROSS SECTION AND THE FISSION CROSS SECTION OF ^{235}U AND ^{239}Pu FOR 2 eV-20-keV NEUTRONS

A. A. Van'kov, Yu. V. Grigor'ev,
V. F. Ukraintsev, T. Bakalov,
G. Ilchev, S. Toshkov,
Chan-Khan'-Mai, and N. Yaneva

UDC 621.039.51

When fast reactors are calculated with the aid of the system of BNAB group constants [1], one must know both the average group cross sections of the fuel nuclides and the design materials and the factors of their resonance self-shielding. These factors are calculated from the resonance parameters of the corresponding nuclides. In the range of unresolved resonances, the errors of both the computer model and the initial data (average resonance parameters) imply considerable errors of the factors of self-shielding (~20-30%) [2]. It is therefore necessary to directly measure the average characteristics of the resonance structures of the cross sections at resolved and unresolved resonances.

The present work presented the results of measurements of those characteristics; the measurements were made with the technique of neutron transmission and self-indication in ^{235}U and ^{239}Pu: the average total cross sections and the factors of the resonance self-shielding of the total cross section and the fission cross section were determined at 2 eV-20 keV.

Experimental Technique. The transmission function and the fission self-indication function

$$\langle T(x)\rangle = \int_{\Delta E} \varphi(E)\,\varepsilon(E)\,\exp[-\sigma_t(E)\,x]\,dE \Big/ \int_{\Delta E} \varphi(E)\,\varepsilon(E)\,dE; \quad (1)$$

$$\langle T_f(x)\rangle = \int_{\Delta E} \varphi(E)\,\sigma_f(E)\,\exp[-\sigma_t(E)\,x]\,dE \Big/ \int_{\Delta E} \varphi(E)\,\sigma_f(E)\,dE \quad (2)$$

were calculated, where $\sigma_t(E)$ and $\sigma_f(E)$ denote the total cross section and the fission cross section of the isotope under consideration; $\varphi(E)$, neutron spectrum; $\varepsilon(E)$, efficiency of the neutron detector; x, sample thickness; and ΔE, interval over which the energy was averaged.

The experimental $\langle T(x)\rangle$ and $\langle T_f(x)\rangle$ values can be used to determine the parameters of the resonance structure of the cross sections and the factors of resonance self-shielding of both the total cross section and the fission cross section [3]:

$$f_t = \frac{1}{\langle\sigma_t\rangle}\left[\left(\left\langle\frac{1}{\sigma_t+\sigma_0}\right\rangle \Big/ \left\langle\frac{1}{(\sigma_t+\sigma_0)^2}\right\rangle\right) - \sigma_0\right]; \quad (3)$$

$$f_f = \frac{1}{\langle\sigma_f\rangle}\left\langle\frac{\sigma_f}{(\sigma_t+\sigma_0)}\right\rangle \Big/ \left\langle\frac{1}{\sigma_t+\sigma_0}\right\rangle, \quad (4)$$

where σ_0 denotes the cross section of neutron thinning.

T(x) and $T_f(x)$ were determined from the flight time with the aid of a neutron spectrometer on the base of a pulsed fast IBR-30 reactor. Counters with ^3He [4] were used as neutron detectors in the measurements of the transmissivity T(x). The resolution was about 100 nsec/m. Fast-response multilayer fission chambers containing uranium and plutonium layers [5] were used as detectors for the self-indication of fission. The ^{235}U layer thickness was 2 mg/cm^2, the total amount of ^{235}U was 2 g; the corresponding figures for ^{239}Pu were 0.5 mg/cm^2 and 0.5 g. The efficiency of fission fragment recording in the fission chambers was measured at the individual resonances and amounted to 50-70%. The resolution in the measurements of self-indication $T_f(x)$ was 53 nsec/m.

The samples were disks of metallic uranium (with 10% ^{238}U) and plutonium having a diameter of 50-80 mm; the disks had been placed into sealed stainless-steel jackets. The ^{238}U correction was calculated from the parameters obtained from the evaluation of the transmissivity data [6].

Translated from Atomnaya Énergiya, Vol. 48, No. 6, pp. 377-381, June, 1980. Original article submitted August 6, 1978.

0038-531X/80/4806-0381 $07.50

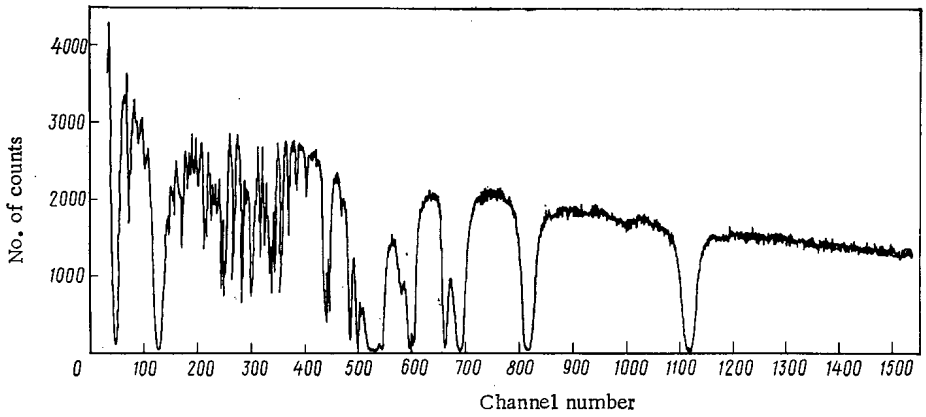

Fig. 1. Instrument spectrum of the flight time (base length of the flight path 1000 m; channel width 32 μsec) for a better detector with ^{3}He; ^{239}Pu sample and manganese and tungsten resonance filters inserted into the neutron beam.

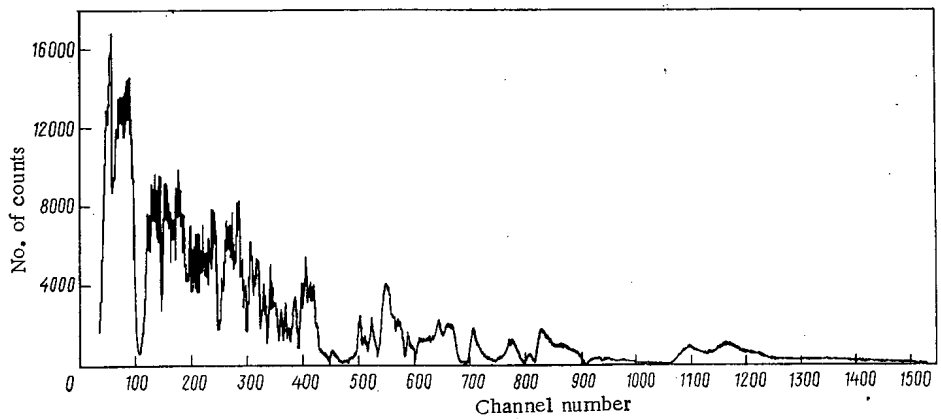

Fig. 2. Instrument spectrum of the flight time (base length of the flight path 59 m, channel width 2 μsec) for a uranium fission chamber; ^{235}U sample and manganese and tungsten resonance filters inserted into the neutron beam.

TABLE 1. Factors of Resonance Self-Shielding of the Total Cross Section and the Fission Cross Section of ^{235}U

No. of group	E_n	Experiment							
		$f_t(\sigma_0)$				$f_f(\sigma_0)$			
		0	10	100	10^3	0	10	10^2	10^3
11	21,5—10 keV	0,923	0,930	0,965	0,994	0,959	0,966	0,987	0,998
12	10—4,65	0,882	0,905	0,967	0,995	0,931	0,949	0,984	0,998
13	4,65—2,15	0,779	0,830	0,948	0,993	0,912	0,937	0,982	0,997
14	2,15—1,0	0,734	0,772	0,907	0,987	0,883	0,907	0,968	0,995
15	1000—465 eV	0,606	0,700	0,825	0,953	0,740	0,817	0,945	0,992
16	465—215	0,545	0,592	0,812	0,972	0,622	0,696	0,887	0,989
17	215—100	0,507	0,545	0,759	0,961	0,624	0,679	0,861	0,979
18	100—46,5	0,377	0,407	0,633	0,933	0,530	0,584	0,796	0,966
19	46,5—21,5	0,296	0,335	0,542	0,861	0,407	0,476	0,701	0,928
20	21,5—10,0	0,269	0,290	0,406	0,705	0,409	0,450	0,609	0,860
21	10,0—4,65	0,270	0,332	0,489	0,832	0,344	0,379	0,559	0,838
22	4,65—2,15	0,578	0,667	0,826	0,963	0,672	0,725	0,872	0,977

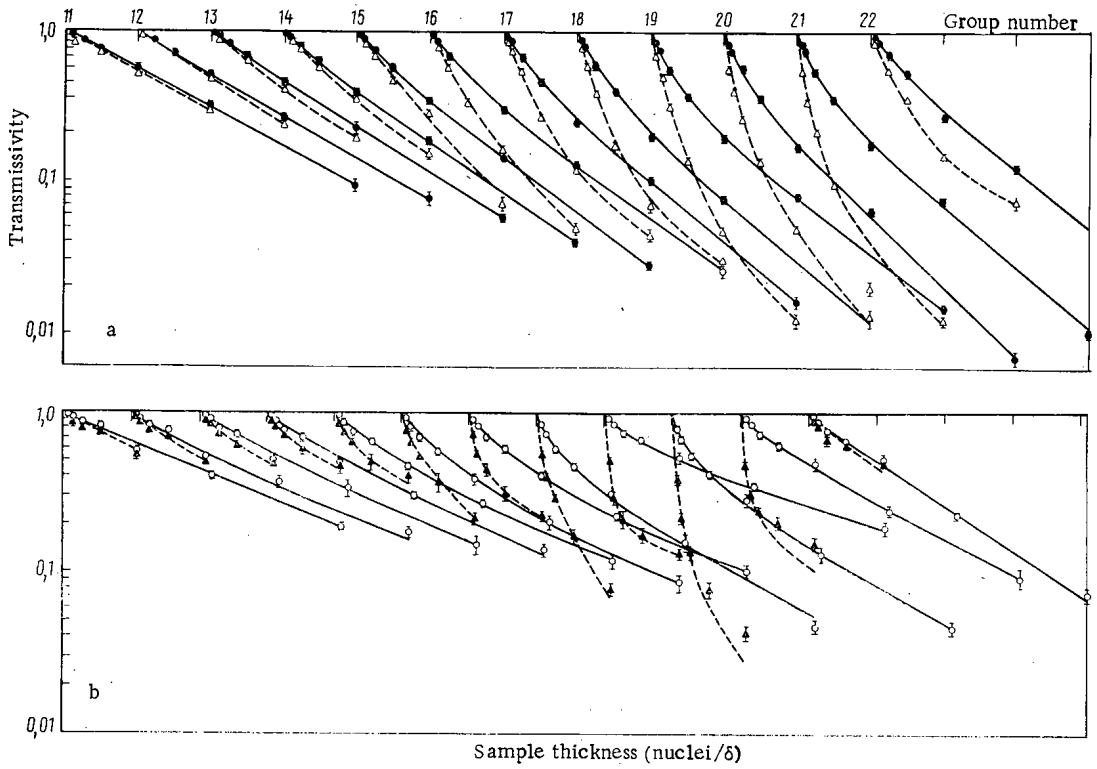

Fig. 3. Transmission function T(x) and $T_f(x)$ for a) ^{235}U and b) ^{239}Pu; averaging in the energy group of BNAB: ○) T(x); ▲) $T_f(x)$.

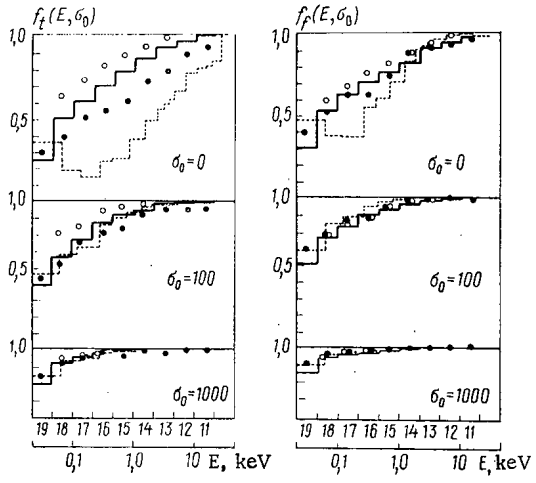

Fig. 4

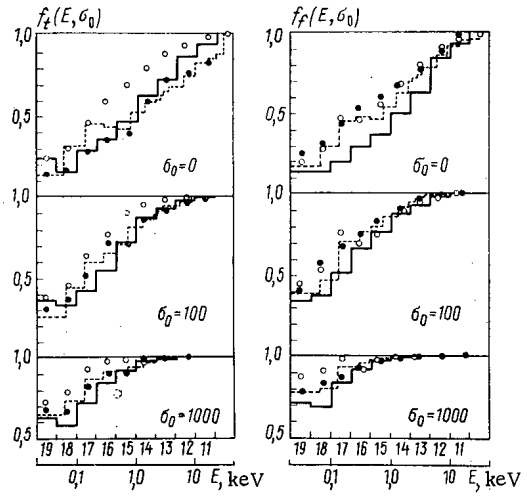

Fig. 5

Fig. 4. Factors of resonance self-shielding of the total cross section (f_t) and of the fission cross section (f_f) for ^{235}U at various cross sections σ_0 of thinning: ●) present work; ——) BNAB-78; ---) [9]; ○) [10]; the group numbers are indicated on the upper abscissa scale.

Fig. 5. Factors of resonance self-shielding of the total cross section (f_t) and of the fission cross section (f_f) for ^{239}Pu at various cross sections σ_0 of thinning (the notation is the same as in Fig. 4).

TABLE 2. Factors of the Resonance Self-Shielding of the Total Cross Section and the Fission Cross Section of ^{239}Pu

No of group	E_n	Experiment							
		$f_t(\sigma_0)$				$f_f(\sigma_0)$			
		0	10	10^2	10^3	0	10	10^2	10^3
11	21,5—10keV	0,836	0,918	0,986	0,998	0,974	0,987	0,999	1,000
12	10—4,65	0,785	0,880	0,978	0,998	0,872	0,928	0,986	0,998
13	4,65—2,15	0,728	0,778	0,924	0,990	0,765	0,826	0,948	0,994
14	2,15—1	0,598	0,650	0,858	0,981	0,688	0,758	0,920	0,990
15	1000—465eV	0,386	0,475	0,696	0,909	0,598	0,676	0,831	0,960
16	465—215	0,361	0,450	0,716	0,909	0,541	0,605	0,757	0,927
17	215—100	0,269	0,300	0,521	0,829	0,435	0,485	0,664	0,888
18	100—46,5	0,165	0,190	0,357	0,672	0,300	0,360	0,658	0,835
19	46,5—21,5	0,162	0,184	0,304	0,660	0,235	0,260	0,399	0,778
20	21,5—10	0,124	0,134	0,229	0,609	0,167	0,199	0,366	0,757
21	10—4,65	0,224	0,233	0,303	0,605	0,198	0,225	0,367	0,736

TABLE 3. Total Cross Sections (b) of ^{235}U and ^{239}Pu at the Center of Groups

No. of group	E_n	$\langle\sigma_t\rangle$ for ^{235}U		$\langle\sigma_t\rangle$ for ^{239}Pu	
		expt.	calc. with BNAB-78	expt.	calc. with BNAB-78
11	10—21,5keV	14,7±0,6	14,7	14,5±0,6	14,8
12	4,65—10	16,8±0,6	17,2	19,8±0,9	15,7
13	2,65—4,65	20,4±0,8	21,5	20,1±0,9	18,0
14	1—2,65	24,2±0,9	26,0	20,9±0,8	20,7
15	0,465—1	27,2±1,2	30,8	33,5±1,3	28,4
16	215—465eV	37,5±1,3	36,4	42,6±1,7	38,9
17	100—215	46,1±1,5	45,6	56,8±2,4	50,3
18	46,5—100	63,1±1,5	62,1	112±6	99,9
19	21,5—46,5	80,1±2,4	83,1	66±4	62,4
20	10—21,5	108±4	102,5	179±8	178,7
21	4,65—10	94±3	94,1	76±4	76,6

The intrinsic background of the detectors was checked during the measurements. In the case of the counters with ^3He the background was small and reached 0.4% for the maximum thickness of the uranium. The intrinsic background of the fission chambers was higher and amounted to ~11 and 18% for the maximum sample thickness in the uranium and plutonium chambers, respectively. The time-dependent background of the reactor was determined in the open beam for each sample thickness with the technique of resonance filters. Titanium, manganese, tungsten, indium, and cadmium were used as filters. Furthermore, the background could be determined at the resonance energies of uranium and plutonium with $n\sigma_{max} \gg 1$ (where σ_{max} denotes the cross section at the resonance maximum). Figure 1 shows the equipment-dependent spectrum of the counters with ^3He in the measurements involving a 0.00822-nuclei/b (1 b = 10^{-28} m^2) plutonium sample and manganese and tungsten filters. Figure 2 shows the equipment-dependent spectrum of the uranium chamber in measurements with a 0.00515-nuclei/b uranium sample and the same filters. The energy range above 3 keV falls within the first few dozen channels. In this region the background was determined by placing into the beam a titanium filter which led to the development of resonance minima at 3.8 and 18 keV. The dependence of the background upon the channel number was approximated with a polynomial on a computer and subtracted from the instrument spectrum.

The background in the beam without sample reached 2-5% in the case of the detector with ^3He and amounted to 20-40% for the maximum of the sample thickness. In the case of the fission chambers, the corresponding figures were 5-15% in the beam without sample and up to 30-60% at the maximum of the sample thickness.

Results of the Measurements. Figure 3 shows the thickness dependence of the transmissivity and the fission self-indication of ^{235}U and ^{239}Pu for the energy intervals assumed in the system of the BNAB constants. The error of the results depended basically upon the error made in evaluating the background measurements. The statistical error of the transmissivity at the center of a group did not exceed 0.5% in all measurement series.

Some time ago [7, 8] the results of measurements of the self-indication of uranium and plutonium fission in the thickness ranges 0.00035-0.014 and 0.00015-0.0079 nuclei/b, respectively, were published. Our data on the self-indication are in rather good agreement with those data within the thickness and energy intervals compared.

In order to determine the parameters of the structure of the cross section in the form of subgroup parameters [3], the transmissivity and self-indication functions were processed with programs of the least-square method. These parameters were used to determine the factors of the resonance self-shielding for the various cross sections σ_0 of thinning. The data are indicated in Tables 1 and 2. Figures 4 and 5 show the energy dependence of the factors of self-shielding of the total cross section $f_t(\sigma_0)$ and of the fission cross section $f_f(\sigma_0)$ for the cross sections 0.100 and 1000 b of thinning. The figures include for comparison the calculated foreign data [9, 10] and the FEI determinations made on the basis of BNAB-78 (calculations of [1] with certain corrections). The error of the factors f_t of self-shielding at 1-21 keV and $\sigma_0 = 0$ amounts to 8-10%, but reaches only 5-7% below 1 keV. For the factors f_f, the error amounted to ~5% at the same energy to 3-5% at energies below 1 keV. The accuracy of f_t and f_f increases with increasing σ_0. The results for $\langle\sigma_t\rangle$ are listed in Table 3.

Conclusions. It follows from Fig. 4 and 5 that the spread in the calculations of the factors of resonance self-shielding is extremely large. Our data for ^{235}U and ^{239}Pu are in regard to the factors f_t systematically below the calculated values at energies above 1 keV. The experimental values are much larger than the values calculated with BNAB for the factors f_f of ^{239}Pu.

The authors consider it a pleasant duty to express their gratitude to L. B. Pikel'ner, M. N. Nikolaev, and A. M. Tsibul' for useful discussions.

LITERATURE CITED

1. L. P. Abagyan et al., Grouped Constants for the Calculation of Nuclear Reactors [in Russian], Atomizdat, Moscow (1964).
2. Dermott E. Cullen and F. Ernest, Trans. Am. Nucl. Soc., 17, 490 (1973).
3. M. N. Nikolaev et al., At. Energ., 30, No. 5, 426 (1971).
4. B. Bemer, A. A. Van'kov, and Yu. V. Grigor'ev, Prib. Tekh. Eksp., 6, 57 (1974).
5. A. A. Bogdzel' et al., Communication of the Joint Institute of Nuclear Research 3-9012 [in Russian], Dubna (1975).
6. A. A. Van'kov et al., in: Nucl. Data for Reactors, 1, 559, IAEA, Vienna (1970).
7. R. Bramblett and J. Czirr, Nucl. Sci. Eng., 35, No. 3, 350 (1969).
8. J. Czirr and R. Bramblett, Nucl. Sci. Eng., 28, No. 1, 62 (1967).
9. R. Kidman and R. Schenter, Group Constants for Fast Reactor Calculations, HEDL-TME-71-36 (1971).
10. E. Menapace, M. Motta, and G. Panini, A 26-Group Library with Self-Shielding Factors for Fast Reactor Calculations with the UK Nuclear Data Files, RT/FI (73) 15 (1973).

WAVEGUIDE PROBING USED FOR THE DOSIMETRY OF BREMSSTRAHLUNG IN HIGH-CURRENT ACCELERATORS

Yu. P. Bakulin, A. P. Korotov Kikh, and N. N. Morozov

UDC 539.12.08

The development of experimental investigations in the bremsstrahlung fields of high-current accelerators is closely related to the development of dosimetry techniques which must have broad dynamic ranges from 10^3 to 10^{10} A/kg and a resolution of nanoseconds. Most widely employed are techniques based on luminescent and optical properties of solids [1-3] and semiconductor detectors [4] at dose rates below 10^7 A/kg [5-7].

In the last few years methods having an upper limit of the dynamic range at 10^{10} A/kg were proposed; these methods are based on direct-charge detectors [8], pyroelectric detectors of radiation [9], and bolometers. But the problem of developing methods with a metrological foundation and instruments for absolute measurements of the dose rate of ionizing radiations with high intensity was not solved because of the well-known difficulties encountered in calibrating the instruments.

Calibration in reference fields with a low dose rate (10^{-2} A/kg) and with a monoenergetic radiation spectrum, followed by the transfer of the units to the range of high dose rates, is most frequently employed. This technique does not allow to create a measuring system with errors consistuent with the requirements of practical applications.

The method: listed above are based on solid-state converters of the energy of the ionizing radiation, though when work is done in a field of pulsed photon radiation, the use of a material of low density (gas) is not less promising. It should be noted that the physical limit of the ionization technique is 10^{15} A/kg [10] but conventional ionization chambers allow measurements of the exposure dose rate of at most 10^2 A/kg with a resolution not greater than 10^{-5} sec.

Superhigh quality probing makes it possible to extend the dynamic range of the ionization technique to 10^9 A/kg with a resolution of nanoseconds [11, 12]. For measuring a dose rate in excess of 10^3 A/kg with a probing technique with a waveguide is most promising.

Absolute measurements of the dose rate with the aid of ionization techniques suggest that a volume of homogeneous sensitivity be employed. In our work we used a wall chamber in the form of a cylindrical 5-mm-thick radiator made from an air-equivalent plastic $(C_5H_8O_2)_n$ with an air-filled Bragg plane (height ~0.5 mm). The measuring waveguide had the form of a strip line of special design the conductors of which were distributed on flat surfaces enclosing a cavity. The conductors were in the form of an aluminum coating with a thickness of ~10 μm. In order to avoid an additional dependence related to the rigidity caused by the metal, a 20-30-μm-thick layer of the $(C_5H_8O_2)_n$ plastic was applied on top of the metallized coating. The dimensions of the detector did not exceed 50 × 10 mm.

The probing was made at 400 MHz so that at a ~120-nsec-long emission pulse, the fine structure of the pulse could be distinguished, that the hf noise generated during accelerator operation could be eliminated, and that long (~30 m) cables could be employed at relatively low losses of hf power in the measuring system.

The attenuation of the wave in the waveguide containing the ionizing gas was directly measured:

$$\eta(t) = \ln E_0/E(t),$$

where E(t) and E_0 denote the amplitude of the probing field at the output of the waveguide with and without plasma, respectively.

The attenuation $\eta(t)$ is related to the conductivity σ of the ionized air (conductivity averaged over the volume) by the formula

$$\eta(t) = \frac{2\pi L}{c}\sigma(t),$$

Translated from Atomnaya Énergiya, Vol. 48, No. 6, pp. 381-383, June, 1980. Original article submitted August 20, 1979.

0038-531X/80/4806-0386$07.50

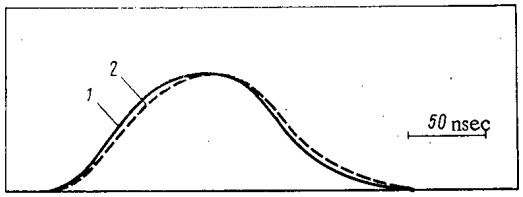

Fig. 1. Normalized oscillograms of the time dependence of the dose rate recorded with: 1) scintillation and 2) hf detectors.

TABLE 1. Comparison of the Results of Dose Measurements Made with the Ionization Technique (IT) and Thermoluminescence Technique (TT)

No. of expt.	Dose (P) per pulse		IT/TT	Ratio of peak ampls.
	IT	TT		
1	15,7	15,2	0,97	10,4
2	22,4	22,5	1,14	11,7
3	9,3	10,7	1,15	12,3
4	10,7	12,6	1,17	9,5
5	13,0	13,8	1,06	10,5
6	11,2	13,4	1,20	8,9
7	15,9	17,5	1,10	12,6
8	19,6	20,2	1,03	13,1
9	12,8	15,3	1,20	12,6
10	13,3	12,6	0,95	12,1

where L denotes the length of the plasma-filled waveguide.

It was shown in [12] that the conductivity of the air (conductivity defined by the usual constants such as the lifetime and the mobility of the electrons) depends upon the ionization I which, in turn, according to the Bragg–Grey theory, is related to the dose absorbed by the walls of the radiator:

$$D_\gamma = k\varepsilon S_{\text{rel}} I.$$

The notation is interpreted as follows: k, coefficient depending upon the system of units employed; ε, average energy of forming an ion in the gas filling the cavity; S_{rel}, linear stopping power of the radiator relative to the gas.

In the case of the air-equivalent $(C_5H_8O_2)_n$ plastic, $S_{rel} \approx 0.92$ and the dependence upon the rigidity did not exceed 15% at $E \approx 0.05$ MeV [13]. In the source of pulsed photon emission used in our experiments, the relative quantum yield was less than 10% at $E \leq 100$ keV [14] which implies an additional error of <4% in the measurements of the absolute values of the exposure dose rate.

The temporal resolution of the technique depends upon the lifetime of the conduction electron in the gas and amounts to $9 \cdot 10^{-9}$ sec in the case of air under standard conditions. The resolution can be improved by one order of magnitude by adding a small amount (~0.1%) of sulfur hexafluoride to the air. In this case the upper limit of the dynamic range is improved by one or two orders of magnitude. It appears unsuitable to employ larger quantities of SF_6 because even at a partial pressure of the order of several hundred Pascals, the capture of electrons by the molecules reaches saturation [15], as confirmed by preliminary experiments made on linear electron accelerators.

Two identical chambers were employed in our experiments: one was filled with dry air under normal pressure, the other with a mixture of air and SF_6 (partial pressure of air and SF_6: $1.01 \cdot 10^5$ and $1.33 \cdot 10^2$ Pa, respectively).

The results of measuring the dose rate with the ionization technique were compared with readings of integral thermoluminescent LiF dosimeters, and the shape of the dose rate curve with the shape of the pulse appearing at the output of a scintillation detector (see Fig. 1). A broadband S8-12 oscilloscope with a bandwidth of 50 MHz was used to record the pulsed component of wave attenuation in the waveguide. The results of the measurements are listed in Table 1. The ratio of the peak values of attenuation in air and the corresponding attenuation in a gas mixture (gas + SF_6) are listed in the last column.

The discrepancy of the results obtained with the ionization technique and the thermoluminescence technique does not exceed 20%. The readings obtained with the air-filled chamber differ from the readings of the same chamber filled with a mixture of gas and SF_6 by more than one order of magnitude. The spread of the ratio of the peak values of attenuation seems to be associated with gradients of the field of photon radiation and the errors made in the measurement of the voltage pulsed.

The errors of the technique depend mainly upon the errors of the known values of the constants (lifetime and mobility of the conduction electrons), and upon the errors of the instruments used to measure the nanosecond voltage pulse. In the experiments the error of measuring the voltage pulsed did not exceed 10%. The lifetime of the electrons in air was experimentally measured with an error of 15% [16]. In [17] the effective mobility of the electrons was determined in air and the values obtained agree within a 5% limit with the values listed in [18]. This means that there is reason to assume that the total error made in the determination of the absolute dose rate does not exceed 30%.

LITERATURE CITED

1. M. M. Grube et al., Izv. Akad. Nauk Latv. SSR, Ser. Fiz. Tekh., Nauk, No. 4, 55 (1967).
2. I. A. Bochvar et al., At. Energ., 15, No. 3, 48 (1963).
3. K. K. Schwarz, Thermoluminescence Dosimetry [Russian translation], Atomizdat, Moscow (1967).
4. Z. A. Al'bikov, A. I. Veretennikov, and O. V. Kozlov, Detectors of Pulsed Radiation [in Russian], Atomizdat, Moscow (1978).
5. E. Tochilin and N. Goldstein, Health Phys., 12, 1705 (1966).
6. I. A. Bochvar et al., A Method of IKS Dosimetry [in Russian], Atomizdat, Moscow (1977).
7. Z. A. Al'bikov et al., Prib. Tekh. Eksp., No. 1, 58 (1977).
8. G. V. Kulakov et al., Metrologiya, No. 5, 69 (1974).
9. L. S. Kremenchugskii and R. Ya. Strakovskaya, At. Energ., 41, No. 3, 190 (1976).
10. B. Michael, Proc. IAEA Symp. "Sterilization by Ionizing Radiation," Vienna (1974), p. 270.
11. Yu. A. Medvedev et al., At. Energ., 40, No. 1, 53 (1976).
12. Yu. A. Medvedev, N. N. Morozov, and B. M. Stepanov, At. Energ., 45, No. 5, 374 (1978).
13. M. Frank and V. Stolz, Solid-State Dosimetry of Ionizing Radiation [Russian translation], Atomizdat, Moscow (1973), p. 62.
14. E. A. Abramyan et al., Prib. Tekh. Eksp., No. 3, 223 (1971).
15. N. S. Bugel'nikova, Zh. Eksp. Teor. Fiz., 35, No. 5, 1119 (1958).
16. G. L. Kabanov et al., Zh. Tekh. Fiz., 43, No. 6, 1275 (1973).
17. V. N. Kapinos and N. N. Morozov, in: Problems of Metrology and Techniques of Optical Measurements in Physics [in Russian], Standartov, Moscow (1975), p. 48.
18. V. Gilinsky, Phys. Rev., 137A, 50 (1965).

A METHOD FOR DETERMINING ISOTOPE COMPOSITION BY COULOMB EXCITATION OF NUCLEI

V. N. Bugrov, V. V. Kamanin, and S. A. Karamyan

UDC 539.183.2

Many physical methods for the analysis of a substance are known [1-3]. Of considerable importance among these are nuclear-physics methods, based on a knowledge of the specific properties of the nuclei of elements and isotopes. Investigators have developed many variants of analysis methods specially designed to determine a particular element. The advantage of a method for determining a specific element is its selectivity, increasing the reliability of the determination, but such methods are not universal. The most widespread method is that of neutron activation analysis, designed for determining a large number of elements by choosing special conditions for each of them or for certain groups of elements. An even more universal method is of x-ray fluorescent analysis. The possibilities of using these and some other nuclear-physics methods of element analysis to determine the isotope composition of a substance are limited. For isotopic analysis we can use only a method based on a physical process which indicates all the stable isotopes of a given element and differentiates between them. These requirements are fairly special, and therefore nuclear methods of isotopic analysis have been developed only for a small number of elements. The methods most widely used for isotopic analysis are mass-spectrum methods based on taking samples which are chemically treated and are completely used up during the analysis.

The purpose of the present study is to propose a relative instrumental method [4] of isotopic analysis suitable for many elements, and in some cases also suitable for element analysis based on the process of Coulomb excitation of nuclei. We describe below an experiment testing the method in the special case of the analysis of a single-crystal tungsten target made of a substance enriched in the isotope ^{186}W, using a beam of accelerated ions of ^{40}Ar. The use of a beam of heavy ions limits the possibility of applying the proposed method, since a heavy-ion accelerator has not yet become a common piece of apparatus in an analytical laboratory. However, it has now been shown to be possible to accelerate heavy ions with currently available equipment, in particular moderate-sized equipment such as U-120 cyclotrons and tandem generators. On the other hand, the need for isotopic analysis usually arises only in the solution of special problems of scientific or applied research. Therefore the number of capabilities of devices that can accelerate heavy ions are sufficient for the isotopic analysis of elements by using the proposed method.

Physical Bases of the Method. It is known [5] that the measurement of the absolute probability of exciting with heavy ions the nuclei of some stable isotope contained in the target in a known proportion leads to the determination of the nuclear characteristic of the isotope – the reduced probability of electromagnetic transition of the nucleus from the ground state to an excited level. In the concrete case of the excitation of the first level 2^+ in an even–even nucleus the yield of γ quanta in the Coulomb excitation reaction is connected with the reduced probability of transition B (E2, $O^+ \rightarrow 2^+$) by the following relation:

$$N_\gamma(2^+ \rightarrow 0^+) = \frac{1.802 \cdot 10^{10} K B(E2, 0^+ \rightarrow 2^+) A, Q}{A_2 Z_2^2 (1 + A_1/A_2)^2} \frac{\int_0^{E_{max}} (E - \Delta E') \sqrt{E} f(\xi) dE}{(dE/d\rho x)|_{E_0} \sqrt{E_0} Z_i}, \quad (1)$$

where K is the relative amount of the given isotope in the target; A_1, A_2, mass numbers of the particle and target nuclei; Z_2, ordinal number of the target nucleus; Z_i, ion charge; Q, integral of the ion current in μC; $(dE/d\rho x)|_{E_0}$, specific losses of the particle in the target material for an initial energy E_0, MeV/mg · cm^2; $\Delta E' = (1 + A_1/A_2) \cdot \Delta E$, ΔE, energy of the observed transition, MeV; $f(\xi)$, Coulomb excitation function [5].

If the cross section of Coulomb excitation is large, we must use the theory of multiple Coulomb excitation [6], in which the cross section of excitation of each level depends on the set of reduced probabilities of the electromagnetic transitions between the various levels of the nucleus.

Translated from Atomnaya Énergiya, Vol. 48, No. 6, pp. 383-385, June, 1980. Original article submitted May 14, 1979.

0038-531X/80/4806-0389$07.50

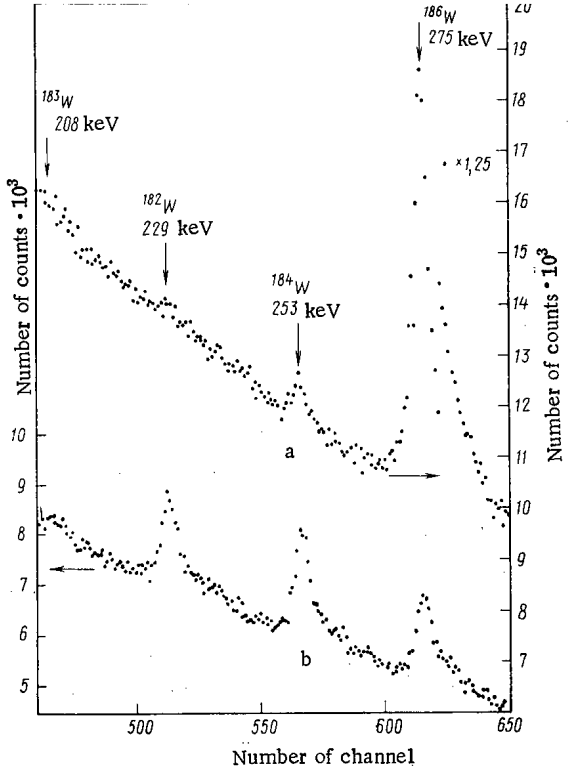

Fig. 1. γ spectra of the investigated target (a) and the standard target (b).

In the inverse formulation of the problem, the measurement of the cross section of Coulomb excitation of the levels of the nucleus for which the determination is being made and the theoretical analysis of the result obtained by means of formula (1) or more complicated formulas make it possible to find the absolute number of nuclei being determined in the target. However, such a formulation of the problem assumes absolute measurements of the efficiency of the apparatus, the ion-beam current, the retardation losses of the ions in the material in the case of a thick target, etc., and also absolute calculations of the probability of the Coulomb excitation reaction.

In the present study the process of Coulomb excitation of nuclei was used for determining the isotope composition of a specimen in relative measurements by comparison of the γ spectra of Coulomb excitation of the target being investigated and a similar target with a natural isotope composition. We denote the natural isotope content by the sequence of symbols P_i, subject to the condition $\Sigma P_i = 1$, with P_i' and $\Sigma P_i' = 1$ in the specimen being investigated, and we denote the number of recorded γ quanta belonging to the various isotopes i in the γ spectra of the Coulomb excitation by N_i and N_i' for the standard and investigated target, respectively. It is not difficult to determine that the desired values of P_i' can be expressed in terms of the known values P_i and the measured values N_i and N_i' as follows:

$$P_i' = N_i' P_i / N_i \sum_{i=1}^{n} N_i' P_i / N_i, \qquad (2)$$

where n is the number of isotopes of the element being investigated. The accuracy of the determination of the amount of the isotopes P_i' present depends on the experimental accuracy of the measurement of N_i and N_i' and the accuracy of the tabulated values of the natural isotope content, P_i.

Formula (2) contains the results obtained by relative measurement for the standard and investigated targets. It is readily seen that formula (2) does not require an absolute connection between these measurements, since the ratio N_i'/N_i occurs twice in it. In the experiment we need only observe the conditions that ensure equal ratios of the probabilities of Coulomb excitation and recording of γ radiation for different isotopes in the two measurements. These requirements include constant energy in the ion beam, uniform distribution of the investigated isotopes through the thickness of the target, and identical variation of the efficiency of recording of γ rays as a function of energy for the two measurements. We can have different geometric

efficiencies of recording, and we do not need to know the ratio of the integral fluxes of particles to the target in the two measurements.

Even more important, for determining the isotope content in this case we do not need to know the reduced probability of electromagnetic transitions in the nuclei being investigated. All of these facts improve the accuracy of the result and reduce the labor involved in handling the experimental data.

Experiment and Results. The method was tested in an experiment designed to determine the isotope composition of a single crystal of tungsten enriched in ^{186}W. A single crystal was used in experiments to measure the lifetimes of the constituent nuclei by means of the shadow effect [7]. The standard used was a single crystal with a natural mixture of tungsten isotopes.

The standard and investigated targets were irradiated for several hours in the U-300 cyclotron of the JINR Nuclear Reactions Laboratory by means of a beam of ^{40}Ar ions having an energy of 135 MeV, after it had passed through retarding foils, at a current of ~1 nA on the target. The γ-ray spectrum of the Coulomb excitation was recorded by means of a semiconductor Ge(Li) detector which had a volume of 37 cm^3, with an energy resolution of 2.0 keV (on the basis of the ^{57}Co lines). The detector was placed 3 cm from the target. Figure 1 shows the γ spectra for the investigated and standard targets. The identification of the γ lines in the spectrum was made by using the tabulated nuclear-spectroscopy data of [8]. The spectra do not contain any γ peak for ^{180}W because the amount of this isotope even in a natural mixture is 0.135%, which is less than the sensitivity of the measurement, determined from the statistical error. Consequently, the value given below signifies the limit of sensitivity of the method.

The percentage composition of the isotopes in the single crystal investigated, obtained by processing of the experimental results and calculation by formula (2), is the following: $(0.02 \pm 0.35)\%$ for ^{180}W, $(0.73 \pm 0.40)\%$ for ^{182}W, $(1.3 \pm 1.0)\%$ for ^{183}W, $(3.75 \pm 0.75)\%$ for ^{184}W, and $(94.2 \pm 2.5)\%$ for ^{186}W. From these results it can be seen that the minimum level of an isotope that can be determined under the specific conditions of the experiment is ~0.5%.

Besides the above-described advantages of this relative instrumental method of analysis, we should also mention the absence of activation of the specimen (since the ion energy is lower than the Coulomb barrier of nuclear interaction) and the possibility of analyzing substances having different chemical forms and mechanical states.

One of the limitations of the use of this method is the fact that its limiting sensitivity becomes insufficient for elements whose nuclei are characterized by a low reduced probability of electromagnetic transitions. Among such nuclei are, e.g., spherical nuclei which are almost doubly magic. The method is also ineffective for the analysis of light elements, since the cross section of Coulomb excitation is proportional to $(Z_1Z_2)^2$, where Z_1 and Z_2 are the atomic numbers of the nuclei of the target and of the bombarding particle. However, if we use ^{40}Ar or heavier ions as the bombarding particles, the cross section of the Coulomb excitation reaction becomes large enough for practically all elements, except for the lightest elements and those with magic Z (tin, lead). In addition to isotope composition, the above-described method can also be used for determining the element composition of mixtures, alloys, or chemical compounds, provided that the atomic numbers of all the components of the mixture do not differ by too much (for a correct choice of the particle energy with respect to the Coulomb barrier of all the nuclei) and that each component has at least one isotope whose Coulomb excitation cross section is sufficiently large.

The authors are grateful to Yu. A. Aleksandrov for his comments on the results obtained.

LITERATURE CITED

1. H. Bowen and A. Gibbons, Radioactivation Analysis [Russian translation], Atomizdat, Moscow (1968).
2. B. G. Egizarov, L. A. Korytko, and Yu. P. Sel'dyakov, Measurement Techniques in Instrumental Neutron Activation Analysis [in Russian], Atomizdat, Moscow (1972).
3. V. T. Tustanovskii, Evaluation of the Accuracy and Sensitivity of Activation Analysis [in Russian], Atomizdat, Moscow (1976).
4. V. N. Bugrov, V. V. Kamanin, and S. A. Karamyan, Byull. OIPOTZ, No. 14, 157 (1978). Inventor's Certificate No. 602835.
5. K. Alder et al., in: Deformation of Atomic Nuclei [Russian translation], L. A. Sliv (editor), IL (1958).
6. I. Ya. Berson, Izv. Akad. Nauk LatvSSR, Ser. Fiz. Tekh. Nauk, 6, 3 (1965); 1, 3 (1965); I. Berson, Nucl. Phys., 67, 296 (1965).
7. V. V. Kamanin et al., Yad. Fiz., 16, 447 (1972).
8. C. Lederer, J. Hollander, and I. Perlman, Table of Isotopes, Wiley (1967).

MODELS FOR E_1 CENTER ACCUMULATION IN QUARTZ IN URANIUM ORE

B. M. Moiseev and M. V. Petropavlov

UDC 539.12.08

It has been shown [1-4] that paleodosimetry can be used in combination with geological and geochemical studies in locating and studying uranium deposits. The main objects of the method are to examine the migration of uranium and to estimate the age of the ore by measuring the E_1 center concentration (C_E) for quartz. Here we use various models for the distributions of the quartz grains and uranium mineralization in the ore in the calculation of the E_1 center concentration due to α and γ rays from the uranium.

The calculations can be checked for small values of the dose, when the time decay of C_E is unimportant, i.e., when there is a linear relationship between the concentration and the time of contact between the quartz and the uranium mineralization [2].

Here we consider the accumulation of the dose in quartz in sedimentary ores containing finely divided and uniformly distributed uranium minerals. The following models have been used in calculating the α-particle flux.

1. For uranium mineralization of this type in sandstone we use the following model: a quartz grain (sphere of radius radius R) is surrounded by a film of thickness l. Then with $l \ll 2R$ we can assume that we have a film emitting α particles at the surface of a planar detector. The formulas of [5] can then be used.

Under conditions of radioactive equilibrium, nuclides in the uranium series emit eight α particles [6], and the α-particle flux N at the quartz grain is

$$N = 3 \cdot 10^6 C_U / 100\% \, (m_1 + m_2) \, [1 - (l/2R_\alpha)], \tag{1}$$

where C_U is the mass proportion of uranium in %; m_1, mass of the quartz grain; m_2, mass of the intergranular material; and R_α, α-particle range in the intergranular material.

As $m_1 = 4/3\pi R^3 \rho_{qu}$; $m_2 = 4\pi R^3 \, (l/R + l^2/R^2 + l^3/3R^3)\rho$, where ρ is the mean density of the intergranular material, we have that the concentration of radiation defects C_E due to the α particles acting on the quartz grain is

$$C_E = 1.6 K C_U t 10^{10} \left(1 - \frac{l}{2R_\alpha}\right) \left[1 + 3 \frac{\rho}{\rho_{qu}} \left(\frac{l}{R} + \frac{l^2}{R^2} + \frac{l^3}{3R^3}\right)\right] \text{ spins/g.} \tag{2}$$

In (2), K is the radiation sensitivity of the quartz, i.e., the number of radiation defects (E_1 centers) formed by the absorption of one α particle, while t is the time of contact in years between the quartz and the uranium mineralization. For example, for K = 0.2, C_U = 1%, l = 10 μm, R_α = 27 μm, ρ = 2.9 g/cm^3, ρ_{qu} = 2.6 g/cm^3, we get $C_E/t \approx 100$ spins/g · sec.

2. The following model is used for uranium mineralization in a quartz–feldspar rock: the detectors (quartz grains) are in a mineral conglomerate in which uranium is uniformly distributed, with the layer thickness greater than the α-particle range in the medium. The elementary α-particle flux dN from a spherical layer of thickness dx at a distance x (x > R) from the center of the quartz grain is the following at the quartz grain itself:

$$dN = \frac{3x^2 \, dx \nu_0}{(R + R_\alpha)^3 - R^3} (1 - \cos\alpha), \tag{3}$$

where R_α is the α-particle range in the medium; ν_0, total number of decays in the layer of thickness R_α; and 2α, solid angle within which lies the detector (quartz grain) and whose vertex lies at any point in the layer of thickness R_α.

Translated from Atomnaya Énergiya, Vol. 48, No. 6, pp. 386-387, June, 1980. Original article submitted August 22, 1978.

0038-531X/80/4806-0392 $07.50

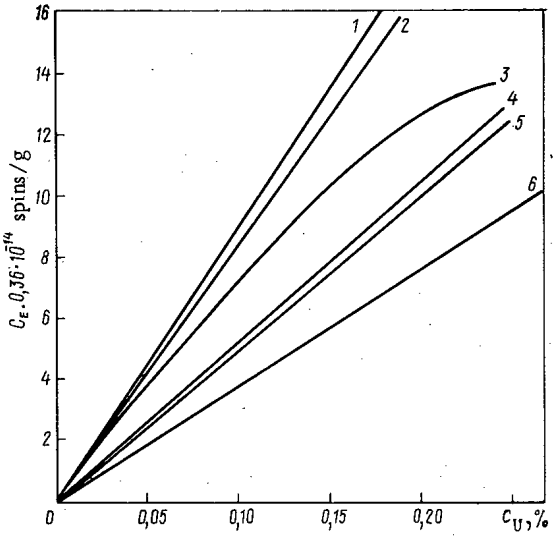

Fig. 1. Observed relation between C_E and mass proportion of uranium C_U for various models: 1) complete absorption of all α particles; 2) result from measurement of flux with an α radiometer; 3) result from ESR measurement; 4) uniform distribution of quartz grains in emitting medium; 5) model for quartz bearing a film of thickness 10 μm; 6) uniform distribution of α-ray sources in a medium with average density ρ_{av}.

We calculate the α-particle flux at the quartz grain and transform the equation to get a formula for the radiation-defect concentration:

$$N = \frac{3}{4}\frac{v_0 R^2 R_\alpha}{[(R+R_\alpha)^3 - R^3]}; \quad C_E = 2{,}3\cdot 10^{10}\frac{K\rho C_U R_\alpha t}{\rho_{qu} R}\left(\frac{m_1}{m_2}+1\right) \text{ spins/g}. \tag{4}$$

With the condition of (2) we get for a quartz content in the rock of about 70% $C_E/t \approx 140$ spins/g · sec.

3. The model with uniform distribution of the α-ray sources in a medium with a certain average density ρ_{av}, which is dependent on the proportion of quartz. If the quartz is uniformly distributed in the medium and the mean α-particle range is R_α, the quartz effectively absorbs a fraction l_1/R_α of all the α particles, where l_1 is the part of the α-particle range in the quartz, $l_1 \approx R\alpha[1 + (\rho_{qu}/\rho)(m_2/m_1)]^{-1}$; the concentration is then given by the formula

$$C_E = \left(3C_U Kt \Big/ 1 + \frac{\rho qu}{\rho}\frac{m_2}{m_1}\right) 10^{10} \text{ spins/g}. \tag{5}$$

The condition of (2) gives $C_E/t \approx 150$ spins/g · sec.

The correctness of the results obtained from these theoretical models was evaluated by measuring the actual α-particle fluxes; there was good agreement between theory and experiment. The C_E were measured for ores by ESR methods, and these are given along with the values calculated from the models in Fig. 1.

The ESR data for quartz need to be corrected from estimation of the contribution of the γ rays to C_E. In the above models, the main proportion of the radiation dose comes from the α particles. For example, for the limiting case corresponding to model 1 and film thickness equal to the α-particle range, i.e., with the maximum self-absorption of the α particles in the conglomerate and absorption of all the γ rays by the quartz we get from (2) that the energy absorbed by the quartz from the α particles with E = 5 MeV is $5.3 \cdot 10^{-18}$ J/g (mass proportion of uranium 0.7%). Under the same conditions, the γ-ray energy absorbed by the quartz (along with the contribution from the β particles) is $1.6 \cdot 10^4$ J/g.

Experiment shows that $C_{E(\alpha)}/D = 0.24 \cdot 10^{12}$ spins/J and $C_{E(\gamma)}/D = 0.31 \cdot 10^{12}$ spins/J, where D is the radiation dose.

For these data we get

$$C_{E(\alpha)} = 1.3 \cdot 10^{16}\ ; \qquad C_{E(\gamma)} = 0.5 \cdot 10^{15}\ \text{spins/g}.$$

The inequality becomes stronger in the other cases. The α particles also produce most of the E_1 centers in previously thermally activated specimens, since for such a specimen $C_{E(\alpha)}$ increases on average by a factor 1.1, while $C_{E(\gamma)}$ increases by a factor 4.5.

LITERATURE CITED

1. Ya. M. Kislyakov et al., Geol. Rudn. Mest., 15, No. 3, 86 (1975).
2. B. M. Moiseev and L. T. Rakov, Dokl. Akad. Nauk SSSR, 233, No. 4, 679 (1977).
3. K. G. Korolev et al., Izv. Akad. Nauk SSSR, Ser. Geol., No. 4, 74 (1977).
4. A. M. Danilevich and V. V. Pavshukov, Abstracts for the Second All-Union Radiogeochemical Conference [in Russian], Dushanbe, Izd. Akad. Nauk SSSR, AN Tadzhik SSR i Min. Geol. SSSR, Dushanbe (1975), p. 215.
5. V. I. Ivanov, Textbook on Dosimetry [in Russian], Atomizdat, Moscow (1970).
6. L. V. Gorbushina et al., Radiometry and Nuclear Geophysics [in Russian], Nedra, Moscow (1974).

THREE-DIMENSIONAL CALCULATIONS OF A HETEROGENEOUS REACTOR

B. P. Kochurov and V. M. Malofeev

UDC 621.039.51.12:539.125.52

An efficient method of calculating a heterogeneous reactor, called by the author the quasialbedo method, was proposed in [1] and developed further in [2] for three-dimensional problems. A more direct approach was used in [3] to obtain the approximate equations of a heterogeneous reactor in difference form. It is shown in the present note that by expanding in a Fourier series in the axial variable, the generalization of the equations in [3] to the three-dimensional case is elementary. Some results of the calculations are presented.

Suppose the solution in the moderator of a reactor of height H with slugs which are nonuniform vertically is given by the expansion

$$N(r, z) = \Sigma N_n(r) \sin \alpha n z, \quad \alpha = \pi/H, \quad r \equiv (x, y). \tag{1}$$

The coefficients $N_n(r)$ satisfy the equations

$$\Delta N_n^g(r) - (\xi_g + \alpha^2 n^2) N_n^g(r) = -\xi_{g-1} N_n^{g-1}(r), \tag{2}$$

so that the form of the general solution is similar to that for the two-dimensional case [3] (notation same as in [3]):

$$N = C\mathcal{F}A; \quad \mathcal{F} = \operatorname*{diag}_k \operatorname*{diag}_n \{K_0(\varkappa_n | r - r_k|)\}, \quad \varkappa_n^2 = \xi_g + \alpha^2 n^2. \tag{3}$$

Assuming that in the boundary condition on the surfaces of the slugs

$$\rho(\partial N/\partial \rho) = \Lambda N \tag{4}$$

the matrix Λ depends on z, multiplying (4) by $\sin \alpha$ mz and integrating with respect to z, we obtain an equation of the form of (4) in which the properties of the slugs are characterized by the matrices

$$\Lambda_{k,\,mn} = \Lambda^c_{k,\,m-n} - \Lambda^c_{k,\,m+n};$$
$$\Lambda^c_{k,\,l} \equiv \frac{\alpha}{\pi} \int_0^{\pi/\alpha} \Lambda_k(z) \cos \alpha l z \, dz. \tag{5}$$

Equations (3) and (4) have the same form as in the two-dimensional case, and the procedure used in [3] to determine the equations in difference form

$$(P + R\gamma_2) N = (P I_0^{-1} K_0 + R)(\gamma_1/\lambda) N \tag{6}$$

is completely applicable to them. The parameters of the difference scheme are determined, as in [3], by the numbers $\varkappa_n a$, where a is the lattice pitch.

We note certain properties of the scheme presented: the operators P and R are diagonal with respect to the number of the vertical harmonic; the interaction of the harmonics is contained in the γ (or Λ) matrices, and in view of the representation (5), the required storage increases linearly with the number of harmonics. In Eqs. (6) the number of harmonics can be chosen differently for different slugs; in particular, their number can be increased in certain regions with local inhomogeneities. The use of a Fourier expansion provides sufficient flexibility to take account of a relatively small change in position of control rods (CR). If the computational net has large steps along the vertical, the quasialbedo method [2] apparently encounters some difficulties.

Figure 1 shows the character of the convergence of the energy distribution along a fuel channel adjacent to a partially inserted CR as a function of the number of harmonics. A heavy water reactor with a hexagonal lattice (Fig. 2) having channel parameters typical of the KS-150 reactor [4] was chosen as a model. Table 1 shows that a small number of harmonics suffices for the sufficiently accurate calculation of such integral reactor characteristics as the neutron multiplication factor k_{eff}, the CR effectiveness ρ, the channel power

Translated from Atomnaya Énergiya, Vol. 48, No. 6, pp. 387-388, June, 1980. Original article submitted July 9, 1979.

0038-531X/80/4806-0395$07.50

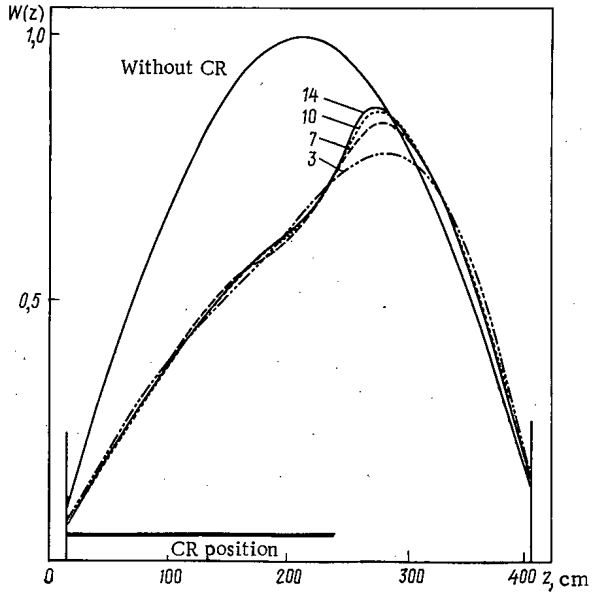

Fig. 1. Energy distribution along a fuel channel W(z) adjacent to a partially inserted CR as a function of harmonics of the neutron distribution (numbers on curves).

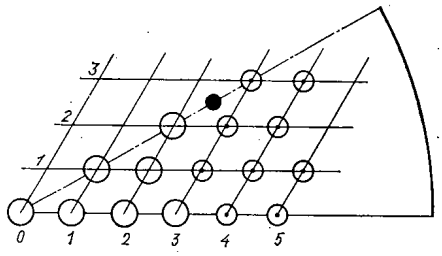

Fig. 2. Part of cartogram of reactor: ○, ⊙) fuel channels of central and peripheral regions: ●) partially inserted CR.

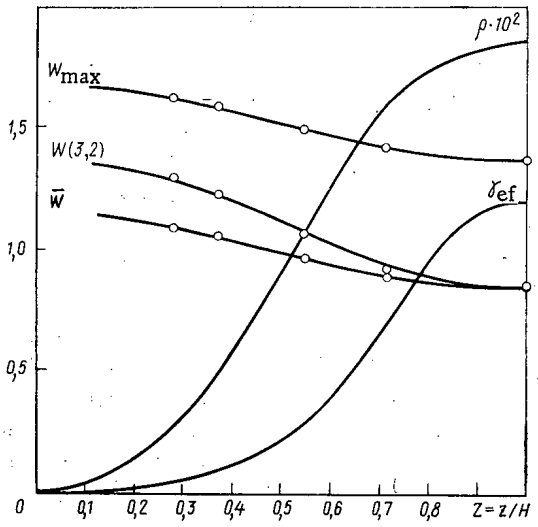

Fig. 3. Certain characteristics of the two-dimensional energy distribution in a reactor as a function of the relative depth of insertion Z of a CR; ρ) CR effectiveness; γ_{eff}) thermal constant of effective CR; $\overline{W}$, W_{max}, and W (3, 2)) average and maximum power of peripheral channel (3, 2) adjacent to a CR; ○) analogous values from calculation with effective CR.

TABLE 1. Characteristics of Reactor of Fig. 2 as a function of Number of Harmonics

Parameter	n				
	3	5	7	10	14
k_{eff}	1,04920 (0,083)*	1,04956 (0,049)	1,04978 (0,028)	1,04996 (0,010)	1,05007 (0)
ρ	0,0132 (6,9)	0,0128 (4,1)	0,0126 (2,4)	0,0124 (0,81)	0,0123 (0)
W (1,1)	1,784 (0,51)	1,781 (0,34)	1,779 (0,23)	1,776 (0,056)	1,775 (0)
W (3,2)	0,795 (0,87)	0,796 (0,75)	0,798 (0,50)	0,801 (0,12)	0,802 (0)
μ_z (1,1)	1,448 (0,34)	1,452 (0,07)	1,452 (0,07)	1,453 (0)	1,453 (0)
μ_z (3,2)	1,512 (8,9)	1,583 (4,6)	1,614 (2,7)	1,648 (0,66)	1,659 (0)
μ_c	1,217 (0,33)	1,216 (0,25)	1,215 (0,16)	1,214 (0,08)	1,213 (0)
μ_p	1,559 (0,32)	1,557 (0,19)	1,555 (0,06)	1,555 (0,06)	1,554 (0)

*Numbers in parentheses are % deviations from results of calculation with 14 harmonics.

over height $\bar{W}$, and the total coefficients of nonuniformity of the energy distribution in the central and peripheral zones $\mu_{c,p}$ with sufficient precision are calculated also for a small number of harmonics (see Table 1).

A highly accurate calculation of the energy distribution along the vertical, characterized by the coefficient of nonuniformity μ_z, requires a somewhat larger number of harmonics. The comparison of radial characteristics of the energy distribution shown in Fig. 3 illustrates the possibility of calculating two-dimensional distributions by replacing a partially inserted CR by a certain effective CR completely inserted into the reactor. The thermal constant γ_{eff} of the effective CR was selected from the condition of equal compensation of reactivity. In a number of cases the small differences of the characteristics of the radial energy distribution justify the use of two-dimensional calculations.

LITERATURE CITED

1. S. S. Gorodkov, Preprint IAE-2251, Moscow (1973).
2. S. S. Gorodkov and N. L. Pozdnyakov, Preprint IAE-2728, Moscow (1976).
3. B. P. Kochurov and V. M. Malofeev, At. Energ., 42, No. 2, 87 (1977).
4. V. M. Abramov et al., At. Energ., 36, No. 2, 113 (1974).

USE OF A LOW-ENERGY ACCELERATOR FOR ELEMENT ANALYSIS ON THE BASIS OF PROTON-EXCITED X RAYS

B. A. D'yachkov, G. V. Kazantsev, and V. Ya. Pavlov

UDC 543.53:537.531:621.3.038.625:546.53

In recent years the use of accelerated ions for the diagnosis of the surface of a solid has been given increased attention by investigators [1]. The development of diagnosis methods has been stimulated by the growing needs of science and technology in the structural and analytic investigations of materials. In particular, for the structural study of solid specimens and the element analysis of the composition of a material [1-5] ion-x-ray spectroscopy methods based on the use of x rays excited in a specimen accelerated ions have come into widespread use. In connection with this, charged-particle accelerators have come to be increasingly used for investigating specimens on the basis of the characteristic x rays induced by ions. Ion-x-ray spectroscopy methods are being used for monitoring environmental contamination, analysis of metals and alloys, analysis of surfaces, structural research on crystal specimens, element analysis of biological materials, etc.

In most studies devoted to the analysis of x rays excited by accelerated particles, the incident particles used are protons. Proton excitation, which ensures fairly low detection limit for the elements involved, is convenient because the x-ray spectra obtained are relatively simple and are analogous to the spectra excited by electrons or photons. Although even lower detection limits can be obtained in the case of excitation by heavy ions, the x-ray spectra in such cases are much more complicated and more difficult to interpret [2].

Coulomb interaction between accelerated protons and atomic electrons of the inner shells are characterized by ionization cross sections whose maximum for most elements is in the 2-10-MeV proton energy range [3]. However, the use of low-energy protons whose energies are of the order of several hundred kiloelectron volts [3-5] is of considerable practical interest. This is because low-energy ion accelerators are widely available and simple to service and have a fairly low detection limit, reaching 10^{-8}-10^{-9} g for thick specimens [5]. It should be noted that the less efficient ionization cross section of the atoms can be compensated in the case of irradiation with protons having energies of the order of several hundred kiloelectron volts by increasing the proton flux, thereby obtaining the same characteristic x-ray intensity as is provided by a beam of protons with energies of several megaelectron volts on an electrostatic generator [2]. The increase in the heating of the target because of the larger beam power can be reduced by cooling the specimen. Furthermore, as is known, ion irradiation gives rise to bremsstrahlung caused by secondary electrons, with energies of $E_X \leq (4m/M)E_1$, where E_X is the x-ray energy; E_1, proton energy; m and M, the masses of the electron and the proton, respectively. Therefore, the use of protons with energies of several megaelectron volts results in strong background radiation in the x-ray region (3-5 keV or less), which complicates the analysis of the elements on the basis of characteristic radiation lines lying in this region. When specimens are irradiated with low-energy protons, the background in this x-ray region is substantially lower. Because of the short flight path of the low-energy protons, it is possible to use them in analyzing surface layers from several microns to several angstroms thick. The analysis of such layers is of great interest, e.g., in the investigation of ion-implantation processes.

For the element analysis in the present study we used a low-energy (200-kV) linear accelerator and studied the possibility of analyzing light elements by using protons with energies of 175 keV. To do this, we a analyzed aluminum (K_α = 1.49 keV) and silicon (K_α = 1.74 keV) in binary alloys of aluminum and silicon with copper.

The experimental apparatus used in this study consists of a linear accelerator, a target chamber, and a detection system with the appropriate electronic equipment. The focused beam of accelerated protons, passing through an evacuated drift tube enters the target chamber. The drift tube cooled with liquid nitrogen is also a differential-evacuation tube which serves to improve the vacuum in the target chamber and prevent the migration of oil vapors from the vacuum system of the accelerator into the chamber (Fig. 1). The diaphragms

Translated from Atomnaya Énergiya, Vol. 48, No. 6, pp. 389-390, June, 1980. Original article submitted July 30, 1979.

0038-531X/80/4806-0398$07.50

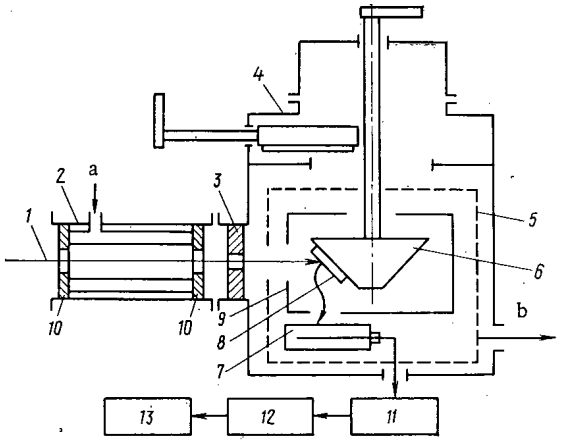

Fig. 1. Schematic diagram of target chamber and measuring equipment: 1) proton beam; 2) drift tube; 3) graphite diaphragm; 4) vacuum lock; 5) cooled screen; 6) target holder; 7) proportional counter; 8) target; 9) electron-delay diaphragm; 10) diaphragm; 11) preamplifier; 12) pulse analyzer; 13) information output unit; a) liquid nitrogen; b) evacuation.

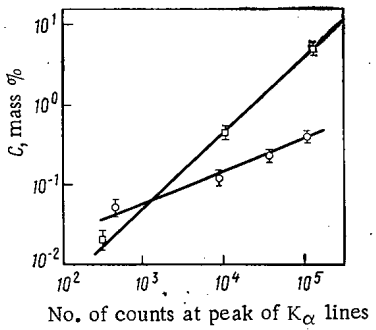

Fig. 2

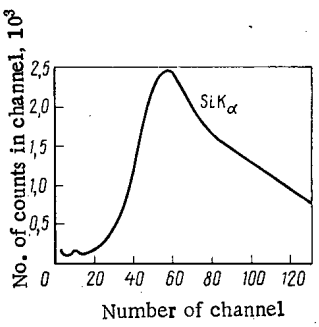

Fig. 3

Fig. 2. Calibration graph for determining the aluminum (□) and silicon (○) content of copper.

Fig. 3. X-ray spectrum 8 of copper–silicon alloy.

TABLE 1. Results of the Analysis of Specimens of Aluminum and Silicon with Copper

No. of specimen	Element being analyzed	Element content C, mass %	
		x-ray analysis	chemical analysis
1	Al	2,7±16 *	2,5±4 *
2		$2{,}7\cdot10^{-1}\pm22$	$2{,}8\cdot10^{-1}\pm10$
3		$2{,}4\cdot10^{-1}\pm26$	$2{,}4\cdot10^{-1}\pm10$
4		$2{,}5\cdot10^{-1}\pm20$	$2{,}0\cdot10^{-1}\pm10$
5		$1{,}6\cdot10^{-1}\pm19$	$1{,}1\cdot10^{-1}\pm10$
6	Si	$3{,}8\cdot10^{-1}\pm17$	$3{,}4\cdot10^{-1}\pm10$
7		$2{,}5\cdot10^{-1}\pm18$	$3{,}1\cdot10^{-1}\pm10$
8		$2{,}4\cdot10^{-1}\pm16$	$2{,}6\cdot10^{-1}\pm10$
9		$1{,}8\cdot10^{-1}\pm15$	$1{,}6\cdot10^{-1}\pm10$
10		$1{,}9\cdot10^{-1}\pm15$	$1{,}5\cdot10^{-1}\pm10$
11		$1{,}4\cdot10^{-1}\pm15$	$1{,}0\cdot10^{-1}\pm10$
12		$1{,}2\cdot10^{-1}\pm26$	$9{,}5\cdot10^{-2}\pm20$
13		$4{,}4\cdot10^{-2}\pm24$	$5\cdot10^{-2}\pm20$

*Here in relative %.

of the differential-evacuation chamber, which have an opening 10 mm in diameter, are at a distance of 100 cm from each other. In the stainless-steel target chamber the specimens can be heated to 400°C. The NORD-250 magnetic-discharge pump provides a working vacuum of $\sim 10^{-5}$ Pa in the chamber. Through a vacuum lock which makes it possible to place specimens under the proton beam and remove them from the chamber without disturbing the vacuum, we introduce into the target chamber a target holder capable of holding eight targets at one time. By rotating the target-holder shaft handle, we can place different specimens under the beam. Before hitting the target, the proton beam is collimated by means of a graphite diaphragm with a 3 × 8 mm opening. In order to prevent the deposition of oil vapors on the specimen, the target holder is surrounded by a screen cooled with liquid nitrogen.

The x rays in the target by the protons are recorded by an x-ray detector, which in our case was a sealed-off SRPO-12 proportional counter. The angle between the direction of the proton beam and the normal to the entry window of the detector is 90°, and the target is placed at an angle of 45° to both of these directions, in order to equalize the path lengths transversed in the specimen by the protons and the x rays recorded by the counter. The signal from the preamplifier output is transmitted to the input of a pulse-amplitude analyzer and then to the information output unit.

Flat specimens measuring 10 × 10 mm and 1-2 mm thick were cut from alloy ingots; before being placed in the target chamber, they were polished and washed with distilled water and rectified ethyl alcohol. As our calibration standards, we used specimens of analogous alloys subjected to careful chemical analysis. The specimens were irradiated for 5 min at proton-beam current of 0.1-0.25 μA. Figure 2 shows the calibration graph constructed from the standard specimens of alloys of copper with silicon and aluminum and used for analyzing the test specimens. As an illustration, we show in Fig. 3 part of the x-ray spectrum of specimen 8 of a silicon–copper alloy. The distortion of the shape of the Si K_α peak on the high-energy side of the spectrum is due to the effect of the x-ray background of the matrix of the specimen. It should be noted that the characteristic Cu K_α radiation (8.04 keV) is only 1/60 to 1/30 as intense as the Si K_α and Al K_α lines.

A comparison of the results of the chemical analysis and the analysis based on the characteristic x rays (see Table 1) indicates satisfactory agreement. We also estimated the detection limits C_{min} for aluminum and silicon in copper by the method described in [5]. We obtained the following values: $(9.5 \cdot 10^{-3} \pm 30)\%$ for aluminum and $(2.2 \cdot 10^{-3} \pm 30)\%$ for silicon. These estimates agree with the results of [5], which gave an estimate of the detection limits for elements in light matrices (carbon and silicon) and a heavy matrix (iron); they indicate that an efficient analysis of light elements is possible. It should be noted that in the analysis of medium to heavy elements on the basis of the L and M lines of the characteristic x-ray emission, as well as in an analysis in light matrices, it is possible to attain an even lower detection limit [5]. Thus, the use of low-energy accelerators enables researchers to conduct a fairly efficient quantitative element analysis on the basis of the characteristic x-ray emission excited by protons.

LITERATURE CITED

1. N. N. Petrov and I. A. Abroyan, Surface Diagnosis Using Ion Beams [in Russian], Leningrad State Univ. (1977).
2. M. A. Blokhin and S. M. Blokhin, Zavod. Lab., 43, No. 12, 1452 (1977).
3. R. Boro and S. Cipolla, Nucl. Instrum. Methods, 131, 343 (1975).
4. V. A. Arkhipovich et al., in: Apparatus and Methods of X-ray Analysis No. XV [in Russian], Mashinostroenie, Leningrad (1974), p. 92.
5. A. S. Akin'shin et al., At. Energ., 43, No. 1, 60 (1977).

INVESTIGATION OF THE PHONON CURRENT IN NEUTRON IONIZATION CHAMBERS

V. P. Ivanov, E. K. Malyshev,
R. A. Milovanova, A. A. Sysoev,
and P. N. Chistyakov

UDC 539.074.22:539.1.074.8

In order to monitor the neutron flux in control and protection systems of nuclear reactors, one widely employs ionization chambers with a solid boron radiator. At temperatures exceeding 300°C one observes in the chambers a phonon current increasing the lower limit of the flux which can be monitored. The goal of the present work is to establish the nature of this current.

Investigation of the Components Forming the Phonon Current. The experimental equipment had plane-parallel stainless-steel electrodes covered with a boron layer. In order to separate the electron and the ion components of the phonon current in vacuum of $\sim 10^{-6}$ mm Hg (1 mm Hg =133.3 Pa), the chamber was placed into the field of a permanent magnet, the field being directed parallel to the plane of the electrodes. The strength of the electric and magnetic fields, as well as the distance between the electrodes, were chosen so that, in the presence of a magnetic field, the electrons returned to the electrode from which they had been emitted, whereas ions of any mass, starting from H^+ and H^- (positive as well as negative ions), were incident on neighboring collector electrodes for charged particles and were recorded. When no magnetic field was applied, the electrons were also incident on the collector electrodes and the current generated by the electrons was recorded as part of the overall current. The results of the measurement made on the current with this instrument with and without magnetic field have shown that the contribution of the electrons to the total current is significant at 400°C, but that basically (by 70-90%) the current consists of positive and negative ions [1].

In neutron chambers the neighboring electrodes (cathode and anode) are of the same area and can become emitters of charged particles: the cathode emits negative ions and electrons, and the anode, positive ions. It is therefore difficult to determine the sign of the charge of the ions of which the current is mainly composed. An experiment for determining the sign of the charged particles was made with an instrument having coaxial cylindrical electrodes with a surface ratio of 0.01. Thus, the charged particles are supplied mainly by the outer electrode of significantly larger area.

Figure 1 shows the results of measuring at 100-400°C the current of the outer cylinder having an emitting surface of 500 cm^2. When the outer cylinder was positive and, hence, was an emitter of positive ions, the current was in the entire range higher than in the case of a negative outer cylinder, i.e., when negative ions and electrons were emitted from the cylinder. At 400°C the current of the positive ions amounted to $2.4 \cdot 10^{-8}$ A, and the current of the negative ions and electrons to $0.9 \cdot 10^{-8}$ A. When the average fraction of electrons in the total current is assumed as 20%, the current of positive and negative ions amounts to 70 and 10%, respectively. At lower temperatures, the current formed by the positive ions is even more important.

Investigation of the Ionic Component of the Phonon Current. In order to analyze the composition of the positive component of the phonon current, an ion source with surface ionization was developed [2]. High efficiency of ion collection is the characteristic feature of this source. A doublet of quadrupole lenses was placed into the source to the form the wedge-shaped beam required for normal operation of the analyzer. With this source the instrument had a resolution of 180 at the 10% level. The experiments were made on an MI-1309 mass spectrometer with an SI-03 ion counter; in combination with the ion source developed, at a fixed mass ion current of up to 10^{-18} A could be recorded. At 400-600°C the ions originated from the surface of the boron layer applied to a stainless-steel plate. The ions separated from the surface of the plate were focused by the field generated by the electrode system of the ion source and were then directed into the magnetic analyzer. A first measurement of the ion current was made from a stainless-steel plate 5 h after the plate had been heated to 400°C. When the spectra of the ions emitted from the plate at that temperature were measured, lines corresponding to potassium and sodium ions were observed.

Translated from Atomnaya Énergiya, Vol. 48, No. 6, pp. 391-392, June, 1980. Original article submitted August 20, 1979; revision submitted December 13, 1979.

0038-531X/80/4806-0401$07.50

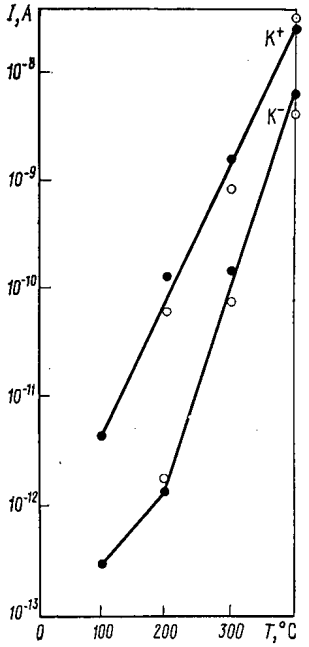

Fig. 1

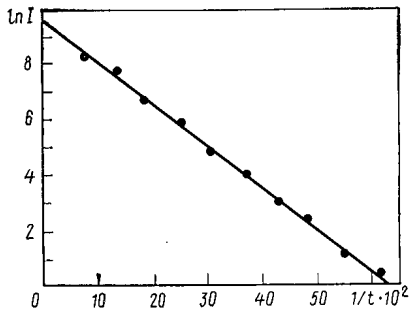

Fig. 2

Fig. 1. Temperature dependence of the current for the components of the phonon current; the components were created by charged carriers with positive (K^+) and negative (K^-) charges after heating for 30 (●) and 50 (○) h. Voltage: 300 V.

Fig. 2. Time dependence of the current of the K^+ ions (● – experimental results).

The basic results were obtained with a boron-coated plate. After 5 h heating at 400°C, the temperature of the plate was increased to 600°C, and a considerable number of lines was obtained; lines corresponding to ions with mass 87 (current $3.6 \cdot 10^{-12}$ A) and 85 (current $1.6 \cdot 10^{-13}$ A) predominated. It seems that those lines must be ascribed to heavy hydrocarbons resulting from surface ionization of the molecules of the organic matter composing the residue of the binder which was used when the boron layer was applied to the substrate. One can assume that upon heating the layer, the hydrocarbon molecules decompose in the layer in the presence of boron and the substrate material and are partially evaporated as ions into the vacuum. After 25 h heating the plate in vacuum at 400°C, the lines corresponding to ions of masses 87 and 85 had disappeared in the spectrum measured at 600°C.

Lines corresponding to masses 39 and 41 were the main lines of the spectrum; these lines must be ascribed to potassium isotopes. The intensity of the ^{39}K line was 10^{-12} A. Furthermore, extremely weak lines corresponding to ions with masses 75, 77, and 155 and caused by hydrocarbon ions were observed.

When the temperature of the plate was reduced to 400°C, it was observed that the intensity of the potassium lines decreased sharply: the ^{39}K line had an intensity of $2 \cdot 10^{-14}$ A. Lines of ions of masses 75, 77, and 115 were missing in the spectrum. Thus, when the plate with the boron coating is heated, heavy hydrocarbon ions are most intensively liberated at the beginning; after that, lines corresponding to ions of the potassium isotopes become most important in the spectrum and a noticeable current is produced by these ions even at 400°C. It should be noted that the current of the K ions depends entirely upon the temperature of the substrate and is independent of the conditions of heating, because the K^+ current results from the presence of potassium in the form of an admixture to the substrate material and, during the heating, atoms of this element are transferred to the surface of the boron by bulk diffusion and are then ionized [3].

Influence of the Diffusion Processes upon the Phonon Current. When the emission of K^+ ions from the surface of the boron applied to a stainless-steel substrate was investigated, a significant nonstationary time dependence of the process was observed. At the beginning, the increase in the temperature of the emitter was accompanied by a sharp increase in the emission of K^+ ions as a consequence of the temperature dependence of the ion emission according to the Saha–Langmuir formula for ionization from a surface [4]. In this case,

potassium ions were emitted from a part of the substrate surface not coated with boron. It was found in a microscopical inspection of the substrate that the area of the "spots" amounted to 5-10% of the entire emitter area.

When the emitter temperature is kept constant, a change in the K^+ current as a function of time is observed. The further increase in the emission at constant temperature of the substrate results from a change in the work function in the course of time, the diffusion of potassium from the bulk of the substrate through the boron film on its surface, the evaporation of boron from the surface, which leads to an increase in the area of "spots" on the emitter surface not coated with boron, and from other processes.

When the time dependence of the potassium ion current is taken into consideration, one can neglect the influence of the boron evaporation from the surface. During the characteristic time within which the K^+ current changes (22 min), the work function cannot substantially change and cause a significant (about two orders of magnitude) increase in the K^+ current. Experiments with substrates of stainless steel and molybdenum without a coating have confirmed the above conclusion. The emission of potassium ions from such emitters was not time dependent.

Estimates of the rate of diffusion of potassium through the boron indicate for the given conditions that the time dependence of the K^+ emission is determined by the latter process when a coating is present on a stainless-steel substrate. This dependence is shown in Fig. 2 for the following experimental conditions: emitter temperature 870°C, film thickness 1 μm. The dependence $\ln I = f(1/t)$ is a straight line; the coefficient of potassium diffusion in boron was determined from the slope of this line relative to the ordinate axis and was equal to $1.7 \cdot 10^{-11}$ cm^2/sec.

Conclusions. Investigations of the photon current in neutron ionization chambers have shown that the main contribution stems from positive ions. Investigations made with the mass spectrometric technique to determine the composition of those ions have led to the conclusion that a significant portion of the ions emitted from a surface which had been heated for 5 h are hydrocarbon ions. This is a consequence of the ionization of the molecules of the material of which the residue of the binder is composed. Prolonged heating (25 h) makes it possible to eliminate hydrocarbon lines from the mass spectrum. However, the spectrum still comprises lines resulting from the current of the K^+ ions which determine the lower limit of the phonon current in neutron chambers.

LITERATURE CITED

1. B. P. Ivanov et al., in: Abstracts of the Reports of the 17th All-Union Conference of Emission Electronics [in Russian], LIYaF, Leningrad (1978), p. 76.
2. V. P. Ivanov et al., Prib. Tekh. Eksp., No. 4, 196 (1978).
3. V. P. Ivanov et al., in: Abstracts of the Reports of the 17th All-Union Conference of Emission Electronics [in Russian], LIYaF, Leningrad (1978), p. 104.
4. É. Ya. Zandberg and N. I. Ionov, Surface Ionization [in Russian], Nauka, Moscow (1969), p. 432.

PHYSICOCHEMICAL PROPERTIES OF IRRADIATED INORGANIC COMPOUNDS OF LITHIUM: OXIDE, ALUMINATE, AND SILICATES

V. G. Vasil'ev, S. R. Borisov,
N. N. Ryazantseva, and A. A. Vashman

UDC 546.66.085

Inorganic compounds of lithium, primarily the thermally stable Li_2O, $LiAlO_2$, Li_2SiO_3, and Li_4SiO_4, are now considered as starting materials for the production of tritium in a thermonuclear reactor [1-5]. In view of this, we were interested in analyzing the influence of radiation on the indicated lithium compounds and evaluating the possibilities of reproduction of tritium in the blanket of a thermonuclear reactor.

The opening of ampules irradiated on a γ setup with ^{60}Co showed the absence of a gas phase. The results of irradiation of ampules in a nuclear reactor are cited in Table 1. The basic component of the gas phase of these ampules is helium. The amount of tritium in the gas does not exceed 2% of its total content in the salt. On the basis of the ESR spectra of irradiated salts, we calculated the concentrations of paramagnetic centers (Table 2). The comparatively low concentration of paramagnetic centers may indicate a high radiation chemical stability of these lithium compounds. Increasing the absorbed dose from 10^{22} to 10^{25} eV/g leads to the appearance of an established concentration of paramagnetic centers at a level of 10^{16}-10^{17} g^{-1}. Preliminary analysis shows that the ESR spectra of γ irradiated samples differ from those obtained for samples irradiated in a reactor. In the case of salts irradiated to a fluence of ~10^{18} neutrons/g, the ESR signals have a narrow line, which is typical of colloidal lithium [6].

TABLE 1. Amount and Composition of Gas in Ampules after Irradiation (V_{free} : V_{bound} = 3 : 1)

Chemical compound	Ampule No.	Wt. of salt sample, g	Amount of titanium in sample, Ci/g	Vol. of gas in sample, neutrons · cm³	Composition of gas, vol. %								
					He	H_2	HT	CH_4	H_2O	N_2	O_2	CO	CO_2
Li_2O	1	24,40	0,03	0,05	30	3		10		5	2	30	20
	2	26,32	0,09	—									
$LiAlO_2$	1	24,45	0,016	0,02	46					23	6	23	2
	2	24,90	0,088	—									
Li_2SiO_3	1	27,70	0,035	—									
	2	24,70	0,092	0,90	46	49	4	1					
Li_4SiO_4	1	31,3	0,017	—									
	2	24,7	0,18	0,94	99,1	0,5		0,4					

TABLE 2. Concentration of Paramagnetic Centers in Irradiated Salts

Chemical compound	Irradiation of ^{60}Co		Irradiation in nuclear reactor			
	dose, eV/g	concn. of centers, g^{-1}	amount of tritium, Ci/g	No. of tritium nuclei per g	dose, eV/g	concn. of centers, g^{-1}
Li_2O	$1,1 \cdot 10^{22}$	10^{15}	0,03	$6 \cdot 10^{17}$	$3 \cdot 10^{24}$	$4 \cdot 10^{16}$
			0,09	$1,8 \cdot 10^{18}$	$9 \cdot 10^{24}$	$4 \cdot 10^{16}$
$LiAlO_2$	$8 \cdot 10^{22}$	$2 \cdot 10^{17}$	0,016	$3,2 \cdot 10^{17}$	$1,6 \cdot 10^{24}$	$1 \cdot 10^{16}$
			0,088	$1,76 \cdot 10^{18}$	$8,8 \cdot 10^{24}$	$1 \cdot 10^{16}$
Li_2SiO_2	$8 \cdot 10^{22}$	$1 \cdot 10^{17}$	0,035	$7 \cdot 10^{17}$	$3,5 \cdot 10^{14}$	$2 \cdot 10^{17}$
			0,092	$1,84 \cdot 10^{18}$	$9,2 \cdot 10^{24}$	$1 \cdot 10^{17}$
Li_4SiO_4	—	—	0,17	$3,4 \cdot 10^{17}$	$1,7 \cdot 10^{24}$	$2 \cdot 10^{17}$
			0,18	$3,6 \cdot 10^{18}$	$1,8 \cdot 10^{25}$	$2 \cdot 10^{17}$

Translated from Atomnaya Énergiya, Vol. 48, No. 6, pp. 392-394, June, 1980. Original article submitted August 20, 1979.

0038-531X/80/4806-0404$07.50

TABLE 3. Liberation of Helium from Irradiated Salts

Compound	Amount of He formed during irr., neutrons · cm^3/g	Amt. of helium in ampule during irr., % of ΣHe	System of heat treatment	Liberation of helium during heat treat., % of ΣHe
Li_2O	0,066	—	500° C, 1 h	60
$LiAlO_2$	0,064	—	600° C, 1 h	
Li_2SiO_3	0,068	25	800° C, 1 h	78
			800° C, 1 h	70
Li_4SiO_4	0,134	28	600° C, 1 h	66
			700° C, 1 h	

TABLE 4. Amount of Tritium Liberated in Molecular Form (HT, T_2) in Heat Treatment for 1 h at a Given Temperature

Chemical compound	Amount of tritium, Ci/g	Temp., °C	Ratio (TH/T_2), % of total amount of tritium
Li_2O	0,09	300	< 1,0
		400	< 1,0
		500	< 1,0
$LiAlO_2$	0,088	400	2,6
		500	5,3
		600	6,0
Li_2SiO_3	0,092	200	2,0
		300	4,0
		400	5,0
		500	5,0
		600	7,0
Li_4SiO_4	0,18	200	2,5
		300	1,0
		400	1,5
		500	2,0
		600	3,5

TABLE 5. Characteristics of Lithium Compounds (time of heat treatment 1 h)

Chemical compound	Melting point, °C	Liberation of tritium		Liberation of helium	
		temp., °C	%	temp., °C	%
Li_2O	1600	350	50	500	100
		450	100		
		500	50		
$LiAlO_2$	1600	800	100	800	100
		500	50		
Li_2SiO_2	1250	700	100	800	100
		450	50		
Li_4SiO_4	1250	700	100	700	100

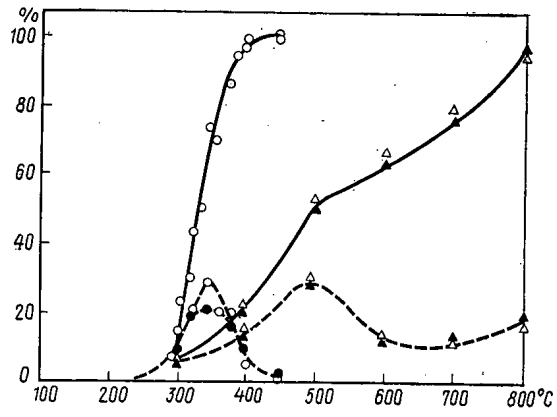

Fig. 1

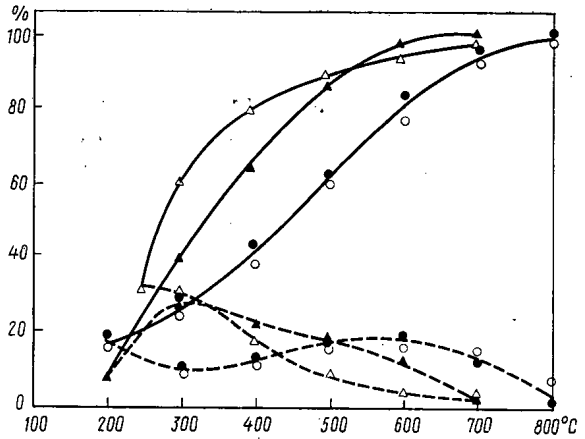

Fig. 2

Fig. 1. Liberation of tritium from LiO_2: ○) $3 \cdot 10^{-2}$ Ci/g; ●) $9 \cdot 10^{-2}$ Ci/g; from $LiAlO_2$: △) $1.6 \cdot 10^{-2}$ Ci/g; ▲) $8.8 \cdot 10^{-2}$ Ci/g.

Fig. 2. Liberation of tritium from Li_2SiO_3: ○) $3.5 \cdot 10^{-2}$ Ci/g; ●) $9.2 \cdot 10^{-2}$ Ci/g; from Li_4SiO_4: △) $1.7 \cdot 10^{-2}$ Ci/g; ▲) $1.8 \cdot 10^{-1}$ Ci/g.

Heat treatment of samples irradiated in a reactor showed the absence of gaseous radiolysis products and a correlation with the results of a determination of the concentration of paramagnetic centers. Data on the liberation of helium during heat treatment (Table 3) can be considered preliminary, noting only that the temperature interval of the liberation of helium falls in the region of 600-800°C. A study of the liberation of tritium from irradiated salts showed that the bulk of the tritium is in the form of HTO (T_2O), which condenses in a trap with liquid nitrogen. The results of heat treatment of a salt sample of particles with a size of ~0.15 mm with a total mass of 0.5 g for 1 h under a vacuum of ~13 Pa during condensation of water vapors in a trap with liquid nitrogen are cited in Table 4 and in Figs. 1 and 2. Thus, inorganic compounds of lithium Li_2O, $LiAlO_2$, Li_2SiO_3, and Li_4SiO_4 possess high radiation stability, since the concentration of radiolysis products in the molecular and radical forms is 10 times or more lower than the concentration of tritium formed. At an initial tritium concentration $\sim 10^{-2}$-10^{-1} Ci/g (1 Ci = $3.7 \cdot 10^{10}$ Bq), its liberation under vacuum (chiefly in the form of the oxide) and in helium occurs in different temperature intervals: from lithium oxide at 300-450°C, from lithium aluminate and silicates at 200-800°C. According to the characteristics of lithium compounds with respect to the liberation of helium and tritium (Table 5), it is evidently expedient to investigate the kinetics of the liberation of tritium and helium, as well as the nature of the radiolysis products in the solid phase.

The liberation of tritium oxide from irradiated lithium oxide is described by the kinetic equation $k = 2.3/\tau(\log 1/1 - x)$. The kinetic curves of the liberation of tritium [7] show that within the investigated temperature range 300-400°C, the initial step of the process has an activation energy 18.8 kcal/mole, while the final step is slower than the initial one, with activation energy ~13 kcal/mole. Taking into account the polymer nature of the investigated inorganic compounds of lithium and considering the kinetic principles, we can consider the process as a chemical reaction of polycondensation [8], resulting in the formation of tritium oxide and an inorganic polymer.

It can be asserted that when the temperature system is correctly selected, the use of lithium material will permit the isolation of tritium and helium directly in the process of irradiation [4, 5]. The compounds under consideration are characterized by different lithium contents per unit volume, which must be taken into account in the creation of elements of the lithium zone.

LITERATURE CITED

1. E. P. Velikhov et al., "A hybrid tokamak thermonuclear reactor for the production of fissionable fuel and electric power," Report at the All-Union Conference on Engineering Problems of Thermonuclear Reactors [in Russian], Vol. 1, Izd. NIIEFA, Leningrad (1977), p. 5.
2. V. Kotov and G. Shatalov, in: Proc. US–USSR Symp. Fusion–Fission Reactors, July, 13-16, 1976. Conf. 760773, p. 129.
3. H. Kubo and K. Tanaka, Radiochem. Radioanal. Lett., 23, (2) 57 (1975).
4. "Method of continuous production of tritium," Czech. Patent No. 130.871 from June 15, 1962.
5. "Production of tritium by irradiation of lithium oxide," Japanese Patent No. 50.125.199 from March 20, 1974.
6. L. I. Dzhordzhishvili et al., in: Electronic Processes in Solids [in Russian], Metsniereba, Tbilisi (1965), p. 19.
7. H. Kudo, K. Tanaka, and H. Amano, J. Inorg. Nucl. Chem., 40, 363 (1978).
8. G. S. Kolesnikov, in: Polymerization and Polycondensation [in Russian], D. I. Mendeleev Moscow Chemicotechnological Institute (1970), p. 115.

THEORETICAL STUDIES ON THE ACCUMULATION OF ^{232}U, ^{236}Pu, AND ^{238}Pu IN THE BREEDING ZONES OF HYBRID AND FAST REACTORS

Yu. G. Bobkov, V. G. Ilyunin,
V. M. Murogov, M. F. Troyanov,
L. N. Usachev, A. G. Tsikunov,
I. Kh. Ganev, A. D. Zhirnov,
L. V. Tochenyi, and A. N. Shmelev

UDC 621.039.516.22

The problems in implementing an external fuel cycle are largely determined by the accumulation of uranium and plutonium nuclides in the fuel, which govern the inherent activity [1, 2]. We have therefore calculated the accumulation of ^{232}U, ^{236}Pu, and ^{238}Pu on the irradiation of uranium and thorium in the breeding zone of a fast reactor type BN-1600 [3] and in the blanket of a hybrid fusion–fission reactor [4]. The latter can also be considered as a potential source of secondary nuclear fuel [5].

The above nuclides of uranium and plutonium accumulate via threshold (n, 2n) reactions, and therefore the yields should vary substantially with the neutron energy spectrum. Figure 1 shows the characteristic neutron spectra for a fast reactor and for the blanket of a hybrid reactor. The spectra were calculated for the blanket via the BLANK program [6] and for the fast reactor via the M-26 program [7]. These spectra were used in averaging the group constants that were used in calculating the burnup and accumulation of the nuclides, for which purpose the PERS program was used [8]. The group constants generated from the library files (mainly the ENDL library) corresponded to the latest recommendations [9].

Table 1 gives mean cross sections for some reactions for these two forms of spectra; even a general overview of the neutron cross sections indicates that there is a considerable difference in the rates of the various processes that determine the isotope positions of uranium and thorium irradiated in such reactors.

U–Pu Fuel Cycle. Table 2 gives results on the accumulation of ^{236}Pu, ^{232}U, ^{238}Pu, and ^{239}Pu in the irradiation of uranium; plutonium accumulates in the breeding zone of a fast reactor, and the ^{236}Pu content there is $5 \cdot 10^{-9}$–$2 \cdot 10^{-7}$%, the exact level being dependent on the accumulation of plutonium in the uranium (maximum accumulation 3-40 kg of Pu/ton U correspondingly). The concentration of ^{232}U in the uranium is correspondingly $1 \cdot 10^{-13}$–$5 \cdot 10^{-10}$%. On the assumption that all of the ^{236}Pu goes over to ^{232}U on storage, the concentration of the latter may rise to $6 \cdot 10^{-9}$%.

The calculations (Table 2) show that a given level of accumulation of plutonium in the uranium (i.e., an identical volume of reprocessing per unit of fuel) will imply ^{236}Pu and ^{238}Pu contents of the plutonium in the blanket of a fusion reactor 10^5 times larger for ^{236}Pu and more than 10^2 times larger for ^{238}Pu than the values for plutonium accumulated in the breeding zone of a fast reactor. The ^{232}U concentration for uranium in the blanket of a fusion reactor will be more than 10^5 times that in the breeding zone of a fast reactor. As a result the ^{238}Pu content of plutonium may exceed 1%, while the ^{236}Pu concentration may attain values characteristic of the ^{232}U concentration in ^{233}U in the thorium fuel cycle, viz., $(10\text{-}100) \cdot 10^{-4}$%. The calculations also show that the relationships are not substantially altered if the accumulation is transferred to the peripheral layers of the blanket. On the other hand, the rate of accumulation of plutonium, which is one of the desirable features of a hybrid reactor [5], is substantially reduced.

Thorium Fuel Cycle. From the viewpoint of the remote future of nuclear power, it is of interest to examine the accumulation of ^{233}U in various types of breeder reactor. From published data, the current level of the external fuel cycle industry allows one to employ ^{233}U with ^{232}U content of $(1\text{-}10) \cdot 10^{-4}$% [10]. In the future, it should be possible in principle to process fuel with a ^{232}U content of $(300\text{-}400) \cdot 10^{-4}$% [11]. In what follows, we assume this level of ^{232}U as the limiting permissible one. Then Table 3 shows that the level of accumulation of ^{233}U in thorium in the breeding zone is practically unlimited. On the other hand, the maximum accumulation of ^{233}U in the thorium blanket of a hybrid reactor should not exceed about 0.3 kg of ^{233}U per ton of Th (20

Translated from Atomnaya Énergiya, Vol. 48, No. 6, pp. 395-396, June, 1980. Original article submitted September 28, 1979.

0038-531X/80/4806-0407$07.50

TABLE 1. Mean Cross Sections of Neutron Reactions in b for the Breeding Zone of a Fast Reactor and a Blanket of a Hybrid Fusion Reactor

Nuclide	Blanket of a hybrid reactor				Breeding zone of a fast reactor		
	$n\gamma$	nf	$n, 2n$	$n, 3n$	$n\gamma$	nf	$n, 2n$
^{235}U	0,60	1,70	—	—	1,30	3,0	—
^{236}U	0,65	1,15	—	—	1,2	0,055	—
^{238}U	0,33	0,069	0,066	0,0018	0,73	0,022	0,00059
^{237}Np	1,61	0,352	0,027	0,0446	3,10	0,18	0,00012
^{239}Pu	0,46	2,03	0,025	0,0410	1,40	2,47	0,00012
^{240}Pu	0,71	0,46	—	—	1,0	0,25	—

*1 b = 10^{-28} m^2.

TABLE 2. Accumulation of ^{236}Pu, ^{238}Pu, and ^{232}U in the Breeding Zone of a Fast Reactor and in the Blanket of a Hybrid Reactor

Breeding zone	Nuclide accumulation	Max. accumulation of plutonium in irradiated uranium, kg of Pu/ton of U			
		3	5	10	20
Fast reactor	^{236}Pu, g/ton ^{239}Pu	$4,6\cdot10^{-5}$	$1\cdot10^{-4}$	$3\cdot10^{-4}$	$6\cdot10^{-4}$
	^{238}Pu, g/ton ^{239}Pu	3,0	4,8	11,5	25
	^{232}U, g/ton ^{238}U	$9\cdot10^{-10}$	$3,5\cdot10^{-9}$	$5\cdot10^{-8}$	$2,1\cdot10^{-7}$
Blanket of hybrid reactor	^{236}Pu, g/ton ^{239}Pu	10	19	42	90
	^{238}Pu, g/ton ^{239}Pu	935	2800	4700	11100
	^{232}U, g/ton ^{238}U	$2\cdot10^{-4}$	$1\cdot10^{-3}$	$1,4\cdot10^{-2}$	$8,5\cdot10^{-2}$

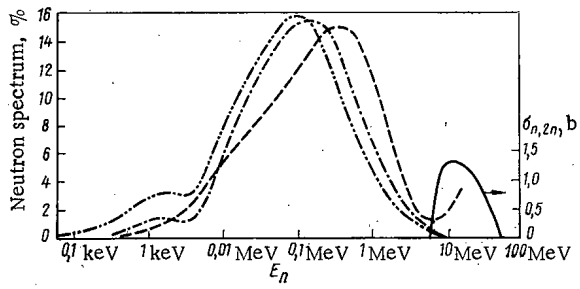

Fig. 1. Neutron spectra in the blanket of a hybrid reactor (---), in the core of a fast reactor (-·-) and in the breeding zone of the latter (—·—); the solid line is $\sigma_{n,2n}(E_n)$ for ^{238}U.

TABLE 3. Accumulation of ^{232}U in the Thorium Zone of a Fast Reactor and in the Thorium Blanket of a Hybrid Reactor, g ^{232}U per ton of ^{233}U

Max. accumul. of ^{233}U (with allowance for ^{233}Pa in irrad. thorium), kg/ton Th	Breeding zone of fast reactor	Blanket of hybrid reactor [11]	Max. accumul. of ^{233}U (with allowance for ^{233}Pa in irrad. thorium), kg/ton Th	Breeding zone of fast reactor	Blanket of hybrid reactor [11]
1,0	1	1300	6,0	15	7500
3,0	5	4300	10	26	$> 10^4$
5,0	11	6000			

days of irradiation). This very low accumulation level (less by an order of magnitude than the ^{235}U content of depleted uranium) will not only increase the volume of chemical processing by about a factor 100 but will also require practically continuous reloading of the blanket. At an economically applicable level of ^{233}U in throium (about 10 kg of ^{233}U per ton of Th), the ^{232}U concentration in the ^{233}U would exceed 1%. This is considerably larger than the equilibrium level of ^{232}U in ^{233}U for a thermal-neutron thorium reactor [11].

We are indebted to A. S. Krivtsov, A. N. Sosnin, and V. N. Sosnin for assistance in the calculations.

LITERATURE CITED

1. O. D. Bakumenko, At. Energ., 44, No. 2, 140 (1978).
2. K. Tasaka et al., Nucl. Sci. Technol., 14, No. 7, 519 (1977).
3. L. A. Kochetkov and Yu. E. Bagdasarov, Design, Construction, and Operating Experience of Demonstration LMFBR, Vienna, IAEA (1978), p. 79.
4. B. D. Gornostaev, in: Proceedings of the Second Soviet–American Seminar on Fusion–Fission [in Russian], Atomizdat, Moscow (1978), p. 94.
5. E. P. Velikhov et al., At. Energ., 45, No. 1, 3 (1978).
6. G. E. Shatalov, Preprint IAE-2832, Moscow (1977).
7. Sh. S. Nikolaishvili et al., in: Papers from the Symposium of COMECON Member Countries on the State of the Art and Development Prospects for Nuclear Power Stations with Fast Reactors [in Russian], Vol. 2, FEI, Obninsk (1968), p. 75.
8. Yu. G. Bobkov and A. S. Krivtsov, in: Nuclear Physics Researches in the USSR [in Russian], No. 27, TsNIIatominform, Moscow (1978), p. 15.
9. R. Howerton et al., The LLL Evaluated Nuclear Data Library (ENDL), UCRL-50400, LLL (1976).
10. Rev. Mod. Phys., 50, No. 1, 2 (1978).
11. S. V. Marin, Atom. Tekh. Rubezhom, No. 5, 3 (1978).

MÖSSBAUER SPECTROSCOPY IN THE PHASE-COMPOSITION ANALYSIS OF CORROSION DEPOSITS IN A NUCLEAR POWER STATION

V. M. Sedov, P. G. Krutikov,
E. A. Konstantinov, V. A. Shishkunov,
and A. A. Afanas'ev

UDC 621.039.553:36:620.193.477

The deposition of solid corrosion products on working surfaces in a nuclear power station largely determines the viability; research on these processes is related to the solution of problems in organizing the optimum water treatment, as well as chemical cleaning and decontamination, forecasting of the radiation environment, etc. In turn, it would be impossible to build up a full picture of the physicochemical processes in the system composed of the constructional material and the coolant without detailed knowledge of the chemical, isotopic, and phase compositions of the solid corrosion products.

Physical and physicochemical methods are used along with purely chemical ones to obtain the desired information: x-ray spectroscopy, electron spectroscopy applied to chemical analysis, electron diffraction, and Mössbauer spectroscopy [1-4]. Industrial conditions impose some constraint on the choice of methods in such analysis. The central laboratory at a nuclear power station should use a set of methods that are reasonably simple to operate and that provide the necessary information quickly and reliably.

It is best at present to determine the chemical composition of deposits at a nuclear power station by qualitative and quantitative chemical analysis [5-7]. The apparatus required includes standard Soviet equipment such as spectrophotometers (SF-18 and SF-26) and photocolorimeters (FÉK-56 and FÉK-60). Well-developed methods are available for the analysis of radionuclides present in corrosion products, and γ spectrometers with semiconductor detectors may be used with the AI-1024 and AI-4096 as standard equipment for radiometric laboratories at virtually all nuclear power stations. The most complicated stage in the analysis of solid corrosion products is that in determining the phase composition. Various steels are the main constructional materials in a nuclear power station, and therefore the corrosion products consist to

Translated from Atomnaya Énergiya, Vol. 48, No. 6, pp. 396-399, June, 1980. Original article submitted September 28, 1979.

0038-531X/80/4806-0409$07.50

TABLE 1. Characteristics of Surface Deposits in Major Systems in Nuclear Power Stations Containing RBMK-1000 Reactors

System and constructional material	Working temp., °C	Deposits on surface after manufacture	Deposit on operation
Multiple circulation loop			
Steel Kh18N10T	285	Cr_2O_3 Thermal scale	γ-Fe_2O_3 [Fe, Ni] O [Fe, Cr]$_2O_3$ 9,72 g/m^2
Alloy containing 2.5% Zr		[Fe, Ni] O [Fe, Cr]$_2O_3$ 1—5 g/m^2 ZrO_2-Monoclinic form	4,5 g/m^2 Fe_3O_4—1,5 g/m^2 γ-Fe_2O_3 — —0,9 g/m^2
Steam section			
St. 20	270	Thermal form FeO, Fe_2O_3, Fe_3O_4 250—500 g/m^2 Products from atmospheric corrosion α-FeOOH, γ-FeOOH 50—100 g/m^2	γ-Fe_2O_3 (22 %) α-Fe_2O_3 (61 %) Fe_3O_4 (17 %) 30—50 g/m^2
Condensate-feed system			
Steel Kh18N10T	30—160	Monoclinic form Cr_2O_3; [Fe, Ni] O [Fe, Cr]$_2O_3$ 1—5 g/m^2	γ-Fe_2O_3 10—30 g/m^2

TABLE 2. Parameters of Mössbauer Spectra and Positions of Lines of Iron Corrosion Products Relative to Metallic Iron

Iron compound	T, K	Positions of lines on Mössbauer spectra, mm/sec						IS, * mm/sec	QS, mm/sec	H, kOe
		1	2	3	4	5	6			
α-Fe	295	5,323	3,083	0,834	—0,834	—3,084	—5,323	0	0	330
α-Fe_2O_3	295	8,12	4,92	1,85	—1,00	—4,03	—7,23	0,44±0,01	0,20±0,05	518±5
Fe_3O_4, lines Fe^{3+}	295	8,00	4,92	1,60	—0,80	—4,20	—7,82	0,39±0,0	—	505±10
Fe_3O_4, lines Fe^{2+}	295	8,00	4,95	1,46	—0,60	—3,63	—6,82	0,65±0,1	—	450±10
α-FeOOH	78	8,05	5,02	1,73	—0,98	—4,26	—7,55	0,37±0,04	0,21±0,02	493±5
	295	7,00	3,80	1,39	—0,39	—2,82	—4,40	0,48±0,02	0,36±0,04	355±10
β-FeOOH	78	7,60	3,57	1,65	+0,91	—2,82	—5,90	0,37±0,04	0,17±0,03	460±10
	295	0,77	—0,02	—	—	—	—	0,39±0,04	0,75±0,01	0
γ-FeOOH	78	0,72	0,05	—	—	—	—	0,33±0,01	0,780±0,005	0
γ-Fe_2O_3	295	8,00	4,92	1,60	—0,80	—4,20	—7,82	0,39±0,05	0,1±0,1	505±20

*IS, isometric shift; QS, quadrupole splitting of nuclear levels; H, magnetic field (1 Oe = 79.5775 A/m).

90-95% of mixtures of various iron oxides and the like (Fe_3O_4 magnetite, α-Fe_2O_3 hematite, γ-Fe_2O_3 maghemite, α-FeOOH goethite, and γ-FeOOH lepidocrocite), with only a small fraction represented by other compounds, in particular spinels of $CrFe_{3-x}O_4$, $Fe_xCr_{3-x}O_4$ type, etc. This is clear from the deposits in the surfaces of major pipelines in the RBMK-1000 system (Table 1).

The surface state of the metal is evaluated at each shutdown, which includes sampling of the deposits, cutting of metal samples, and extraction of reference specimens [8, 9]. A unit in a nuclear power station is shut down annually for planned prophylactic operations related to fuel reloading (nuclear power stations with water-cooled—water moderated (VVÉR) reactors), and a similar annual shutdown is used in scanning the entire system in continuous operation (power stations with high-powered water-cooled channel (RBMK) reactors). When the major systems are examined, about 150-200 samples of deposits are taken, and about 50 metal specimens are cut from the equipment and pipelines, i.e., about 200-250 samples have to be examined for one unit in a nuclear power station.

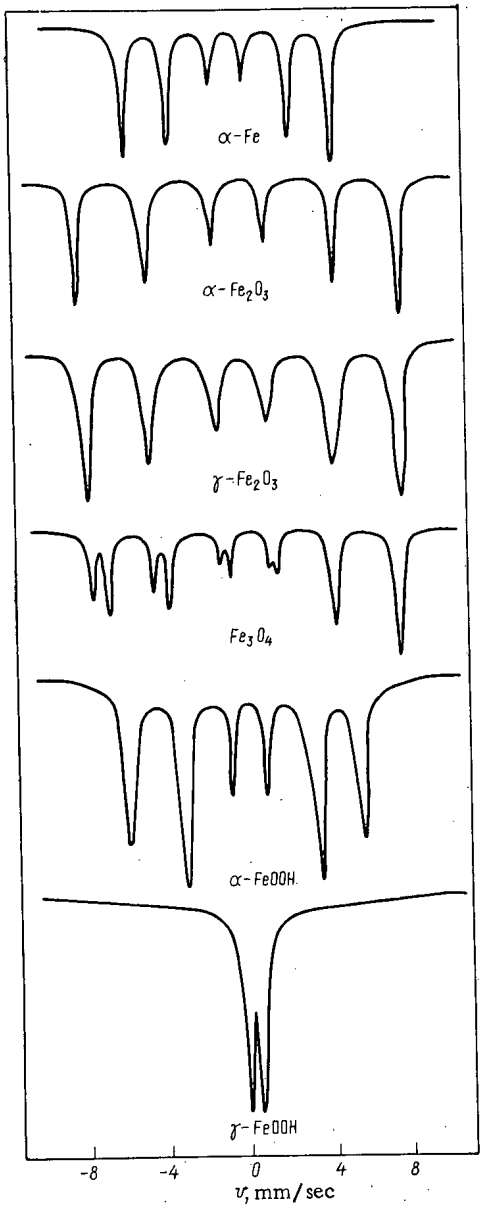

Fig. 1. Mössbauer spectra of standard iron compound.

X-ray spectroscopy is a classical phase-analysis method. However, quantitative evaluation of the phase composition requires additional measurements and consumes much time. Also, the method cannot be applied to corrosion products in the amorphous or finely divided states, which substantially restricts the application to nuclear power stations.

Electron diffraction and electron spectroscopy are also difficult to apply to solid corrosion products, because the specimens required for these methods have to be very thin and are therefore difficult to prepare, and secondly the methods require extremely complicated costly equipment produced in small numbers, which requires highly skilled staff. In recent years there have been many researches on the oxidation of iron alloy by Mössbauer methods [4, 10-12].

The phase composition of an iron-bearing corrosion product can be examined by Mössbauer spectroscopy because the hyperfine structure of the nuclear energy levels is examined for ^{57}Fe (2% of the natural iron isotope mixture), as the levels are dependent on the form of the compound. Various monographs and articles [4, 13] deal with the essence of the processes in Mössbauer spectroscopy. The main components that characterize a Mössbauer spectrum are the isomeric or chemical shift, the nuclear electric quadrupole splitting, and the nuclear magnetic dipole splitting. The parameters of Mössbauer spectra that characterize the hyperfine struc-

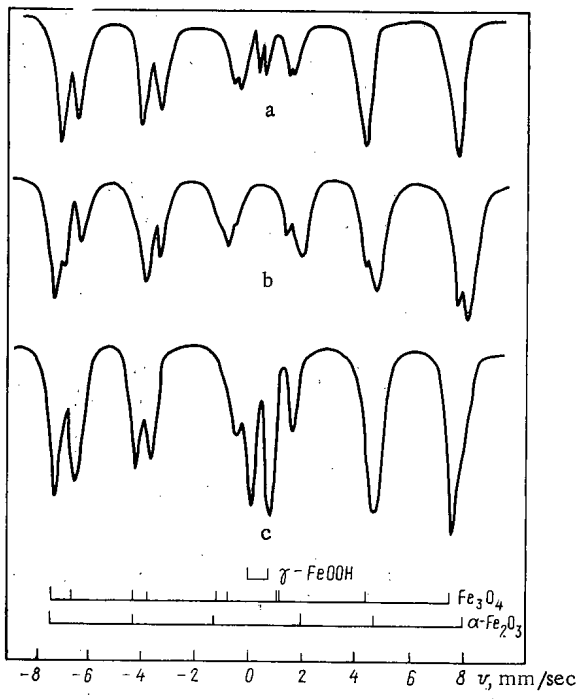

Fig. 2. Spectra of the corrosion products from Leningrad nuclear power station (RBMK-1000): a) deposits from the emergency protection system; b) suspension of corrosion products from the separator drum; c) deposits from the high-pressure cylinder in the separator-superheater.

ture of the ^{57}Fe nucleus are highly individual to the compound, so quantitative and qualitative phase analyses can be performed for iron oxide corrosion products.

The Mössbauer spectra were identified by comparison with the spectra of pure compounds and with published spectra. Figure 1 gives the spectra of some standard compounds, while Table 2 gives the parameters.

Quantitative analysis of particular forms of iron in a corrosion-product mixture is based on the largely linear relationship between the area of the Mössbauer spectra and the content of a particular form of the element within certain limits [14]. The sensitivity of this method is usually not less than 10% (the proportion of a particular phase in a heterogeneous mixture for a sample of 50-100 mg), while the relative error of determination is not more than 15%. These characteristics are no worse than the analogous parameters of x-ray structure analysis, even when a diffractometer is used.

The wide scope for Mössbauer spectroscopy was demonstrated in research on corrosion under various conditions governed by the temperature, oxidant composition, and properties of the constructional material [9, 11, 15]. In particular, mild-steel constructional materials have given α-FeOOH and γ-FeOOH with small amounts of α-Fe_2O_3 and Fe_3O_4. The thermal oxidation of carbon steels gives rise to Fe_3O_4, α-Fe_2O_3, and γ-Fe_2O_3.

Mössbauer measurements have been made on the phase composition for various corrosion products in various systems in a nuclear power station, and the results are fully explicable in relation to the processes of formation and are in agreement with data obtained by other methods, in particular x-ray spectroscopy (Fig. 2) [11, 15]. The Mössbauer spectra were recorded with a YaGRS-4M γ-resonance spectrometer, which is in routine production in this country. These instruments are simple to use and reliable to operate.

Therefore, nuclear γ-resonance spectroscopy should be used in the phase analysis of iron-bearing corrosion products at nuclear power stations, while a YaGRS-4M spectrometer should be present in the radiometry laboratory of the station.

LITERATURE CITED

1. L. M. Kovba and Ts. K. Trunov, X-Ray Phase Analysis [in Russian], Moscow State Univ. (1976).
2. A. G. Akimov, Zashch. Met., 12, 6 (1976).
3. K. Siegbahn, ESCA Applied to Free Molecules, Elsevier (1970).
4. G. K. Wertheim, The Mössbauer Effect [Russian translation], Mir, Moscow (1966).
5. G. Charlot, Methods of Analytical Chemistry [Russian translation], Khimiya, Moscow (1969).
6. Yu. Yu. Lur'e and A. I. Rybnikova, Chemical Analysis of Industrial Effluents [in Russian], Khimiya, Moscow (1974).
7. Z. Marczenko, Spectrophotometric Determination of Elements, Halsted Press (1976).
8. P. G. Krutikov et al., Teploenergetika, 6, 13 (1978).
9. V. M. Sedov et al., At. Energ., 46, No. 1, 23 (1979).
10. B. M. Akarelyan et al., Zavod. Lab., 41, No. 3, 1115 (1975).
11. Corrosion, 32, No. 11, 432 (1976).
12. A. N. Murin, Physical Principles of Radiochemistry [in Russian], Vysshaya Shkola, Moscow (1971), p. 249.
13. V. I. Gol'danskii, The Mössbauer Effect and Its Application in Chemistry [in Russian], Izd. Akad. Nauk SSSR, Moscow (1963).
14. W. Meisel, in: Proc. 5th Int. Conf. on Mössbauer Spectroscopy, Part 1, Bratislava, 3-7 September (1973), p. 200.
15. L. N. Moskvin, At. Energ., 46, No. 1, 28 (1979).

THERMOELECTRIC PROPERTIES OF ZrC, UC – ZrC, AND UC – UN AT 285-450°K

L. I. Gomozov and I. Sh. Akhmedzyanov

UDC 537.32.323:661.879.1

The study of thermoelectric properties in combination with other physical parameters makes it possible to judge the nature of the interatomic bond in interstitial phases [1]. The observed anomalies of the elastic properties of Zr carbides in the region of homogeneity and the solid solution UC–ZrC and UC–UN may be due, in particular, to the unequal porosities of the specimens, and therefore the measurement of the thermo-emf, whose value is not affected by the porosity, is of additional interest as a method for estimating the properties of the interatomic bond.

In order to determine thermoelectric properties, we used specimens 3 mm in diameter and 30-50 mm in length, obtained by powder-metallurgy methods or argon-arc melting with subsequent homogenization. The amount of oxygen impurity in near-stoichiometric specimens of ZrC and (Zr, U)C was ~0.2 atom %; in substoichiometric specimens it rose to 0.9 atom % for $ZrC_{0.76}$, and in UC–UN specimens it varied from 0.1 to 1 atom %. The amount of nitrogen impurity in the specimens, on the basis of the ZrC, did not exceed 0.12 atom %.

The characteristics of the thermo-emf were determined relative to pure copper, for which the coefficient of absolute thermo-emf at 298°K is $\alpha = 1.855$ μV/deg and $d\alpha/dt = 5.225 \cdot 10^{-3}$ μV/deg^2 [2, 3]. In processing the measurement results, we took account of the relation

$$\Delta E = [\alpha + T\,(\overline{d\alpha/dT})]\,\Delta T, \quad (1)$$

where ΔT is the temperature difference between the hot and cold junctions.

The specimens were held in openings in the cooler and the heater by means of quick solder. The temperature of the cold junction was 286°K, and that of the hot junction ranged up to 450°K. The instrument error in the determination of α and $d\alpha/dT$ did not exceed ± 2 and ± 10 relative %, respectively.

The measurement results are shown in Figs. 1-3. As a rule, the extremum points of α as a function of concentration coincide with the extremum points of other physicochemical properties. For ZrC_x (see Fig. 1a) we observe a sharp minimum of the negative values of α in the region of 48 atom % carbon, which coincides

Translated from Atomnaya Énergiya, Vol. 48, No. 6, pp. 399-400, June, 1980. Original article submitted October 22, 1979.

0038-531X/80/4806-0413$07.50

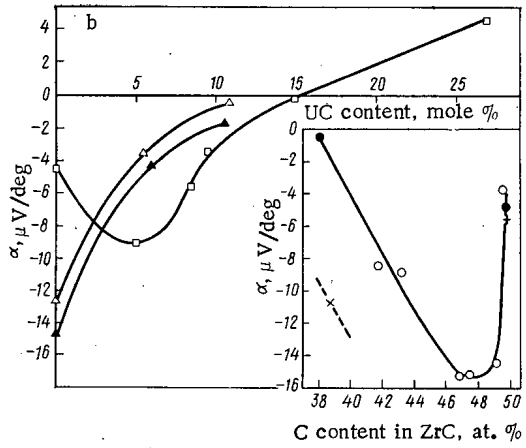

Fig. 1

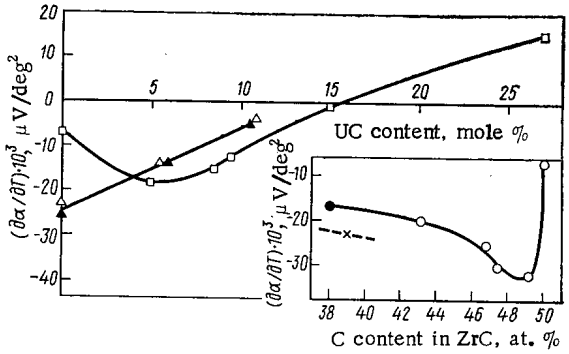

Fig. 2

Fig. 1. Coefficient of absolute thermo-emf at 298°K as a function of the composition of ZrC (a) and ZrC−UC (b): ○, ●) specimens containing 0.2-2 atom % oxygen; +) carbidographite with 2 mass % graphite; ×) oxycarbide $Zr(C_{0.56}, O_{0.08})$; □) $(Zr, U)C_{0.95-1.00}$; ▲) $(Zr, U)C_{0.87}$; △) $(Zr, U)C_{0.82}$.

Fig. 2. Temperature coefficient of absolute thermo-emf in the 285-450°K range as a function of the stoichiometry of ZrC (a) and solid solutions ZrC−UC (b): ○, ●) specimens containing 0.2-2 atom % oxygen; ×) oxycarbide $ZrC_{0.56}O_{0.08}$; □) $(Zr, U)C_{0.95-1.00}$; ▲) $(Zr, U)C_{0.87}$; △) $(Zr, U)C_{0.82}$.

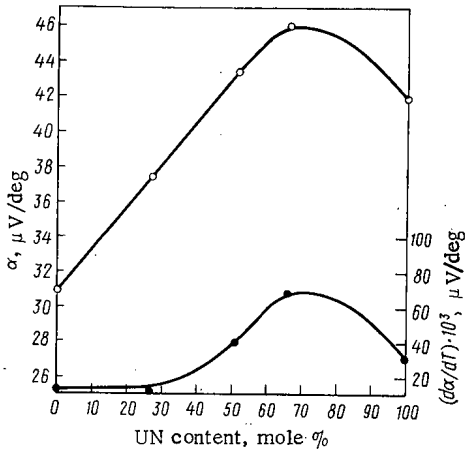

Fig. 3. Variation of the coefficient of absolute thermo-emf and its dependence on temperature in the case of solid solutions of the UC−UN system: ○) α; ●) dα/dT.

with the maximum on the curves of the melting point and the crystal-lattice parameter [1, 4], as well as with an increased growth in microhardness [5]. The values of α for ZrC_x in the region of 38-48 atom % carbon are close to those published in [4], but the earlier experiments did not detect any sharp increase in α for a composition which differed very little from the stoichiometric. The oxycarbide Zr(C, O) of substoichiometric composition was characterized by α values which were more negative. For the solid solutions (Zr, U)C the concentration curves of the thermo-emf has a minimum in the region of 5 mole % UC (see Fig. 1b), which coincides with the position of the maximum of the modulus of elasticity and of the corresponding maximum in microhardness [6]. When we pass to the region of substoichiometric compositions, the variation of α concentration becomes quite different (see Fig. 1b). The partial replacement of ZrC with NbC in the solid solution $(Zr, Nb, U)C_{\sim 1}$ resulted in a displacement of α into the region of negative values, and this displacement (by 1 atom % NbC) amounted to about −0.1 μV/deg for an NbC content of up to 10 atom %, and to about −0.03 μV/

deg for 10-50 atom % NbC. A similar displacement is found in the case of alloying of (Zr, W, U)$C_{\sim 1}$ up to 2 atom % WC.

Changes in composition lead to a qualitatively similar variation of α and $d\alpha/dT$ (see Fig. 2), which follows immediately from the relation [7]

$$\alpha = \frac{\pi^2 k^2}{3e} T \left[\frac{\partial \ln \sigma(\varepsilon)}{\partial \varepsilon} \right]_{\varepsilon = \varepsilon_F}. \quad (2)$$

According to relation (2), the negative value of the absolute thermo-emf indicates that in ZrC and its solid solutions containing up to about 15 mole % UC, the most mobile current carriers are the electrons.

The positive values of α for UN–UC solid solutions (see Fig. 3) in the first approximation indicate hole conductivity. The maximum values of α are observed for UN/UC $\approx$3/1 and coincide with the maxima of the melting point [8] and the modulus of elasticity [9], as well as with the minimum of the microhardness [6] of the UC–UN solid solutions. A comparison of the coefficients of electronic heat capacity [6] shows that the compositive $U(C_{0.25}N_{0.75})$ must be associated with the largest contribution of the homeopolar (covalent) component of the interatomic bond.

LITERATURE CITED

1. L. E. Toth, Transition Metal Carbides and Nitrides, Academic Press (1971).
2. A. A. Rudnitskii, Thermoelectric Properties of Noble Metals [in Russian], Izd. Akad. Nauk SSSR, Moscow (1956).
3. T. V. Samsonov, Sensors for Measuring Temperature in Industry [in Russian], Izd. Akad. Nauk Ukr. SSR, Kiev (1962).
4. T. V. Samsonov, Physical Study of Carbide Materials [in Russian], Naukova Dumka, Kiev (1974).
5. L. I. Gomozov, A. I. Dedyurin, and O. S. Ivanov, in: Physicochemical Analysis of Alloys of Uranium, Thorium, and Zirconium [in Russian], Nauka, Moscow (1974), p. 178.
6. L. I. Gomozov et al., in: Plutonium 1975 and Other Actinides, North-Holland (1976), p. 915.
7. N. Mott and H. Jones, The Theory of Properties of Metals and Alloys, Oxford (1936).
8. R. Benz, J. Nucl. Mater., 31, 93 (1969).
9. A. Padel, A. Groff, and C. De Novion, ibid., 36, 297 (1970).

NUCLEAR-PHYSICS DETERMINATION OF THE STEAM CONTENT IN A REACTOR AT KURSK NUCLEAR POWER STATION

V. I. Kulikov, S. S. Lomakin,
Yu. N. Filimontsev, V. V. Karnaukhov,
Yu. M. Krutogin, A. M. Gryaznov,
and V. V. Volkov

UDC 621.039.534.44

It is important to measure the distribution of the steam content in a pressurized-water reactor channel, since this is involved in improving the reliability and safety of nuclear power stations.

Measurements may be made on the two-phase (water–steam) system in a nuclear power station outside the reactor by several methods involving the responses of the phase to input processes or on the differences in electrical and other characteristics of the vapor and liquid, as well as on the attenuation of neutron or other radiation beams [1]. However, these methods perturb the structure of the medium or else are inapplicable within the core. Therefore, the steam content within the core of a pressurized-water reactor is best determined by a nuclear-physics method involving measurement of the parameters of the neutron spectrum, which are dependent on the proportion of hydrogen in the steam–water mixture [2]. Spectrally sensitive activation detectors are normally employed to measure the parameters of the neutron spectrum within the reactor.

In measurements at the Kursk nuclear power station, we have used thermally resistant activation detectors based on alloys of aluminum with lutetium and gold, as well as copper foils, which were placed at various points along the channel. The detectors were placed in special tubes in such a way as to eliminate the effects of the spacing grids on the parameters.

We measured the epithermal parameter $r\sqrt{T/T_0}$ [3], where r is the proportion of moderated neutrons and T is the neutron gas temperature (T_0 = 293.6°K).

Figure 1 shows experimental and theoretical results, and this implies that the method allows one to identify the economizer section in a channel. The scale for the theoretical value of the volume steam content φ has been chosen in accordance with the variation in $r\sqrt{T/T_0}$, and the mean value of $r\sqrt{T/T_0}$ in the economizer section corresponds to φ = 0. The change in $r\sqrt{T/T_0}$ as φ goes from 0 to 60% is 17%, which agrees with the data from neutron-physics calculations (Fig. 2). The relationship is linear in the working range φ, which enables one to determine the relative variation in the steam content along the height of a channel in the reactor.

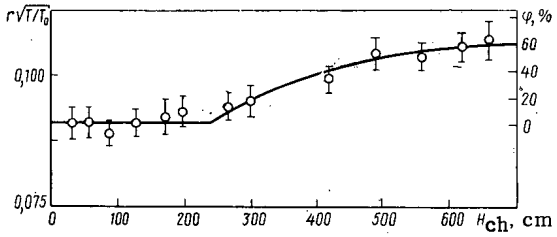

Fig. 1

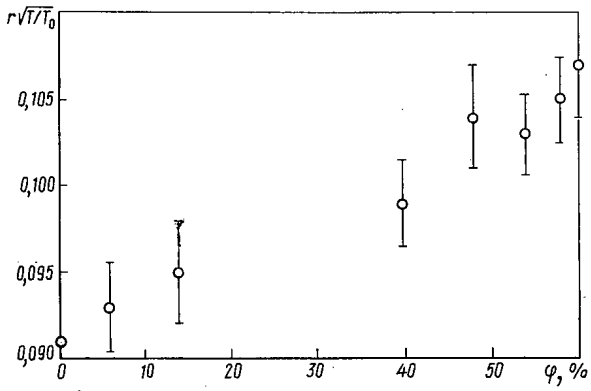

Fig. 2

Fig. 1. Distribution of the epithermal parameter $r\sqrt{T/T_0}$ over the height of a channel: solid line) theoretical value of φ; points) observation.

Fig. 2. Relationship of $r\sqrt{T/T_0}$ to volume steam content φ.

Translated from Atomnaya Énergiya, Vol. 48, No. 6, pp. 400-401, June, 1980. Original article submitted November 13, 1979.

0038-531X/80/4806-0416$07.50

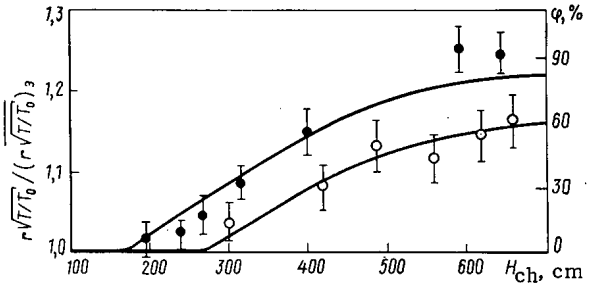

Fig. 3. Normalized distributions of $r\sqrt{T/T_0}$ over the height for power levels in a channel of 2.06 MW (filled points) and 1.15 MW (open points), where the solid line is the theoretical value of φ.

The $r\sqrt{T/T_0}$ parameter was measured in the same channel at a higher reactor power; Fig. 3 shows the measurements normalized to the value of $(r\sqrt{T/T_0})$ for the economizer section. It is clear that the length of the economizer section is reduced when the channel power is higher, and that there is a corresponding increase in $r\sqrt{T/T_0}$.

The measurements were made with the control rods closest to the point of measurement withdrawn. The results showed that it is possible to determine the distribution of the steam content in a working channel in the core of the RBMK reactor by nuclear-physics (activation) methods.

LITERATURE CITED

1. J. Boland, Instruments for Monitoring Nuclear Reactors [Russian translation], Atomizdat, Moscow (1973), p. 207.
2. S. S. Lomakin et al., in: Nuclear Instrumentation [in Russian], No. 17, Atomizdat, Moscow (1972), p. 17.
3. C. Westcott, W. Walker, and T. Alexander, in: Proceedings of the International Conference on the Peaceful Uses of Atomic Energy, United Nations, New York (1958), A/Conf. 15/P202.

MEASUREMENT OF ^{236}U FISSION PRODUCT YIELDS IN A FAST REACTOR

A. N. Gudkov, V. M. Zhivun,
A. V. Zvonarev, V. V. Kovalenko,
A. B. Koldobskii, Yu. F. Koleganov,
V. M. Kolobashkin, V. G. Liforov,
N. S. Piven', V. A. Tolstikov,
and A. O. Tipunkov

UDC 539.173.8

The appreciable yield of ^{236}U fission products formed in the operation of fast reactors can have a considerable effect on both the operational and technological quality of the nuclear-physical installation and the radiation characteristics of irradiated fuel undergoing reprocessing. In view of the clearly inadequate information on the yields of products resulting from the fast-neutron fission of ^{236}U, we measured these yields in the BR-17 reactor. The measurements were made by γ spectroscopy of an unseparated mixture of fission products [1, 2]. A 98-mg sample of ^{236}U with less than a 1% admixture of ^{235}U and ^{238}U was hermetically wrapped in an aluminum jacket and irradiated at the center of the reactor core in a flux density of 10^9 neutrons/cm^2 · sec. The sample was irradiated for 1.5 and 10.35 h. After each irradiation the γ spectrum of the fission product mixture was determined with a Ge(Li) spectrometer having a resolution of 3.2 keV at 1333 keV. The measurements were performed for 30 days over an energy range of 100-1800 keV. The values of the absolute quantum yields and half-lives needed to process the experimental results were taken from [3].

The fission rate in the sample was found by using track detectors. Calibrated layers containing $(4.02 \pm 0.08) \cdot 10^{16}$ ^{236}U nuclei were deposited on glass backing and placed in special containers with collimating openings to determine the efficiency of the track detector. The impurity content of the ^{236}U used in the layers did not exceed $0.155 \pm 0.049\%$. After irradiation the glass was etched, and the tracks developed were counted visually by using an optical microscope.

Our measured values of the cumulative yields and corresponding data from [4] are shown in Table 1. Since in [4] the yields were obtained relative to ^{140}Ba, they were renormalized to our value of the ^{140}Ba yield. Except for the yields for mass numbers 92, 97, and 132, the results agree within the limits of error.

TABLE 1. Cumulative Yields of Products Resulting from the Fission of ^{236}U by Neutrons with a Fission Spectrum

Fission product	$T_{1/2}$	Yield, %		Fission product	$T_{1/2}$	Yield, %	
		present work	data from [4]			present work	data from [4]
^{85m}Kr	4,48 h	1,20±0,06	1,50±0,10	^{132}Te	78 h	4,80±0,20	4,08±0,18
^{87}Kr	76,3 min	2,25±0,15	2,19±0,14	^{133m}Te	55,4 min	2,08±0,14	
^{88}Kr	2,80 h	2,64±0,20	2,80±0,15	^{133}I	20,8 h	7,45±0,35	6,74±0,31
^{91}Sr	9,48 h	5,04±0,20	5,38±0,23	^{134}Te	41,8 min	6,62±0,46	
^{92}Sr	2,71 h	4,94±0,26	5,93±0,26	^{134}I	52,6 min	7,37±0,41	7,71±0,36
^{92}Y	3,53 h	4,86±0,69		^{135}I	6,70 h	6,32±0,26	
^{93}Sr	7,30 min	5,82±0,79	5,38±0,26	^{135}Xe	9,15 h	6,16±0,29	5,48±0,32
^{94}Y	18,7 min	4,82±0,28		^{138}Xe	14,2 min	6,36±0,97	—
^{97}Zr	17,0 h	5,86±0,21	4,77±0,23	^{138}Cs	32,2 min	8,39±0,54	—
^{99}Mo	66,0 h	5,54±0,26	5,61±0,25	^{139}Ba	82,7 min	5,69±0,20	—
^{101}Mo	14,6 min	4,77±0,39		^{140}Ba	12,8 day	5,44±0,23	5,44∓0,23
^{105}Ru	4,40 h	2,42±0,20	2,36±0,12	^{141}Ba	18 min	5,00±0,44	5,27±0,25
^{130m}Sb	40 min	0,839±0,050		^{142}La	92,7 min	4,81±0,17	5,54±0,25
^{131m}Te	30,0 h	0,90±0,11		^{143}Ce	33 h	5,20±0,25	5,82±0,26
^{131}I	8,04 days	3,23±0,15	2,88±0,14				

LITERATURE CITED

1. A. A. Byalko et al., in: Experimental Methods of Nuclear Physics [in Russian], No. 3, V. M. Kolobashkin (editor), Atomizdat, Moscow (1978), p. 82.

Translated from Atomnaya Énergiya, Vol. 48, No. 6, pp. 401-402, June, 1980. Original article submitted December 11, 1979.

 0038-531X/80/4806-0418$07.50

2. A. N. Gudkov et al., ibid., No. 4, p. 105.
3. J. Blachot and C. Fiche, Atomic Data and Nucl. Data Tables, 20, 241 (1977).
4. A. Ferrieu, J. Blachot, and G. Lhospice, Thesis, Univ. of Grenoble (1977).

YIELDS OF ^{165}Tu, ^{166}Tu, ^{167}TU, ^{168}Tu, AND ^{170}Tu IN REACTIONS WITH PROTONS, DEUTERONS, AND α PARTICLES

P. P. Dmitriev, G. A. Molin, and M. V. Panarin

UDC 539.172.12

When erbium is bombarded with protons and deuterons, and holmium with α particles, thulium radionuclides are formed with a high yield. One of these, ^{167}Tu is widely used in nuclear medicine, and therefore it is of particular interest to obtain it with high radioisotopic purity. We have measured the yields of $^{165-168,170}$Tu formed when thick erbium targets were bombarded with 9 to ~22 MeV protons and deuterons, and holmium with α particles having energies from 17 to 43.5 MeV.

Samples of erbium oxide Er_2O_3 (conversion ratio of yield to pure erbium 1.28) and a stack of holmium metal foils of average thickness ~25 mg/cm^2 were irradiated in the deflected beam of the FEI cyclotron. The energy of the protons and deuterons was varied by aluminum foils. The slowing down properties of aluminum and holmium were determined from data in [1]. The radionuclides were identified by γ energies and half-lives.

The activities of $^{165-168,170}$Tu were determined by photopeaks of selected γ lines [8], which were measured on a γ-ray spectrometer with Ge(Li) detectors. The photoefficiency of the detector was determined by using radiators from the OSGI complex. A ^{133}Ba source was used also. Its activity was calibrated by a careful comparison of the 276.38 keV γ photopeak of ^{133}Ba with the 279.19-keV γ photopeak from the OSGI ^{203}Hg source.

The integrated bombardment current was measured by the activity of ^{65}Zn in 18 mg/cm^2 copper monitor foils. The following values of the cross sections of the monitor reactions were used: ^{65}Cu(p, n)^{65}Zn, σ = 46 mb* (E_p = 22.5 MeV) [2]; ^{65}Cu(d, 2n)^{65}Zn, σ = 525 mb (E_d = 22.5 MeV) [3]; ^{63}Cu(α, p, n + 2n)^{65}Zn, σ = 325 mb (E_α = 44 MeV) [4]. The values of the cross sections were obtained from an analysis of data in [2-4] and our measurements of the relative behavior of the excitation functions of the reactions mentioned.

The measured yields of $^{165-168,170}$Tu are shown in Figs. 1-3. The errors in the values of the $^{165-168}$Tu yields are 11-12% and result mainly from systematic errors in measuring the activities of the nuclides and the integrated bombardment current. The error in the values of the ^{170}Tu yield is ~18-20% and was determined

TABLE 1. Comparison of $^{165-168,170}$Tu Yields (for E_α = 44 MeV and E_p = 22 MeV)

Isotope	Ho + α							Er + α		Er + p		
	[6]		[7]		[5]		Present work	[6]		[5]		Present work
	B*	Bк*	B	Bк	B	Bк		B	Bк	B	Bк	
^{165}Tu	295	370	188	248	—	—	224	22	28	19	440	1960
^{166}Tu	3800	6460	2620	4300	—	—	4580	25	41	3960	13600	7000
^{167}Tu	95	119	71	89	58	52	98	72	91	397	355	224
^{168}Tu	0,69	0,67	0,24	0,24	0,36	0,46	0,56	0,35	0,34	6,2	8	7,2
^{170}Tu	—	—	—	—	—	—	—	—	0,07†	1,3	1,7	0,43

*B – yield of nuclide in μCi/μAh for quantum yield used in [6, 7]; Bk – yield of nuclide for new quantum yield [8].
†Estimate of yield.

*1 b = 10^{-28} m^2; 1 Ci = $3.7 \cdot 10^{10}$ Bq.

Translated from Atomnaya Énergiya, Vol. 48, No. 6, pp. 402-404, June, 1980. Original article submitted December 17, 1979.

0038-531X/80/4806-0419$07.50

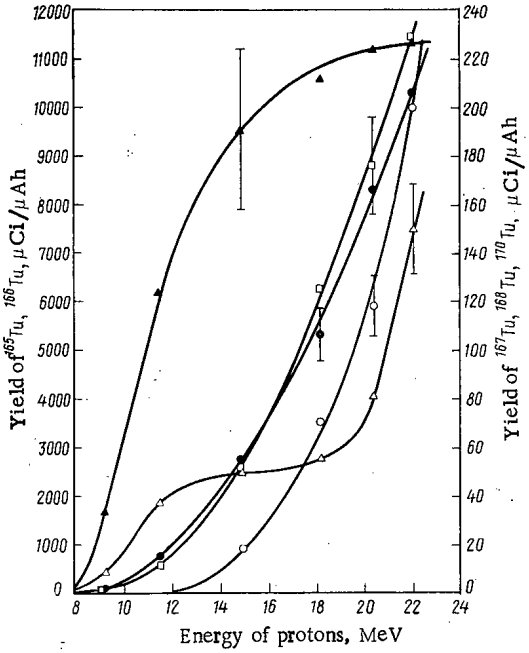

Fig. 1

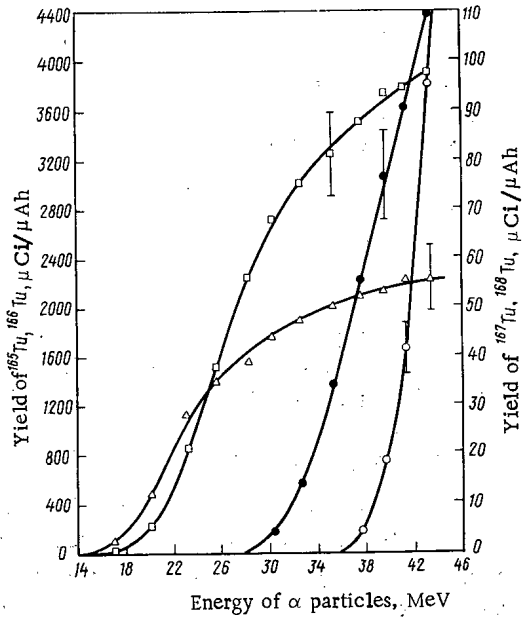

Fig. 2

Fig. 1. Yields of ^{165}Tu, ^{166}Tu, ^{167}Tu, ^{168}Tu, and ^{170}Tu as functions of proton energy for a thick erbium target: ○) ^{165}Tu (×5); ●) ^{166}Tu; □) ^{167}Tu; △) ^{168}Tu (×20); ▲) ^{170}Tu (×500).

Fig. 2. Yields of ^{165}Tu, ^{166}Tu, ^{167}Tu, ^{168}Tu, and ^{170}Tu as functions of deuteron energy for a thick erbium target: ○) ^{165}Tu (×10); ●) ^{166}Tu; □) ^{167}Tu; △) ^{168}Tu (×10); ▲) ^{170}Tu (×50).

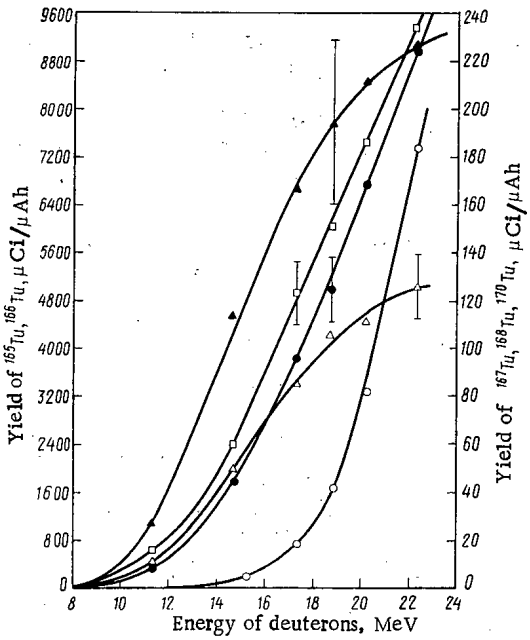

Fig. 3. Yields of ^{165}Tu, ^{166}Tu, ^{167}Tu, and ^{168}Tu as functions of α particle energy for a thick holmium target: ○) ^{165}Tu (×20); ●) ^{168}Tu; □) ^{167}Tu; △) ^{168}Tu (×100).

by eliminating the strong background of the 79.82 keV γ line of ^{168}Tu in the measurement of the photopeak of the 84.26 keV γ line of ^{170}Tu. In [5-7] the activities of the nuclides were measured with a scintillation γ spectrometer by the photopeaks of selected γ lines. The values of the quantum yield and the γ energy used were obsolete, and in a number of cases differ sharply from the current data [8]. Therefore, the yields of the radionuclides were corrected by using the current values of the quantum yield of γ photons. The corrected yields are compared with our results in Table 1. If the cross sections were measured up to lower particles energies, the yield of a nuclide for E_p = 22 MeV and E_α = 44 MeV was found by extrapolating the yield curve using our measured values of the relative behavior of the yield curves. The results are in satisfactory agreement with the measurements of Sau et al. [7] except for ^{168}Tu where Sau et al. obtained values of the reactions cross sections which were too low.

Our data enables us to indicate optimum methods of obtaining thulium nuclides. For example, Fig. 1 shows that obtaining ^{167}Tu by bombarding erbium with protons in the 19-22-MeV range (thin target) decreases the admixture of ^{168}Tu by approximately a factor of 5, and ^{170}Tu by about 1.5 in comparison with bombarding a thick target with 22-MeV protons. The use of a thin holmium target decreases the admixture of ^{168}Tu by a factor of 1.5 (cf. Fig. 3). The use of an enriched ^{167}Er target bombarded with deuterons is very promising. For an enrichment of 96-97% with E_d = 22 MeV one can expect an increase in the ^{167}Tu yield by approximately a factor of 4, and a decrease of the ^{168,170}Tu admixture by approximately a factor of 20.

The method of obtaining ^{167}Tu, from the Er + $\alpha \rightarrow$ ^{167}Tu reaction is worth noting. Here the isotopes ^{165,166,167}Tu are formed mainly through the isobaric nuclei ^{165,166,167}Yb in reactions of the type (α, xn), and ^{168,170}Tu in reactions of the type (α, pxn) with a smaller yield. Reactions of the type (α, pxn) also contribute to the ^{165,166,167}Tu yields, which is taken into account in Table 1 by the known yields of analogous reactions. The relatively low yield of ^{165,166}Tu results from the small ^{164}Er content in natural erbium (1.56%) and the fact that ^{166}Tu is practically in equilibrium with ^{166}Yb ($T_{1/2}$ = 56.7 years). Consequently, the thulium fraction separated from the target, even shortly after bombardment, has a relatively low γ activity. The ^{170}Tu yield was not measured in [6]; we estimated it from the yield of analogous reactions.

The authors thank G. N. Grinenko and Z. P. Dmitrieva for help with the work.

LITERATURE CITED

1. C. Williamson, J. Boujot, and J. Picard, Rapport CEA-R3042 (1966).
2. P. P. Dmitriev et al., At Energ., 24, No. 3, 279 (1968); R. Colle et al., Phys. Rev., C9, 1819 (1974).
3. P. P. Dmitriev and N. N. Krasnov, At. Energ., 18, No. 2, 184 (1965); D. Williams and J. Irvine, Phys. Rev., 130, 265 (1963).
4. N. Porile and D. Morrison, Phys. Rev., 116, 1193 (1959); F. Houck and J. Miller, Phys. Rev., 123, 231 (1961).
5. G. Rayudu and L. Yaffe, Can. J. Chem., 41, 2544 (1963).
6. G. Martin and R. Pilger, Nucl. Phys. A89, 481 (1966).
7. J. Sau et al., Nucl. Phys., A121, 131 (1968).
8. C. Lederer and V. Shirley, Tables of Isotopes, 7th Ed., Wiley, New York (1978).

NEW RUSSIAN JOURNALS

IN ENGLISH TRANSLATION

BIOLOGY BULLETIN
Izvestiya Akademii Nauk SSSR, Seriya Biologicheskaya

The biological proceedings of the Academy of Sciences of the USSR, this prestigious new bimonthly presents the work of the leading academicians on every aspect of the life sciences—from micro- and molecular biology to zoology, physiology, and space medicine.
Volume 7, 1980 (6 issues) $195.00

SOVIET JOURNAL OF MARINE BIOLOGY
Biologiya Morya

Devoted solely to research on marine organisms and their activity, practical considerations for their preservation, and reproduction of the biological resources of the seas and oceans.
Volume 6, 1980 (6 issues) $115.00

WATER RESOURCES
Vodnye Resursy

Evaluates the water resources of specific geographical areas throughout the world and reviews regularities of water resources formation as well as scientific principles of their optimal use.
Volume 7, 1980 (6 issues) $215.00

HUMAN PHYSIOLOGY
Fiziologiya Cheloveka

A new, innovative journal concerned *exclusively* with theoretical and applied aspects of the expanding field of human physiology.
Volume 6, 1980 (6 issues) $195.00

SOVIET JOURNAL OF BIOORGANIC CHEMISTRY
Bioorganicheskaya Khimiya

Features articles on isolation and purification of naturally occurring, biologically active compounds; the establishment of their structure, methods of synthesis, and determination of the relation between structure and biological function.
Volume 6, 1980 (12 issues) $245.00

SOVIET JOURNAL OF COORDINATION CHEMISTRY
Koordinatsionnaya Khimiya

Describes the achievements of modern theoretical and applied coordination chemistry. Topics include the synthesis and properties of new coordination compounds; reactions involving intraspheral substitution and transformation of ligands; complexes with polyfunctional and macromolecular ligands; complexing in solutions; and kinetics and mechanisms of reactions involving the participation of coordination compounds.
Volume 6, 1980 (12 issues) $255.00

THE SOVIET JOURNAL OF GLASS PHYSICS AND CHEMISTRY
Fizika i Khimiya Stekla

Devoted to current theoretical and applied research on three interlinked problems in glass technology; the nature of the chemical bonds in a vitrifying melt and in glass; the structure-statistical principle; and the macroscopic properties of glass.
Volume 6, 1980 (6 issues) $145.00

LITHUANIAN MATHEMATICAL JOURNAL
Litovskii Matematicheskii Sbornik

An international medium for the rapid publication of the latest developments in mathematics, this quarterly keeps western scientists abreast of both practical and theoretical configurations. Among the many areas reported on in depth are the generalized Green's function, the Monte Carlo method, the "innovation theorem," and the Martingale problem.
Volume 20, 1980 (4 issues) $175.00

PROGRAMMING AND COMPUTER SOFTWARE
Programmirovanie

Reports on current progress in programming and the use of computers. Topics covered include logical problems of programming; applied theory of algorithms; control of computational processes; program organization; programming methods connected with the idiosyncracies of input languages, hardware, and problem classes; parallel programming; operating systems; programming systems; programmer aids; software systems; data-control systems; IO systems; and subroutine libraries.
Volume 6, 1980 (6 issues) $115.00

SOVIET MICROELECTRONICS
Mikroelektronika

Reports on the latest advances in solutions of fundamental problems of microelectronics. Discusses new physical principles, materials, and methods for creating components, especially in large systems.
Volume 9, 1980 (6 issues) $160.00

Send for Your Free Examination Copy

PLENUM PUBLISHING CORPORATION, 227 West 17th Street, New York, N.Y. 10011
In United Kingdom: 88/90 Middlesex Street, London E1 7EZ England
Prices slightly higher outside the U.S. Prices subject to change without notice.